A Deconstructable Grout-Reinforced Hybrid Shear Connector for Tall Cross-Laminated Timber Buildings

Experimental Study & Reliability Analysis

by

Samuel Shulman

B. Eng., Concordia University, 2018

A THESIS SUBMITTED IN PARTIAL FULFILLMENT
OF THE REQUIREMENTS FOR THE DEGREE OF

MASTER OF APPLIED SCIENCE

in

THE FACULTY OF GRADUATE AND POSTDOCTORAL STUDIES
(Forestry)

THE UNIVERSITY OF BRITISH COLUMBIA
(Vancouver)

December 2021

The following individuals certify that they have read, and recommend to the Faculty of Graduate and Postdoctoral Studies for acceptance, the thesis entitled:

A Deconstructable Grout-Reinforced Hybrid Shear Connector for Tall Cross-Laminated Timber Buildings

submitted by **Samuel Shulman** in partial fulfillment of the requirements for the degree of **Master of Applied Science** in **Forestry**.

Examining Committee:

Dr. Cristiano Loss, Assistant Professor, Department of Wood Science
Supervisor

Dr. Frank Lam, Professor, Department of Wood Science
Supervisory Committee Member

Dr. Terje Haukaas, Professor, Department of Civil Engineering
Supervisory Committee Member

Dr. Ricardo Foschi, Professor Emeritus, Department of Civil Engineering
Additional Examiner

Abstract

All over the world, the mass timber construction industry is experiencing unprecedented growth. However, as mass timber buildings reach new heights, designers are faced with new challenges regarding constructability, sustainability, and compliance with performance-based design requirements. In particular, there is a need for novel connection solutions that are conducive to off-site prefabrication, quick on-site assembly, and that can provide required seismic resistance without suffering damage, creating the potential for deconstruction and reuse.

This research investigated the structural performance of a novel multi-material shear connector for mass timber and hybrid timber-based buildings, consisting of a threaded steel rod embedded into Cross-Laminated Timber (CLT), reinforced with a ring-layer of epoxy-based grout. The protruding rods may be bolted to steel beams or hold-down plates to form hybrid timber-based floor and shear wall structural assemblies, respectively. The shear connector is to be capacity-protected, resulting in a damage-free connection, allowing for disassembly and potential reuse of the structural timber components.

The response of shear connectors with varying rod diameter and steel strength-class, grout thickness, and CLT grade was analyzed. An insight into the behaviour under quasi-static monotonic incremental loads is given based on a comprehensive experimental campaign, with a total of 240 push-out tests performed on full-scale squared CLT specimens, including baseline samples without grout reinforcement.

Test results revealed significant improvement in shear capacity and stiffness when a grout layer is included, without negatively impacting ductility and failure modes. Strong relationships between rod and grout diameter and yield and maximum shear resistance were established. Reliability analyses established a resistance factor in order to achieve similar levels of reliability across connector types and with dowel-type connectors already in the Canadian wood design standard CSA-O86.

The results are encouraging and serve as a foundation for further research on this novel connector, including testing CLT assemblies and developing reliable mechanics-based models. From a design perspective, the studied multi-material shear connector has great potential for tall and large-scale timber building applications, giving designers a high-capacity alternative to traditional timber connectors.

Lay Summary

Building with wood has historically made use of screws and nails to join elements together. Even as wooden buildings grow taller, thanks to the advent of mass timber, such fasteners continue to be used. Taller buildings mean higher loads, particularly lateral loads from wind and earthquakes, requiring a great number of screws and nails. Not only is this labour-intensive and inefficient, but these connectors also cause permanent damage to the wood upon removal, severely restricting reuse and repair of timber elements. In this research, a novel high-capacity deconstructable shear connector for mass timber buildings is developed and studied. Its primary application is in forming hybrid timber-steel floor and shear wall systems. The main value of this research is in providing a description of the behaviour of these connectors as well as design values for use by engineers.

Preface

This thesis is the original work of the author, Samuel Shulman, in collaboration with thesis supervisor, Dr. Cristiano Loss. In addition to Dr. Loss, the supervisory committee included Dr. Terje Haukaas (Civil Engineering) and Dr. Frank Lam (Wood Science). Part of this work has been published as a report for the funding agency BC Forestry Innovation Investment. Part of this work has also been presented at the 2021 Canadian Society for Civil Engineering Annual Conference.

The processing of the CLT panels was done by Lief Eriksen, Brandon Chan, and Pablo Chung of the UBC Centre for Advanced Wood Processing. Specimens were fabricated by the author, with the assistance of Blériot Vincent Feujofack Kemda, PhD student in the UBC Sustainable Engineered Structural Solutions laboratory. Testing was conducted by the author, with training on the operation of the testing machine provided by Chao Zhang of the UBC Timber Engineering and Advanced Mechanics laboratory. Steel rods were prepared for tensile testing by Angela Hold of the UBC Mechanical Engineering Machine Shop. Tensile testing was provided by Qualitest Canada Ltd. Cross-sectioning of specimens was done by Vancouver Concrete Cutting & Coring Ltd. Assistance with the Bayesian linear regression and reliability analysis was provided by Dr. Terje Haukaas.

Table of Contents

List of Tables

List of Figures

Glossary

CDF Cumulative Distribution Function

CLT Cross-Laminated Timber

CNC Computer Numerical Control

DfD Design for Deconstruction

FORM First-Order Reliability Method

FT Full-Thread

glulam Glue-Laminated Timber

LVDT Linear Voltage Displacement Transducer

LVL Laminated Veneer Lumber

MSR Machine Stress Rated

SORM Second-Order Reliability Method

SPF Spruce-Pine-Fir

UTM Universal Testing Machine

Acknowledgments

I offer my most sincere gratitude to my thesis supervisor, Dr. Cristiano Loss. Your unwavering support, patience, and guidance kept me on course throughout a hectic two and a half years. It is a privilege to become the first student to graduate from your lab at UBC.

I gratefully acknowledge the assistance of Brandon Chan, Pablo Chung, and Lief Eriksen of the UBC Centre for Advanced Wood Processing, George Lee and Chao (Tom) Zhang of the UBC Timber Engineering and Advanced Mechanics laboratory, and Blériot Vincent Feujofack Kemda of the UBC Sustainable Engineered Structural Solutions laboratory.

My thanks are extended to Rothoblaas Canada (Delta, BC) for donating the threaded steel rods, nuts and washers, Hilti Canada (Langley, BC) for discounting the epoxy grout and donating the mixing paddle, Structurlam (Penticton, BC) for discounting the CLT panels, Select Steel (Delta, BC) for including for free the priming of the test jig, and Qualitest (Surrey, BC) for conducting steel rod tensile testing free of charge.

I am also grateful for the financial support I received from the Natural Sciences and Engineering Research Council of Canada (NSERC) through the Canada Graduate Scholarships – Master's program, the Forestry Innovation Investment (FII) of British Columbia through the Wood First program, the Canadian Wood Council through the Catherine Lalonde Memorial Scholarship, the Faculty of Forestry through the Strategic Recruitment Fellowship, Jack and Mavis Toovey through the Jack and Mavis Toovey Gradute Entrance Scholarship in Forestry, and Dr. Irene Bettinger through the Paul Heller Memorial Fellowship in Forestry.

To my bubble, thank you for keeping me sane throughout the pandemic.

Lastly, I would like to thank my parents, Tina and Gary; my brothers, Andrew and Benjamin; and my chosen brothers, Jamie and Joseph. Without your support, encouragement, and love, this thesis would not have come to be.

Chapter 1

Introduction

The best friend on Earth of man is the tree. When we use the tree respectfully and economically, we have one of the greatest resources of the Earth.”
— Frank Lloyd Wright

1.1 Background and Motivation

Wood has been used as a structural material for as long as mankind has sought shelter outside natural geological formations. Beginning from crude nest structures of branches and thatch in the prehistoric era, the development of more sophisticated tools and construction technologies throughout the ancient age allowed larger and more complex wooden structures to be built. Wood framing, as we know it today, was developed in the Roman Empire, and by the Middle Ages, timber was being used to build civil structures, public buildings, and places of worship across the world (Arup, 2019). Some of these structures, like the Hōryū-ji Buddhist temple in Ikaruga, Japan, are still standing today, over one thousand years later. However, the vast majority of historical wooden structures were destroyed by fires, leading to strict regulations on their sizes and heights (Smith and Snow, 2008). Concerns of fire safety, combined with rapid technological advancements during the Industrial Revolution, saw wood replaced by steel and concrete as construction materials of choice. Only in the past fifty years, with newly raised concerns about environmental preservation, climate change, and population growth, has interest been renewed in wood as a structural material (Arup, 2019).

To compete with steel and concrete, timber needed to span greater lengths and carry greater loads. This was achieved with engineered wood products – combinations of strands, veneers, or boards of wood bonded together with adhesives or mechanical fasteners – resulting in composite elements with greater dimensional stability, strength, and stiffness compared to common structural lumber. Common examples of such products include Glue-Laminated Timber (glulam), Cross-Laminated Timber (CLT), and Laminated Veneer Lumber (LVL). Such products, along with a better understanding of fire dynamics and protection, have made timber an attractive lightweight alternative to steel and concrete. However, as the acceptance and application of mass timber continues to grow, so does the need to respond to various concerns surrounding sustainability, building code compliance, and long-term impacts. These three topics are the main motivators for the research presented herein.

1.1.1 Sustainability

The building industry accounts for about a third of global greenhouse gas emissions, resulting from the direct use of energy for heating and cooling as well as the indirect energy required to manufacture building materials (known as embodied energy) (Michael Green Architecture, 2020). With the transition to renewable energy sources and the development of energy-efficient mechanical systems, it is estimated that by 2050, half of the emissions from new construction will be from embodied energy (Röck et al., 2020).

Additionally, UN-Habitat estimates that by 2030, 60% of the global population will live in urban areas and 3 billion people will be in need of affordable housing (United Nations Human Settlements Programme, 2015). This means an unprecedented amount of low-cost housing will need to be constructed at a time when anthropogenic climate change is at its peak. To continue building with traditional construction materials and methods would be both irresponsible and unsustainable.

Wood, as a structural material, has been identified as a sustainable alternative to steel and concrete, with these last two embodying 26% and 57% more energy, respectively, than wood for typical residential construction (Canadian Wood Council, 2004). Not only do wood products require less energy to manufacture, they store carbon throughout their life, keeping greenhouse gasses out of the atmosphere.

Despite the environmental benefits of building with wood, one may reasonably be concerned about the impact the growth of timber construction may have on the world's forests. After all, more timber buildings means more trees being cut down. Deforestation has long been a critical issue in the fight against climate change and in just 15 years between 1990 and 2015, 129 million hectares of global forest were lost, resulting in an 11 gigaton reduction in the forest biomass carbon stock, not to mention damage to species biodiversity, fluctuations in temperature and water cycle regulation, and reduction in global oxygen production (FAO, 2016). However, the vast majority of the forests landmass lost over that 15 year period was the result of land conversion, that is, razing forests to use the land for another purpose, usually agriculture. Not only do the felled trees return their carbon stores to the atmosphere through decomposition or burning, but the previously forested land is now used for the energy-intensive process of growing plants or raising livestock.

Conversely, harvesting forests for lumber is actually beneficial to the environment, when done responsibly. Unlike with land conversion, the forest is replanted after harvesting in order to produce more lumber, and the harvested wood is turned into value-added products. This means that not only are young saplings actively sequestering carbon, but the previously harvested wood continues to passively sequester carbon, significantly increasing the carbon abatement potential of a given forested landmass. This was confirmed by Ximenes et al. (2012), who found that multiple-use production forests have greater greenhouse gas abatement potential (thanks to frequent new growth and long-term carbon storage in its products) compared to conservation forests, which reach a plateau in carbon storage levels. Xu et al. (2018) made similar findings in British Columbia, concluding that “higher utilization” is almost twice as effective at mitigating greenhouse gas emissions compared to “old growth conservation” or “harvest less” strategies. These findings are in line with the Intergovernmental Panel on Climate Change’s recommendation that “in the long term, a sustainable forest-management strategy aimed at maintaining or increasing forest carbon stocks, while producing an annual yield of timber, fibre or energy from the forest, will generate the largest sustained mitigation benefit” (IPCC, 2007). This emphasizes the substantial economic and environmental potential that exists in a symbiotic relationship between the forestry and building sectors.

Though the environmental benefits of timber construction have been explored, to truly assess its sustainability one must consider the full life-cycle of a timber building, particularly its end-of-life. If at the end of a building’s life, the timber elements are left to decompose or are burned, building with wood does not offer a complete solution to climate change, but just a means of delaying it (Michael Green Architecture, 2020). Unfortunately, this is the present case in Canada, which is one of the world's largest solid waste producers, with 25% coming from construction, renovation, and demolition (Earle et al., 2014).

In its state-of-the art report on timber buildings, Arup (2019) has identified "disassembly, adaptation and reuse [as the] ideal disposal option[s] at end-of-life". Similarly, Ximenes et al. (2012) emphasizes the importance of "ensuring timber is processed to long-life products and can be utilised to offset fossil-fuel emissions at the end of their lifespan." It is clear that the potential to deconstruct and reuse timber elements is at the forefront of sustainable construction.

1.1.2 Design for Deconstruction

Design for Deconstruction (DfD) is a design philosophy that has emerged in the last twenty years to address the ever-growing concerns surrounding resource scarcity and demolition waste production. It calls for a change in the design and construction paradigm, shifting from a cradle-to-grave model to a cradle-to-cradle model, in which the end-of-life options for building components are accounted for in the initial design of a building. The ultimate goal of DfD is to increase resource efficiency and reduce pollution and waste production by recovering as much material as possible for reuse and recycling. In particular, wood has been identified as "a highly preferable material in design for deconstruction since it is flexible for both reuse and recycling, a 'natural' material, and can be readily connected using interstitial connecting devices such as bolt" (Guy et al., 2006).

In Canada, the majority of wood-frame buildings are demolished, with the majority of waste sent to landfills. Wood accounts for 30-34% of the waste produced from construction, renovation and demolition, with only about 5.4% salvaged for reuse or recycling (Guy et al., 2006).

The primary barriers to deconstruction and reuse of wooden building elements are the time and cost involved in dismantling and sorting the elements and their connections (Earle et al., 2014). Additionally, it is very difficult to salvage wooden members that have been nailed or screwed. An investigation on the reuse of wooden building elements, conducted by researchers at the University of Florida, found that "human-made damage was the single greatest reason for a down-grade" when grading deconstructed wooden elements. They identified "connecting systems and wood construction designs [...], which do not damage the lumber" as a necessity for deconstruction and reuse (Guy and McLendon, 2000). Similarly, other reports have concluded that damage due to nail holes is the most common deterrent to material reuse (Richardson, 2013) and that reducing the number and variety of connectors may reduce possible damage and speed up the deconstruction process (Guy et al., 2006).

As it stands, the most commonly used fasteners in mass timber construction are self-tapping screws, which work in a similar way as wood screws and nails normally used in light-frame timber construction. Unlike split rings and shear plates, nails and screws rely on multiplicity (i.e. group of fasteners) rather than inherent strength and stiffness to achieve desired performance. This may be acceptable in simple low-rise construction, but to continue using these in high-rise mass timber buildings would be both inefficient and uneconomical. Not only do these connectors permanently damage the wood during installation, as previously mentioned, but they are designed to fail plastically, further damaging the wood in the process.

The use of stronger and stiffer individual connectors in mass timber, akin to split rings and shear plates in light-frame construction, not only reduces the number of connections in a system, simplifying deconstruction, but also allows for careful design for the greater loads on multi-storey timber buildings. In particular, connections may be capacity-protected, such that connectors remain elastic even under extreme loading, preventing any damage in the wood throughout their lifespan.

1.1.3 The Future of Mass Timber Construction

The 2020 edition of Canada's National Building Code will double the allowable height limit of timber buildings in Canada from six storeys to twelve storeys (Sorensen, 2019). Though there is no widely accepted definition of what constitutes a high-rise building, it is safe to say that this new allowance takes timber construction above the mid-rise, mainly residential, market. However, these so-called new heights are actually quite old. Prior to the establishment of the National Building Code in 1941, which imposed a four storey limit on timber construction that lasted until 2015, several timber buildings across Canada exceeded six storeys, many of which still stand today. One such building is The Landing in Vancouver's Gastown district, an eight-storey heavy timber building erected at the turn of the century to serve as a warehouse during the gold rush era. This building, and other like it, are a living testimony to timber's strength and durability.

Since the construction of The Landing, heavy timber has been replaced by engineered wood products, which are stronger, stiffer, and more dimensionally stable. This, in consort with advancements made in the field of fire suppression and a better understanding of the behaviour of mass timber when exposed to fire, makes 12-storey timber construction easily achievable. It is therefore likely that this limit will continue to increase, as has already occurred in the United States with the

2021 edition of the International Building Code defining a new construction type allowing for 18-storey mass timber construction (Breneman et al., 2019).

The real challenge with these new heights is not the greater gravity loads, but the greater lateral loads. As buildings grow taller, the affect of wind loads, and earthquake loads for buildings located in high-seismic regions like Vancouver, become significant. Unlike The Landing, which sits on almost an entire city block, modern timber buildings will be confined to smaller and smaller plots of land, while growing taller in height. This combination of large height and small ground dimensions leads to high lateral demands. Not to mention the trend of open floor plans further increasing lateral demands by restricting the number of shearwalls or braces. There is thus a need for high-capacity and stiff lateral load resisting systems for tall mass timber buildings.

The Canadian timber design code, CSA-O86, imposes a capacity-design approach to the design of lateral load resisting systems by which connections are designed to dissipate energy through plastic deformation while the capacity-protected members are over-designed in order to remain elastic. This is particularly important in timber buildings in which the steel connector elements provide the necessary ductility that timber lacks on its own.

Despite the advancements made in structural timber elements over the past century, very little progress has been made with respect to timber fasteners and connections. Essentially the same fastener technology used for millennia in light-frame wood design, nails and screws, are still being used today. Though improvements have been made with the advent of ductile alloys, ring-shank and spiral-shank nails, as well as self-tapping screws, these pale in comparison to the improvements made in structural timber, evolving from dimensional lumber to glulam and from plywood to CLT.

In order to meet the growing demands allowed by mass timber products and greater building heights, these connectors have relied on high levels of redundancy. As building and loads only continue to grow, the quantity of such fasteners required in a timber building will become prohibitively expensive and require extremely time-consuming on-site labour. Using fewer but larger high-capacity connectors can easily be seen to be more efficient. Additionally, such connectors may be pre-installed off-site, creating connection assemblies that are quickly joined together on-site.

Considering timber fasteners from a DfD perspective, screws and nails are problematic as their removal causes damage to the wood. The use of bolted connections, fastened with easily removed nuts, responds to this issue. However, to be truly deconstructable, the bolted connection must not suffer damage in its service life. As previously mentioned, the steel fasteners in a timber building are traditionally designed to dissipate energy in the event of extreme lateral loading. This energy dissipation comes in the form of plastic deformation of the fastener, causing permanent damage to the wood elements. To respond to this, it is suggested that the fastener be designed to remain elastic, while achieving the required ductility in the plastic deformation of an attached fuse element, such as steel plates, perforated plates, friction-devices, etc. The inclusion of a grout layer allows the connector to reach a high enough stiffness and shear yield capacity to support elastic capacity design. This is particularly applicable to steel-timber hybrid construction, in which timber elements are already joined to steel elements which may act as, or support, a fuse.

To illustrate the applicability of this concept, consider the CLT shearwall design guidelines provided in CSA-O86 (CSA Group, 2014*a*). Various studies have shown that the strength and stiffness of CLT shearwalls are dictated by their connections, while the CLT panel itself mainly behaves as a rigid body (Dujic et al., 2006, Gavric et al., 2014, Popovski et al., 2010). In particular, the connections between the shearwall and the foundation (or the floor beneath) and the connections between adjacent in-plane shearwalls govern the shear resistance of the wall. This rigid-body behaviour and the influence of the shear connectors is illustrated in Figure 1.1. Following capacity-design principles, these connections should be allowed to yield, thus providing the energy dissipation required. This is normally achieved by specifying certain diameters of screws, nails, or other dowel-type connections, which are designed to bend plastically. The non-dissipative connections are over-designed such that their factored resistance is greater than the demand induced on them when the dissipative connections have reached the 95$^{\text{th}}$ percentile of their ultimate resistance, and such that they can tolerate the displacement when the dissipative connections reach their target displacement.

The proposed alternative approach is to achieve the required ductility through the deformation of a fuse to which the fastener is attached, rather than through the deformation of the fasteners themselves. Thus, the fastener may be designed as a non-dissipative element, while the fuse be designed as the dissipative element. In this scenario, plastic behaviour of the connections is achieved while the fastener itself remains elastic. To achieve this, much higher-capacity and stiffer dowel-type fasteners, that do not depend on slenderness, are required than what is currently available.

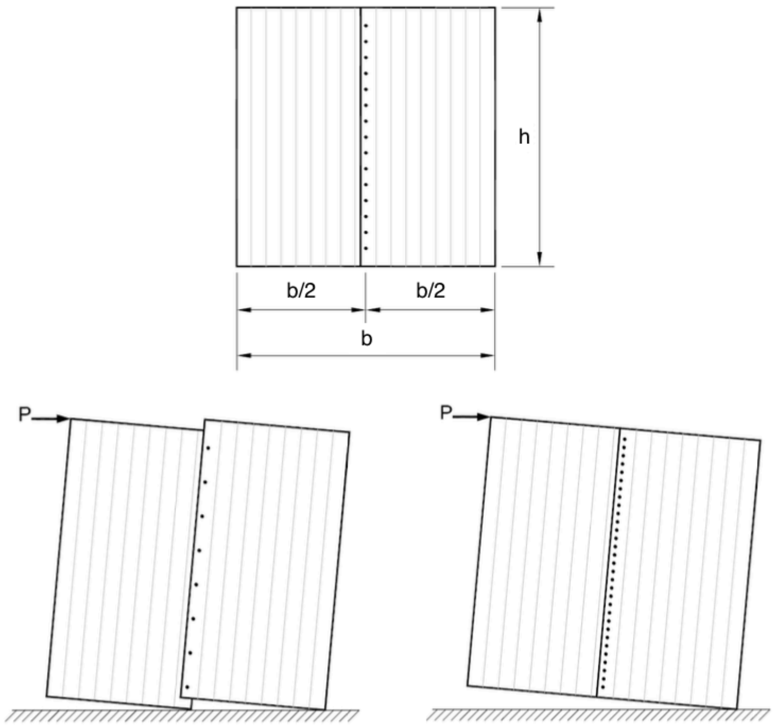

Figure 1.1: Rigid-body rocking behaviour of CLT shearwall segments as governed by interstitial shear connectors. Adapted from Karacabeyli and Gagnon (2019).

1.2 Proposed Shear Connector

The proposed shear connector is conceived as a system in which a Full-Thread (FT) steel rod is embedded into CLT and reinforced by a ring-layer of epoxy-based grout. As a system, such connectors can be designed to respond to the various needs discussed previously. They encourage hybridization and therefore the introduction of more timber components into high-rise buildings, thereby decreasing the building's embodied energy. The protruding FT rod allows for the formation of bolted connections, which are quick and easy to both erect and disassemble without damaging the wood. Additionally, the grout layer allows for high-capacity making possible capacity-based design by which the connector itself remains elastic, transferring the energy dissipation demand to a connected element. This ties back in to the concept of DfD in that the assembly may be deconstructed even after extreme loading events, allowing for the reuse of the structural timber elements and ultimately diverting wood from landfills.

The anticipated application of such a connector is in forming CLT panels with permanently embedded FT steel rod fasteners for use in hybrid timber-based floor and shearwall systems, as illustrated in Figure 1.2. In the case of floors, the panel is fixed to steel beams, transferring composite action from the slab to the beams through the connectors. In the case of shearwalls, the panel is fixed to steel hold-downs with the connectors ensuring that shear forces are transferred to the steel. These steel elements may be designed as the dissipative elements or a sacrificial steel element may be introduced into the connection.

As this is the first time such connectors are being studied, the research is limited to testing simple single-dowel connections under monotonic loading. Multiple design parameters are varied in order to develop a thorough understanding of the connection's behaviour and to assess the influence of each parameter on its structural performance.

1.3 Research Objectives

This research aims to develop and study a novel steel-to-timber shear connector that responds to the need for reliable and deconstructable connection solutions for the next generation of mass timber and hybrid timber-based buildings. Connections are conceived in order to:

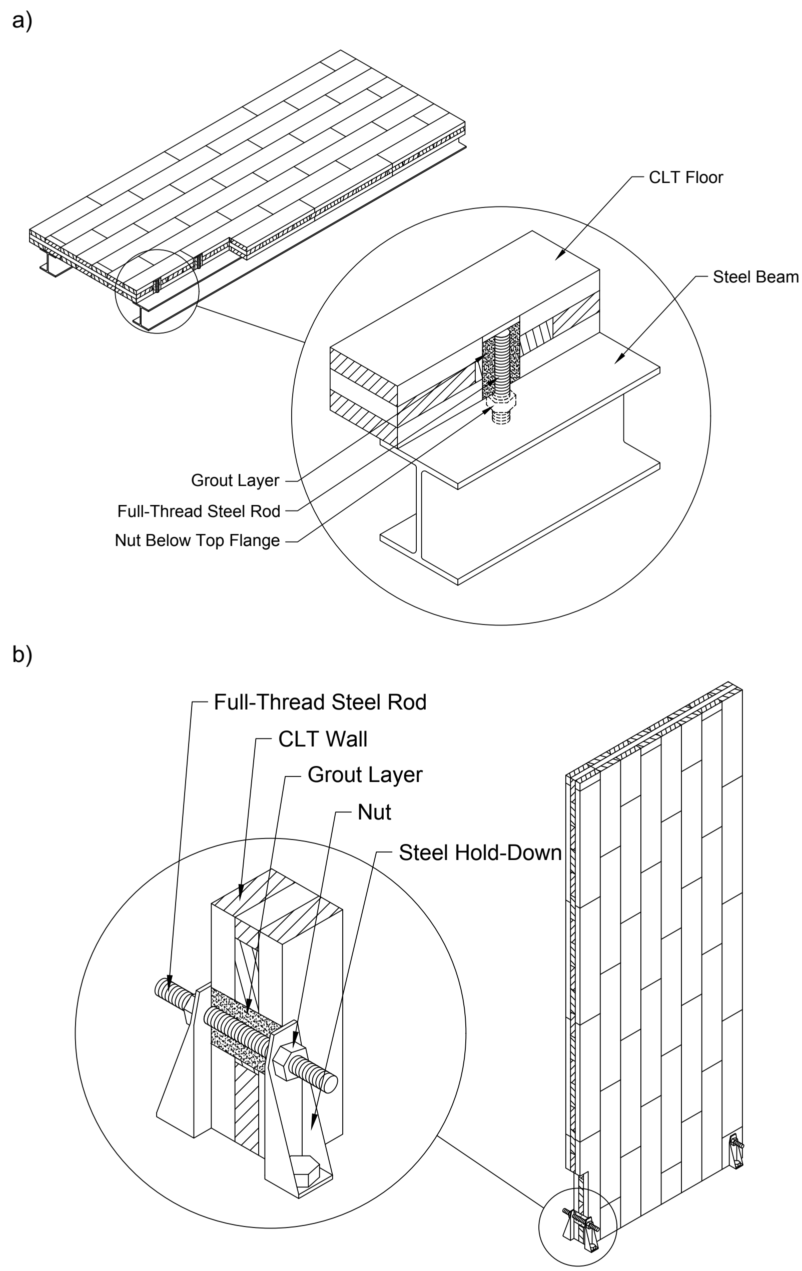

Figure 1.2: Application of proposed shear connector in hybrid steel-timber (a) floor and (b) shearwall systems.

i. offer high individual capacity such that fewer connectors are required to meet the multi-objective structural performance requirements of NBC and CSA-O86 standards,
ii. favour prefabrication and modular construction,
iii. favour quick erection of buildings,
iv. favour quick disassembly and possible reuse of the timber members,
v. provide efficient seismic-resistant structural assemblies.

1.4 Organization of Thesis

Chapter 2 presents a review of the background theory and existing literature related to the design, testing, and modelling of the proposed novel hybrid connection. Chapter 3 describes the experimental program, including the materials used, the fabrication of the test specimens, the design of the test apparatus, the testing procedure, and the derivation of the performance parameters from the raw data. Chapter 4 discusses the results of the tests, including observed failure modes, load-deformation behaviour, and structural performance, as well as the results of the statistical and reliability analyses. Finally, Chapter 5 details the main findings and discusses limitations and future work.

Chapter 2

Review of Background Theory and Existing Literature

This research aims to test and study a novel dowel-type hybrid shear connector for mass timber buildings. Thus, this chapter presents an overview of important theories and previous research related to dowel-type fasteners in wood. This is expanded upon with a discussion on hybrid connectors as well as an insight into the codes and standards referred to throughout the thesis.

2.1 Laterally Loaded Dowel-Type Fasteners for Timber Connections

Research on laterally loaded fastener connections in timber construction dates back to 1932, when Trayer (1932) conducted embedment strength tests on dowel-type wood connections, establishing an empirical relationship between bearing strength and bolt slenderness. Later, Johansen (1949) developed a model for the capacity of dowel-type connectors in timber based on the bending resistance of the dowel and the embedment strength of the wood. Johansen's model was modified by Larsen (1973) and became known as the European Yield Model. Soltis et al. (1986) confirmed that the European Yield Model was a suitable analytical model to describe Trayer's empirical results, with Whale et al. (1987) developing equations for wood embedment for use in the model. Whale's equations, as they appear in Eurocode 5, are as follows:

$$f_{h,0,k} = 0.082(1 - 0.01d_F)\rho_k \tag{2.1}$$

$$f_{h,\alpha,k} = \frac{f_{h,0,k}}{k_{90}\sin^2\alpha + \cos^2\alpha} \tag{2.2}$$

where: $f_{h,0,k}$ is the characteristic embedment strength parallel to the grain, d_F is the fastener diameter, ρ_k is the characteristic wood density, $f_{h,\alpha,k}$ is the characteristic embedment strength at an angle to the gran, α is the load-to-grain angle, and k_{90} is an adjustment factor depending on the diameter of the fastener and the type of wood (softwood, hardwood, or LVL).

The most comprehensive study on dowel-type fasteners in CLT was conducted by Uibel and Blaß (2006). 620 tests were conducted on specimens equipped with smooth dowels, of diameter 8 mm to 24 mm, installed in the panel face, positioned both in areas with and without gaps, and assuming load-grain angles of 0°, 45°, and 90°. A multiple regression analysis resulted in the following formula for the characteristic embedment strength of CLT with dowels installed in the panel face:

$$f_{h,k} = \frac{0.031(1 - 0.015d_F)\rho_k^{1.16}}{1.1\sin^2\alpha + \cos^2\alpha} \tag{2.3}$$

The Whale et al. (1987) model and the Uibel and Blaß (2006) model were compared by Ringhofer et al. (2017) and it was concluded that both exhibit a similar relationship between fastener diameter and wood density and that, with adjustment factors to account for the influence of gaps and the effect of different load-grain angles of adjacent layers, one equation could be used for solid timber, glulam, and CLT.

This is the approach taken in CSA-O86 (CSA Group, 2014*a*), which gives the following equations for CLT embedment strength:

$$f_{iP} = 50G(1-0.01d_F)J_X \tag{2.4}$$

$$f_{iQ} = 22G(1-0.01d_F) \tag{2.5}$$

where: f_{iP} is the embedment strength for a fastener bearing parallel to grain, f_{iQ} is the embedment strength for a fastener bearing perpendicular to grain, G is the mean relative density of the wood, and J_X is an adjustment factor for CLT equal to 0.9. For fasteners bearing at an angle to the grain, the Hankinson formula is used.

A recent Canadian study by Kennedy et al. (2014) questioned the validity of including the fastener diameter as a parameter in the embedment strength equation, since it is a material property of the wood and should not depend on the size of fastener used. After performing 960 tests on Canadian glulam specimens with lag screws, the study concluded that the Canadian formulas tended to overestimate the embedment strength. Furthermore, a statistical analysis showed that the fastener diameter was not a significant predictor of embedment strength. The authors therefore proposed an equation for characteristic embedment strength based solely on the wood density, as follows:

$$f_{h,k} = \frac{42G^{1.7}[27G^{2.2}]}{(1.54G^{-0.5})\sin^2\alpha + \cos^2\alpha} \tag{2.6}$$

As previously stated, the embedment strength is one of the main parameters required for calculating the load-carrying capacity of laterally loaded dowel-type connections according to the European Yield Model. The other relevant parameters are the yield moment (or strength) of the dowel, the diameter of the dowel, and the thicknesses of the connected elements. In developing the load-carrying capacity equations, the possible failure modes are identified and the capacity determined by evaluating a free-body diagram of the failure modes, assuming rigid-plastic material behaviour of the dowel when subjected to bending stresses and the timber when subjected to embedment stresses.

For single-shear timber-timber connections, the European Yield Model identifies six different failure modes, as shown in Figure 2.1:

a embedment failure in member 1,

b embedment failure in member 2,

c embedment failure in both members,

d embedment failure in both members and one plastic hinge in member 2,

e embedment failure in both members and one plastic hinge in member 1,

f embedment failure and plastic hinge in both members.

For double-shear timber-timber connections, the European Yield Model identifies four different failure modes, as shown in Figure 2.2:

a embedment failure in outer members,

b embedment failure in inner member,

c embedment failure in all members and one plastic hinge in inner member,

d embedment failure and plastic hinge in all members.

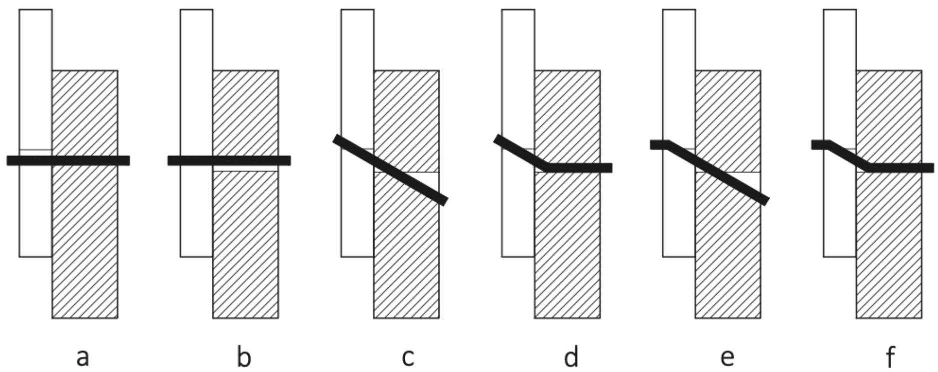

Figure 2.1: European Yield Model single-shear failure modes (Blaß and Sandhaas, 2017). Member 1 is the side member (white) and member 2 is the main member (hatched).

Eurocode 5 presents equations for each of these timber-timber connection failure modes, with an additional twelve failure modes for timber-steel single-shear and double-shear configurations with both thin and thick steel plates. Conversely, CSA-O86 adopts a simplified approach consisting of only seven capacity equations, combining the single-shear and double-shear equations that are identical (i.e., the equations for failure mode (a) and (g) are equivalent). Rather than provide a new set of equations for steel-timber connections, CSA-O86 does not differentiate between timber-timber and steel-timber connections, but simply provides embedment strength equations for non-wood-based material.

The capacity equations given in CSA-O86, per fastener per shear plane, are as follows:

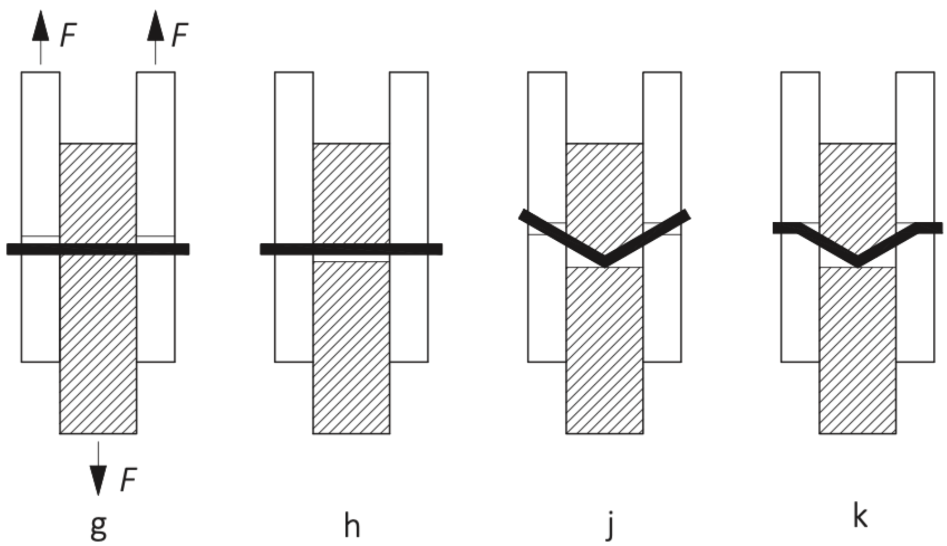

Figure 2.2: European Yield Model double-shear failure modes (Blaß and Sandhaas, 2017). Member 1 is the side member (white) and member 2 is the main member (hatched).

$$n_u = \begin{cases} f_1 d_F t_1 & \text{(a), (g)} \\ f_2 d_F t_2 & \text{(b)} \\ f_1 d_F^2 \left(\sqrt{\frac{1}{6} \frac{f_2}{(f_1+f_2)} \frac{f_y}{f_1}} + \frac{1}{5} \frac{t_1}{d_f} \right) & \text{(e), (j)} \\ f_1 d_F^2 \left(\sqrt{\frac{1}{6} \frac{f_2}{(f_1+f_2)} \frac{f_y}{f_1}} + \frac{1}{5} \frac{t_2}{d_f} \right) & \text{(d)} \\ f_1 d_F^2 \frac{1}{5} \left(\frac{t_1}{d_f} + \frac{f_2}{f_1} \frac{t_2}{d_f} \right) & \text{(c)} \\ f_1 d_F^2 \sqrt{\frac{2}{3} \frac{f_2}{(f_1+f_2)} \frac{f_y}{f_1}} & \text{(f), (k)} \end{cases} \tag{2.7}$$

where: n_u is the unit lateral yielding resistance, f_1 and f_2 are the embedment strengths of members 1 and 2, with member 1 being the side member in the case of a double-shear connection, d_F is the diameter of the fastener, t_1 and t_2 are the member thicknesses, and f_y is the fastener yield strength in bending. The corresponding

European Yield Model failure modes are given to the right of each equation.

In the Johansen model, it is assumed that normal forces do not develop in the axis of the dowel. This may be accurate for smooth shank connectors, but for threaded rods or bolts with washers, that are capable of developing large normal forces under large deformations, this is not a reasonable assumption. As such, in Eurocode 5 a rope effect factor is appended to the capacity equations in all failure modes that involve inclination of the dowel. This factor consists of the axial withdrawal capacity of the fastener multiplied by a friction coefficient of 0.25. This accounts for the compressive component of the force developed in the axis of the fastener, which generates frictional force between the timber members and thus increases the load-bearing capacity of the joint. In CSA-O86, the capacity equations for wood screws account for the rope effect in the term f_3, but it is not accounted for in the previously listed capacity equations for bolts and dowels.

The Canadian standard also stipulates that connections be checked for brittle failure modes dictated by fracture mechanics, including row shear, group tear-out, net tension, and splitting. Such brittle failure modes were not included in the scope of this research project.

In addition to the load-carrying capacity, stiffness is another important property as it describes a connection's elastic load-deformation behaviour. In general, a connection's load-deformation curve will begin with large deformation given little to no applied load, called initial slip. This is the result of fabrication tolerances and is the movement of the dowel through gaps in the connection. Following initial slip, an approximately linear load-deformation behaviour is observed until yielding, at which point the load-deformation behaviour becomes non-linear. A connector's stiffness is then taken as the slope of the linear elastic portion of its load-deformation curve.

Eurocode 5 defines the slip modulus as a stiffness property “used in the calculation of the deformation between two members of a structure” (EN 1995-1-1, 2004). For dowel-type timber-timber connections, it is calculated as follows, based on the work of Ehlbeck and Larsen (1993):

$$K_{ser} = \frac{\rho_m^{1.5} d}{23} \tag{2.8}$$

where: ρ_m is the mean density of the connected timber elements and d is the diameter of the fastener. For steel-timber connections, this value may me multiplied by 2.

To date, CSA-O86 does not have specific provisions accounting for the deformation of dowel-type connections.

2.2 Structural Hybridization and Hybrid Connectors

Hybridization involves the combination of different materials at either the system, component or connection level, with the purpose of forming “a system which utilizes the strength of each material to overcome their weaknesses” (Schober and Tannert, 2016). All timber buildings are hybrid to some extent at the system level, usually in the form of a concrete foundation. Such system hybridization also commonly takes the form of a timber-based gravity system combined with a concrete-core lateral system, as is the case in the 18-storey Brock Commons Tall Wood Building at the University of British Columbia (naturally:wood, 2016).

At the component level, composite structural assemblies are created consisting of different materials. One well-researched and commonly employed example is timber-concrete composite flooring systems. These consist of a base layer of CLT topped with a layer of concrete joined together by shear connectors. Thus, the timber takes on the bending-induced tension that would otherwise crack the concrete, while the concrete provides additional stiffness and improved vibration performance that the timber lacks on its own (Cuerrier-Auclair, 2020). Recently, steel-timber assemblies have become a subject of research, with Loss et al. (2016) developing and testing a vast range of connections for such assemblies.

To understand hybridization at the connection level, one must first be aware of the traditional connection types used in timber construction. Timber connections are usually divided into three categories: carpentry joints, adhesive joints, and mechanically-fastened joints. Carpentry joints represent the oldest type of joint, which relies simply on wood bearing against wood, often seen in the form of dovetail, mortise and tenon, and tongue and groove joints. Though such joints used to require highly specialized labour to manufacture, the advent of Computer Numerical Control (CNC) technology has made possible their applications in modern timber construction (Tannert, 2016).

In adhesive joints, two of more pieces of wood are bonded together by means of an adhesive. This significantly increases the stiffness compared to carpentry joints, but leads to brittle connections. Additionally, in-situ installation of adhesive joints is problematic both due to the difficulty in working the adhesives but also due to the significant influence temperature and humidity have on adhesive properties. However, as off-site prefabrication becomes more popular and with the development of concrete-type adhesives, such connections may find a foothold in mass timber engineering (Schober and Tannert, 2016).

Mechanically-fastened joints are by far the most common and well-understood types of joints in timber construction. These include nails, screws, bolts, dowels, and threaded rods, most often made of steel. From a construction point of view, steel fasteners are readily available and easy to install. From a design point of view, the behaviour of steel is well understood and the fasteners provide timber with the ductility it lacks on its own. For these reasons, mechanically-fastened joints have been heavily researched and their design codified in most timber design standards, including CSA-O86.

Hybridization at the connection level involves the combination of any of these basic timber connection types. One of the most promising of these combinations is that of fastener-adhesive hybrids, benefiting from the ductility of the fastener and the stiffness of the adhesive. This concept, particularly adhesive-reinforced dowel-type connections, was first studied by Hart-Smith (1985) for application in aircraft design. This was expanded to building design by Riberholt (1986) and Townsend and Buchanan (1990). Since then, glued-in-rods have mostly been limited in both research and application to the axial pull-out strength of single rod connections in solid lumber (Yeboah et al., 2011), LVL (Hunger et al., 2016), and glulam (Steiger et al., 2007). Research on glued-in-rods applied to CLT is still in its infancy and similarly limited to axial capacity (Andersen and Høier, 2016, Azinović et al., 2018).

As for the lateral capacity of glued-in-rods applied as shear connectors, very little research has been conducted. Rodd et al. (1989) demonstrated increased load-bearing capacity and stiffness for rods glued in perpendicular to the grain. Davis and Claisse (2001) expanded on this by testing laterally loaded glued-in-rods in timber, glulam, and two different timber composites. For timber and glulam, results showed a reduction in initial slip and bedding-in deformation as well as improved structural performance, though no relationship is given due to the small sample size. However, for the timber composites, the resin leaked through voids in the material and proved to be ineffective. This research is limited by only testing one rod diameter (12 mm), using a viscous adhesive, and only considering the adhesive in the same way as in the axial tests - as a means of filling in the small gap between dowel and wood (in this case 2 mm).

According to the literature review, no research on laterally loaded adhesive-dowel hybrid connectors in CLT has been conducted. Additionally, no research has been conducted considering different sizes of the adhesive layer as a design parameter (rather than considering the adhesive as simply a means of filling a pre-existing gap in the connection). Finally, no related research has been done using Canadian products and for the purpose of informing Canadian design standards.

2.3 Reliability Analysis

Since 1989, the Canadian timber design standard, CSA-O86, follows a reliability-based limit-state design format, based on the fundamental research of Foschi et al. (1989). A summary of reliability analysis is presented here, adopting the same nomenclature as Foschi et al. (1989), and consequently, CSA-O86.

Structural design problems involve the interaction of several variables of uncertain value, also known as random variables. Such variables may either be demand variables, D (influencing the demand or load on the system) or capacity variables, C (influencing the capacity or resistance of the system). Reliability-based design uses principles of probability theory to account for the uncertainty of these random variables. The starting point for reliability analysis is a performance (or limit-state) function, $G(X_1, X_2, X_3, \ldots, X_N)$, which is a function of the N random variables X_i. By convention, the performance function is written as:

$$G = C - D \tag{2.9}$$

This formulation is known as the basic reliability problem and simply expresses that when capacity C exceeds demand D, then $G > 0$, representing adequate performance. Conversely, when demand D exceeds capacity C, then $G < 0$, representing non-performance or failure. When capacity and demand are equal, $G = 0$, and this is known as the limit state between performance and non-performance. The probability of failure is calculated as the probability that $G < 0$ and is quantified by the reliability index β. Given statistical data about the random variables, β is determined using common reliability methods. The most common methods are First-Order Reliability Method (FORM) and Second-Order Reliability Method (SORM). From the reliability index, a corresponding resistance factor can be determined for use in a design equation.

In CSA-O86, performance is assessed by a design equation that takes on the following format:

$$[\alpha_D D_n + \alpha_Q Q_n]S = \phi R_o \tag{2.10}$$

where: $\alpha_D = 1.25$ and $\alpha_Q = 1.50$ are the dead and live load factors, respectively; D_n and Q_n are the design dead and live loads from the NBCC, respectively; S is a parameter that transforms the applied loads into stress (e.g., $\frac{6L^2}{8BH^2}$ for bending of a uniformly-loaded simply supported beams), R_o is the characteristic resistance, usually taken as the 5^{th}-percentile of the distribution of the variable R; and ϕ is the resistance factor.

Assuming linear elastic failure as the limit-state, the performance function can be written as:

$$G = R - (D + Q)S \tag{2.11}$$

where: R, D, and Q are the resistance, dead load, and live load, now given as random variables.

Solving the design equation for S and substituting it into the performance function yields the following:

$$G = R - \phi \frac{R_o}{1.25\gamma + 1.50}(d\gamma + q) \tag{2.12}$$

where: $\gamma = \frac{D_n}{Q_n}$, $d = \frac{D}{D_n}$ and $q = \frac{Q}{Q_n}$. For timber structures, γ is typically taken as 0.25 (Foschi et al., 1989).

Statistical data for the demand variables d and q have been given in Foschi et al. (1989). For the live load demand variable q Foschi et al. (1989) provides distributions for residential occupancy, office occupancy, and various snow loads of cities across Canada. For this study, it was chosen to use the office occupancy live load as this would be a common design live load for tall timber buildings. The statistical properties of the dead and live load distributions used for the reliability analysis are give in Table 2.1.

The statistical properties of R are established from test data. Given statistical data for these random variables, the probability of $G < 0$ for different values of ϕ can be studied. A reliability analysis can then be conducted to establish the relationship between ϕ and β. An appropriate resistance factor, ϕ, can then be selected based on a target value for β, corresponding to an adequate and consistent level of safety across structural materials and components.

Table 2.1: Probability distributions of demand variables.

Load	Distribution Type	Mean	COV
Dead	Normal	1.0	0.1
Live, Office	Extreme Type I	0.925	0.236

Table 2.2: Target reliability indices β (adapted from Massé and Salinas (1989)).

	Type of Failure	
Safety Class	Ductile	Brittle
Not Serious	2.5	3.0
Serious (Normal Building)	3.5	4.0
Very Serious	4.0	4.5

When CSA-O86 was converted from an allowable stress design format to an ultimate limit state design format in 1989, a target reliability analysis of 2.8 was used (Foschi et al., 1989). This was chosen to best match the steel design standard of the time. However, other references offer different levels of reliability based on consequence of failure, type of failure expected (brittle or ductile), return period (in years), and structural level (element or system). These all generally fall within a range of 2.5 to 4.5, with higher values reserved for important structures whose failure would have serious consequences, as well as for elements which tend to fail suddenly. A special report prepared by the CSA, CSA SP S408-1981 (1981), provides target reliability indices for various scenarios, as summarized in Table 2.2. Though CSA-O86 was calibrated for a reliability index of 2.8, at the connector level a target reliability index closer to 3.5 would be more appropriate.

Chapter 3

Experimental Program

The research methodology presented in this chapter includes the development of the shear connector, material processing, fabrication of specimens, design of a test apparatus, testing of specimens, and data processing.

3.1 Materials

The materials used in the experimental program are given in Table 3.1.

3.1.1 Cross-Laminated Timber Panels

A total of 24 3-ply 105 mm thick CLT panels were procured from Structurlam (Penticton, BC). Half of these were V2M1.1 visually graded panels (herein referred to as V grade), consisting of three layers of 35 mm thick Spruce-Pine-Fir (SPF) #2 boards, or better grades, and half were E1M5 electronically graded panels (herein referred to as E grade), consisting of three layers of 35 mm thick boards, of which the interior minor layer is SPF #2 or better grades, and the two face layers are Machine Stress Rated (MSR) 2100 1.8E SPF. The panels were manufactured to

Table 3.1: Materials used in experimental program.

Item	Manufacturer	Description
CLT	Structurlam	V2M1.1 105 V 3-ply, 105 mm thick E1M5 105 E 3-ply, 105 mm thick
Grout	Hilti	CB-G EG 3-component epoxy grout
Threaded Rods	Rothoblaas	20M / 4.8 strength-class 20M / 8.8 strength-class 24M / 4.8 strength-class 24M / 8.8 strength-class 30M / 4.8 strength-class
Nuts & Washers	Rothoblaas	20M 24M 30M

meet the requirements of the Standard for Performance Rated CLT ANSI/APA PRG 320 (2012), with design properties as per the product report APA PR-L314 (2021).

An average moisture content of 9.2% (COV = 9.2%) was determined based on 156 samples, with measurements taken at two locations on the panel face and one location on the panel edge of the CLT specimen, within the interior layer. Measurements were taken from an electric resistance meter with pins embedded at 1-1/8” depth. This is less than the manufacturer-specified moisture content at the time of production of 12% ($\pm$3%) (Structurlam, 2016) and well below 19%, the threshold below which wood is generally considered dry.

The density was estimated from 34 samples of CLT. An average density of 441 kg/m^3 (COV = 6.8%) was determined for the V grade CLT and an average density of 482 kg/m^3 (COV = 5.0%) was determined for the E grade CLT. The manufacturer-specified density for a single piece of SPF lumber is given as $\pm$485 kg/m^3 (Structurlam, 2016). As expected, the density of the CLT itself is less than this, more so for V grade than E grade, accounting for gaps in the finished product.

3.1.2 Steel Rods

Zinc-coated full-thread steel rods measuring 1 m in length were acquired from Rothoblaas Canada (Delta, BC). These included both 4.8 strength-class rods and 8.8 strength-class rods. The strength-class 4.8 rods consisted of rods with a 20M, 24M, and 30M metric thread, while the strength-class 8.8 rods consisted only of rods with a 20M and 24M metric thread. Strength-class 8.8 rods with a 30M metric thread were not readily available from the manufacturer and were therefore not included in the testing program. The rod threads are in accordance with DIN 975 (see Appendix E).

3.1.3 Epoxy-Based Grout

The grout mixture used to bond the rods to the CLT specimens was CB-G EG by Hilti (see Appendix E for the material data sheet). This three-component epoxy grout has a manufacturer-specified 7-day compressive strength of 103 MPa, at an ambient temperature of 23°C, in accordance with testing standard ASTM C579 B. The adhesive formula was initially selected for its availability, high compressive strength, gap-filling properties, and low shrinkage. In addition, the high viscosity of the grout made it perfectly suited to its use in fabricating this type of connector. Davis and Claisse (2001) observed that fabricating glued-in-rod connections in parallel strand lumber with a low-viscosity epoxy resin was inappropriate as the resin tended to flow into the element's internal voids, resulting in leakage and an incomplete encasement of the rod. The epoxy-based grout used here was fluid enough to work into the gap between the rod and the CLT but viscous enough that it did not tend to leak into the small internal voids of the CLT.

3.1.4 Other Material

Wooden rings for sealing the grout were laser-cut from scrap plywood approximately 9 mm in thickness.

Other materials used in the testing program included 20M, 24M, and 30M washers (S235 grade steel, zinc-plated, conforming to DIN 125 A) and nuts (class 8 steel, zinc-plated, conforming to DIN 934) provided by both Rothoblaas Canada (Delta, BC) and Select Steel (Delta, BC). The material data sheets for the nuts and washers are given in Appendix E.

3.2 Material Tests

Three samples of 20M strength-class 4.8 rods and three samples of 20M strength-class 8.8 rods were tested for their tensile strength according to ASTM E8/E8M (2021). The samples were machined to a standard test size with a reduced diameter of 12.5 ± 0.2 mm over a gauge length of 62.5 ± 0.1 mm. Machining of the samples was completed by the Mechanical Engineering Machine Shop at the University of British Columbia and testing was conducted by Qualitest (Surrey, BC). The results of these tests are given in Table 3.2 and the full reports are available in Appendix D.

No material testing was done for the CLT and the epoxy-based grout, relying on the manufacturer-specified mechanical properties.

Table 3.2: Average strength properties of steel rods from tensile testing.

Strength-Class	Av. Yield Strength (MPa)	Av. Ultimate Strength (MPa)
4.8	528.6	562.4
8.8	733.5	878.3

3.3 Design of the Experimental Program

3.3.1 Design of Test Specimens

The proposed shear connector is conceived to give designers multiple design parameters to work with in order to achieve required capacity. Unlike typical dowel-type connectors, whose performance relies primarily on the fastener diameter, the behaviour of the proposed connector depends on the fastener diameter as well as the grout diameter and potentially other properties of the connector. In order to develop a rigorous understanding of the grout-reinforced connector, as many design parameters as reasonably possible were varied and combined in all their permutations. This not only allowed for the development of a robust data set, but also served as a means of studying the feasibility and constructability of such a connector. Additionally, specimens without grout (i.e., typical dowel-type fasteners) were fabricated to serve as a baseline for comparison. In accordance with current construction practices, all elements of the connector were chosen for their availability and ease of procurement from local manufacturers, allowing for the potential of large-scale use without exhausting supplies.

The rod diameter was varied between 20 mm, 24 mm, and 30 mm, all of which are commonly produced and used in construction. Of the 20 mm and 24 mm rods, both strength-class 4.8 and 8.8 steel were used. For the 30 mm rods, only strength-class 4.8 rods were used as strength-class 8.8 rods in this diameter are not commonly used and require placing a special order. The two strength-classes were used in order to assess how the rod strength would impact the capacity and ductility of the connector.

The grout diameter was taken as a multiple of the rod diameter, either twice (2x), three times (3x), or four times (4x). The smallest grout diameter was established in accordance with the minimum gap required to achieve proper filling according to the grout manufacturer. The largest grout diameter was selected in order to have a large, but not excessive, amount of grout. The intermediate grout diameter was selected to assess an intermediate solution between minimum grout and a potentially prohibitively large amount of grout.

The last parameter of interest was the CLT grade, which was varied between visually graded, V, and electronically graded, E. It was desired to assess whether the grade of CLT would influence the behaviour and capacity of the connector and if the inclusion of the grout layer would nullify this impact.

Three replicates of specimens without grout were fabricated for each combination of design parameters, while seven replicates were fabricated for the specimens with grout. In total, 240 specimens were fabricated. Arrangements of specimens based on the varied design parameters, including number of specimens fabricated are given in Table 3.3.

Table 3.3: Specimens fabricated for testing.

ID	Rod Dia.	Rod Strength-Class	CLT Grade	Grout Dia.†	Rep.
20M-4E	20 mm	4.8	E	N/A	3
20M-4E-2x	20 mm	4.8	E	2x	7

Table 3.3 continued from previous page

ID	Rod Dia.	Rod Strength-Class	CLT Grade	Grout Dia.†	Rep.
20M-4E-3x	20 mm	4.8	E	3x	7
20M-4E-4x	20 mm	4.8	E	4x	7
20M-4V	20 mm	4.8	V	N/A	3
20M-4V-2x	20 mm	4.8	V	2x	7
20M-4V-3x	20 mm	4.8	V	3x	7
20M-4V-4x	20 mm	4.8	V	4x	7
20M-8E	20 mm	8.8	E	N/A	3
20M-8E-2x	20 mm	8.8	E	2x	7
20M-8E-3x	20 mm	8.8	E	3x	7
20M-8E-4x	20 mm	8.8	E	4x	7
20M-8V	20 mm	8.8	V	N/A	3
20M-8V-2x	20 mm	8.8	V	2x	7
20M-8V-3x	20 mm	8.8	V	3x	7
20M-8V-4x	20 mm	8.8	V	4x	7
24M-4E	24 mm	4.8	E	N/A	3
24M-4E-2x	24 mm	4.8	E	2x	7
24M-4E-3x	24 mm	4.8	E	3x	7
24M-4E-4x	24 mm	4.8	E	4x	7
24M-4V	24 mm	4.8	V	N/A	3
24M-4V-2x	24 mm	4.8	V	2x	7
24M-4V-3x	24 mm	4.8	V	3x	7
24M-4V-4x	24 mm	4.8	V	4x	7

Table 3.3 continued from previous page

ID	Rod Dia.	Rod Strength-Class	CLT Grade	Grout Dia.†	Rep.
24M-8E	24 mm	8.8	E	N/A	3
24M-8E-2x	24 mm	8.8	E	2x	7*
24M-8E-3x	24 mm	8.8	E	3x	7
24M-8E-4x	24 mm	8.8	E	4x	7
24M-8V	24 mm	8.8	V	N/A	3
24M-8V-2x	24 mm	8.8	V	2x	7
24M-8V-3x	24 mm	8.8	V	3x	7
24M-8V-4x	24 mm	8.8	V	4x	7
30M-4E	30 mm	4.8	E	N/A	3
30M-4E-2x	30 mm	4.8	E	2x	7
30M-4E-3x	30 mm	4.8	E	3x	7
30M-4E-4x	30 mm	4.8	E	4x	7*
30M-4V	30 mm	4.8	V	N/A	3
30M-4V-2x	30 mm	4.8	V	2x	7
30M-4V-3x	30 mm	4.8	V	3x	7
30M-4V-4x	30 mm	4.8	V	4x	7*

† Grout diameter is a multiple of rod diameter.

* Though 7 replicates were fabricated, only 6 were tested.

3.3.2 Fabrication of Test Specimens

Fabrication of the specimens required cutting and drilling the CLT panels in a Hundegger CNC machine. Panels were processed according to the details given in drawing no. 3 given in Appendix A. The 105 mm thick panels were cut into squared specimens with equal width b and height h measuring 280 mm, 340 mm, or 420 mm. Dimensions were dictated by the minimum edge and end distances of fasteners recommended in EN 383 (2007) for dowel-type timber connectors, based on 20 mm, 24 mm, and 30 mm rod diameters, respectively. In each specimen, a hole was drilled through its centre of which 95 mm of the depth had a diameter of D and the remaining 10 mm of depth had a diameter of d, as shown in Figure 3.1. The diameter d is the associated rod diameter, while the diameter D corresponded to either twice, three times, or four times the associated rod diameter. The specimens were then labeled and any debris from the drilling process removed by means of compressed air.

In addition to preparing the CLT for fabrication, the 1 m length steel rods were cut into four sections of approximately 250 mm lengths. This was done using a metal bandsaw. Lastly, wooden rings for centering the rod and enclosing the grout were laser-cut from a sheet of plywood. Laser-cutting ensures a perfectly circular shape and therefore there is no gap between the CLT and ring and the rod is perfectly centred in the hole. These rings had various combinations of inner and outer diameters, d and D, respectively, in accordance with the corresponding specimens.

To control the fabrication process of the specimens, including the alignment of rods, specimens were laid down on wooden rails measuring 72.5 mm thick with the smaller diameter hole facing down. Rods were placed through the holes such that the bottom end made contact with the ground, ensuring that they protruded 72.5 mm from each side of the specimens. The epoxy grout was mixed according to the manufacturer's instructions and then poured into the gap between the rod and the CLT, until it was approximately half full. The grout was tamped down and then the hole was filled and the grout tamped again. The wooden rings were then placed in the hole and set flush to the CLT surface using a rubber mallet. This served to centre the rod and further compact the grout such that it filled any small voids. The specimens were left to cure for at least two hours, according to manufacturer recommendations, before being moved to long-term storage, where they were left to continue curing for at least seven days before testing.

The specimen fabrication instructional drawing is given in Appendix A (drawing no. 2) and pictures of the fabrication procedure are given in Appendix B.

3.3.3 Design of Test Apparatus

A steel test apparatus was custom-designed for testing the specimens and fabricated by Select Steel (Delta, BC). It was designed in accordance with the Canadian steel design standard CSA-S16 (CSA Group, 2014*b*) in order to resist a maximum load of 300 kN. It consists of a 105mm x 105mm x 105 mm welded steel box, two loading arms, and a platform with welded angle sections to hold the specimen in place. The steel box consists of a top plate and a base plate connected together by two side plates having four bolt holes, arranged two by two, as well as a stiffener plate that connects the two side plates in the centre. At their top end, the loading arms have four bolts holes, by which they are connected to the side plates of the box with high-strength bolts and nuts. At their bottom end, they have three bolt holes aligned

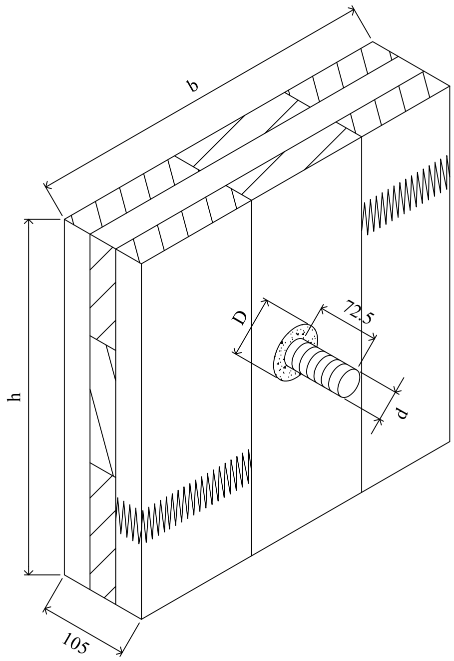

(a) Isometric view.

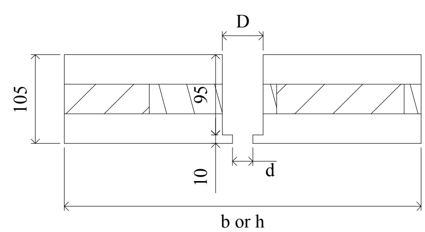

(b) Cross-section.

Figure 3.1: A typical specimen (units in mm).

vertically, corresponding to the three rod diameters of 20 mm, 24 mm, and 30 mm. It is through these holes that the steel rod protruding from the specimen is placed and fastened by means of nuts and washers without preloading. The shop drawing of the test apparatus is given in Appendix A (drawing no. 1).

3.3.4 Testing Procedure

Specimens were tested monotonically in displacement-controlled loading in a double-shear push-out configuration, in accordance with ASTM D5764 (2018). The test apparatus was setup within a model 318.25 MTS 810 Universal Testing Machine (UTM), which is capable of applying a maximum load of 250 kN. The custom steel platform, complete with welded-on angles to stabilize the specimen, was placed on the machine platform. A specimen was centred on the plate and then the loading arms fixed to the steel rod with washers and nuts. The loading arms were then affixed, at their top ends, to the box by means of eight high-strength bolts, nuts, and washers. The hydraulic actuator was then engaged in order to achieve contact between the load cell of the UTM and the top plate of the test apparatus. Two Linear Voltage Displacement Transducer (LVDT)s were then attached to each side of the specimen by means of a clamp drilled into the CLT. The plunger of the LVDT rests on a magnetic bracket attached to the loading arm. As the specimen is displaced upward by the hydraulic actuator, the LVDTs measure the relative displacement of the CLT and the rod, which is fixed to the loading arms. The load was measured by the load cell built into the UTM with a 6kHz sampling rate.

Within this experimental campaign, specimens were tested at a 0° load-to-grain angle with respect to the external layers, assuming this as the strong direction for the shear connector capacity. Displacement-controlled loading was applied monotonically at a rate of 1.2 mm/min or 1.8 mm/min in order to reach maximum load within 10 minutes, as stipulated by ASTM D5764 (2018). Testing was conducted until failure or a relative displacement of 15 mm was reached, whichever occurred first. The testing setup is shown in Figure 3.2 and Figure 3.3.

3.4 Calculation of Structural Performance Parameters

Structural performance parameters extracted from the test data were the maximum and ultimate load-carrying capacity, yield load, elastic limit, elastic stiffness, and ductility.

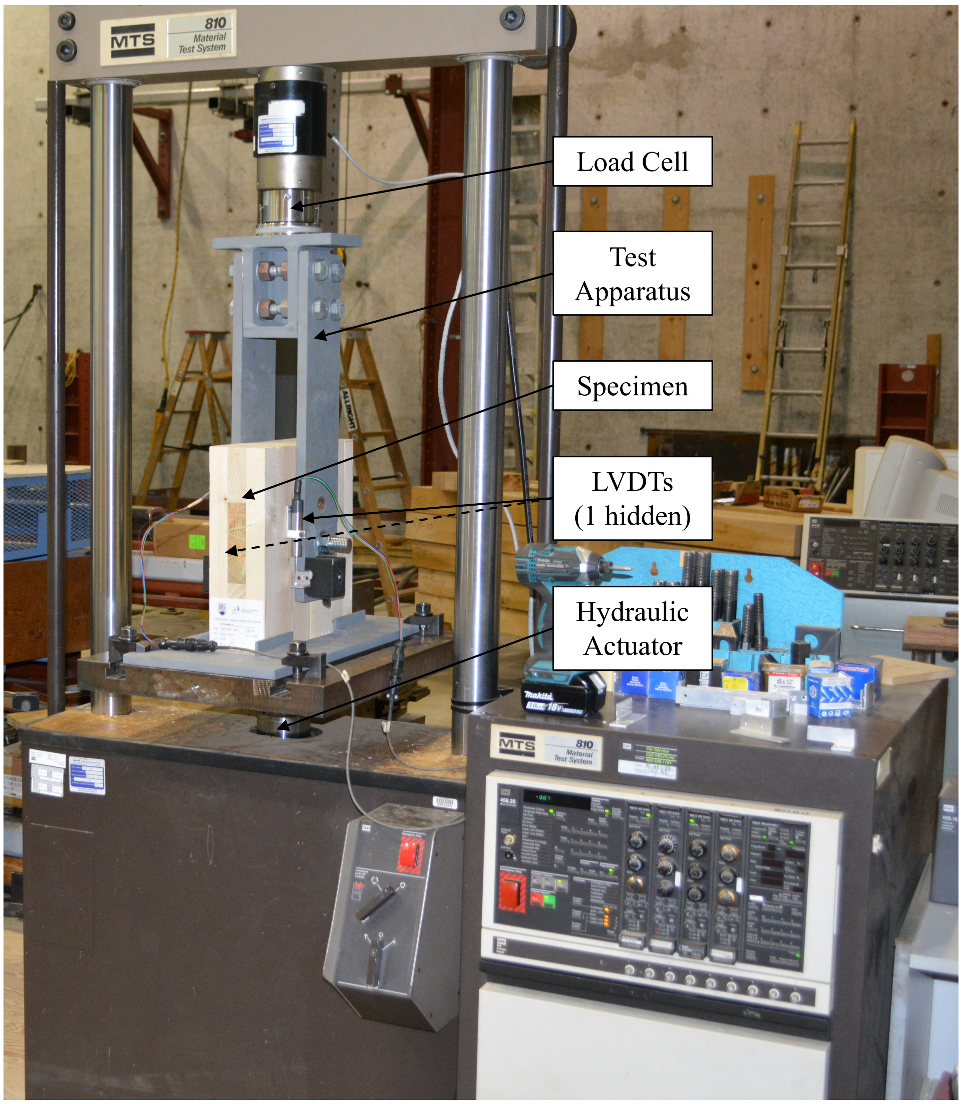

Figure 3.2: Specimen loaded into test apparatus and ready for testing.

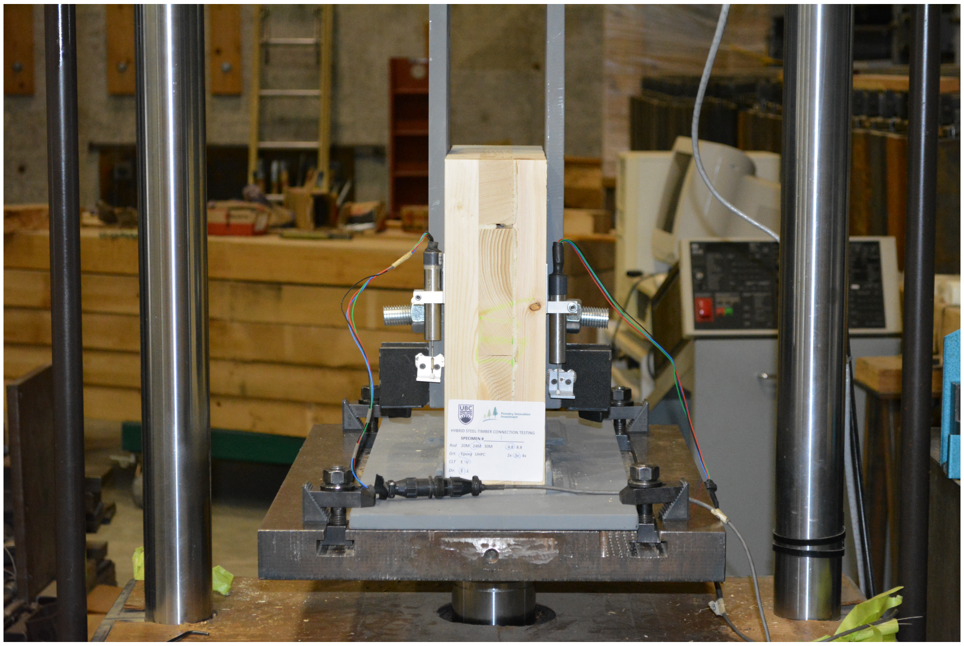

Figure 3.3: Close-up of specimen in test apparatus.

3.4.1 Load-Carrying Capacity

The load-carrying capacity of the connector was taken as the maximum recorded force during testing, F_{max}. The corresponding deformation was also extracted.

Additionally, the ultimate force F_{ult} was taken to be the final recorded force, whether it be at failure or at 15 mm, or 80% of the maximum recorded force, whichever was greater. The corresponding deformation was also extracted.

Finally, the loss of strength (LoS) from maximum to ultimate load was calculated as follows:

$$LoS = \frac{|F_{ult} - F_{max}|}{F_{max}} \tag{3.1}$$

3.4.2 Yield Point and Elastic Limit

The yield capacity F_y was calculated according to the 5% fastener diameter offset method, as specified by ASTM D5764 (2018). A line was fit to the initial linear portion of the load-deformation curve (see Section 3.4.3) and then displaced positively along the x-axis by a value of 5% of the rod diameter. Where this line intersects the load-deformation curve is taken to be the yield point and the corresponding deformation the yield deformation.

The elastic limit is the point at which the load-deformation curve becomes nonlinear, though there is no standard procedure for determining this point. Herein, the elastic limit was determined by first calculating the elastic stiffness, as defined below. Next, the slope of a line with the same starting point as the stiffness line but ending at the next recorded data point is calculated. This is repeated for each consecutive data point until the slope of this new line deviates from the stiffness by more than 5%.

3.4.3 Elastic Stiffness

The elastic stiffness was determined according to Equation 3.2 given in EN 26891 (1991), since ASTM D5764 (2018) does not specify a method for determining stiffness. The elastic stiffness is taken as:

$$k = \frac{0.4F_{max} - 0.1F_{max}}{\delta_{04} - \delta_{01}} \tag{3.2}$$

where: δ_{04} and δ_{01} are the slips measured at 40% and 10% of the maximum load, respectively. F_{max} has been previously defined.

3.4.4 Ductility

Ductility is defined as a material or assembly's capacity to undergo plastic deformation before reaching failure. The two most accepted definitions, and those specified in the testing standard for the cyclic testing of mechanical joints in timber EN 12512 (2001), are as follows:

$$\mu_m = \frac{\delta_m}{\delta_y} \tag{3.3}$$

$$\mu_u = \frac{\delta_u}{\delta_y} \tag{3.4}$$

where: μ_m is the ductility ratio of the maximum deformation δ_m with respect to the yield deformation δ_y and μ_u is the ductility ratio of the ultimate deformation δ_u with respect to the yield deformation δ_y.

The choice of which ductility model to use depends on the shape of the load-deformation curve. In general, Equation 3.4 provides the most realistic assessment of ductility, encapsulating the entire plastic range from yielding to failure. However, as Smith et al. (2006) points out, it may not always be possible to define a consistent ultimate deformation. For highly ductile connections that exhibit post-yield hardening, the testing machine may not have sufficient capacity or range to reach failure. They therefore suggest calculating ductility from the maximum deformation. This has the advantage of allowing for comparison between different types of connection as there is no ambiguity regarding maximum load and deformation.

However, for connections that reach a maximum load very soon after yielding and then exhibit a plateau or slight decrease in load with respect to deformation, the first measure will be much smaller than the second. In such cases, the second definition of ductility is more appropriate, despite the ambiguity in defining the ultimate deformation. Accordingly, this is the method used in this thesis. The consistent definition of ultimate load and deformation, as defined in Section 3.4.1, allow for comparisons between specimen types.

3.5 Matlab Code

The previously discussed structural performance parameters were all calculated in a Matlab script written by the author, portions of which are given in Appendix F. The raw data recorded from the tests consisted of the load readings from the load cell and the two deformation recordings from the LVDTs. The dataset was first screened for any instrument errors before being imported into Matlab. An average deformation was calculated from the readings of the two LVDTs and they were converted from inches to millimeters. The data was then truncated in two ways. For specimens that achieved the target displacement of 15 mm, any data recorded after this point was discarded. For specimens where failure occurred before 15 mm, all post-failure data was discarded.

For each individual test, the aforementioned structural parameters were calculated. An average of the structural parameters was then calculated for each set of replicates, as well as the coefficient of variation. For the capacity parameters, the characteristic value was also calculated as the 5^{th}-percentile value, determined at a confidence level of 75%. This is done by fitting a lognormal distribution to the extracted capacity data, confirming the fit with a Kolmogrov-Smirnov test, and then calculating the 5^{th}-percentile of the distribution.

The following portion of the code plotted the average and envelope load-deformation curves for each shear connector arrangement. Due to the nature of the LVDT recordings, no two sets of data had the same deformation readings. Therefore, deformation intervals of 0.1 mm were defined in which all deformation readings for a given specimen within a range of ± 0.05 mm were averaged. The average load-deformation curve was built by plotting these deformation intervals against the average corresponding load calculated from the replicates. The envelope curves were similarly plotted using these deformation intervals, except that the maximum values were used for the maximum envelope and the minimum values were used for the minimum envelope.

3.6 Statistical Analyses

3.6.1 Linear Regression Analysis

In order to quantify the observations made from the test results and load-deformation curves, a regression analysis was conducted. In particular, a linear regression analysis, in which the design variables (rod diameter, grout diameter, steel strength-class, and CLT grade) were taken as the independent variables and the yield resistance, maximum shear resistance, and stiffness were taken as the dependent variable. The purpose of the regression analysis was to determine which design variables significantly impact the resistance and stiffness. Since this is a novel shear connector and a mechanics-based model has yet to be developed, no assumptions could be made about the relationship between any of the design parameters and the resistance or stiffness. Therefore, it was chosen to conduct a linear regression analysis, which makes the most simple assumption of a linear relationship between the independent variables and the dependent variable. Though the purpose of this analysis was to assess the impact of the independent variables, and not to develop a model or equation, it is still useful to display the linear regression model as follows:

$$R = C_0 + C_1 d_{rod} + C_2 d_{grout} + C_3 f_{y/u,s} + C_4 g + \varepsilon \tag{3.5}$$

where: R is the resistance (yield F_y or maximum F_{max}), d_{rod}[1] is the rod diameter in mm, d_{grout}[1] is the grout diameter in mm, $f_{y/u,s}$ is the rod yield strength or ultimate strength in MPa (representing steel strength-class), and g is a categorical variable where 1 represents V grade CLT and 0 represents E grade CLT. C_0, C_1, C_2, C_3, and C_4 are the regression coefficients and ε is the model error.

The specific method used, implemented in Matlab, was a stepwise multi-variable linear regression. As in any regression analysis, the inclusion of an independent variable in the final model depends on its significance, measured by its p-value. If an independent variable's p-value is less than 0.05, it is considered insignificant and discarded. If its p-value is greater than 0.05, it is considered significant and is included in the model. Stepwise multi-variable linear regression is an iterative process by which one independent variable is added at a time and its significance is assessed. If upon the addition of a new independent variable a previously significant variable is found to have become insignificant, it is removed from the model. Removed variable are reintroduced again and their significance assessed in the event that the inclusion of another variable has impacted their significance. Once all combinations of variables have been assessed, the strongest model is produced. The strength of the model is determined by its coefficient of determination, also known as its R-squared value. This value quantifies how much of the variance in

[1] The symbols for rod and grout diameter have been changed to avoid confusion with the symbol for dead load d in the reliability analysis.

the dependent variable is explained by the independent variables. An R-squared value of 1 indicates that the variance in the dependent variable is explained entirely by the independent variables.

Though the R-squared value provides a measure of the model's ability to explain the variance in the dependent variable, it does not provide insight into each independent variable's contribution. To quantify this, the semi-partial correlation coefficient for each independent variable is calculated as follows:

$$sr_i^2 = \frac{F_i}{df_{res}}(1 - r^2) \tag{3.6}$$

where: sr^2 is the semi-partial correlation coefficient for variable i, F_i is the F-ratio of variable i, df_{res} is the degrees of freedom of the residuals, and r^2 is the coefficient of determination of the model.

The magnitude of sr^2 (between 0 and 1) serves as a quantifiable measure of an independent variable's ability to explain variance in the dependent variable.

It was chosen to focus the analyses on yield resistance, maximum shear resistance, and stiffness. The yield resistance would be the primary value used for design in capacity-based design, whereas maximum shear resistance would be the primary value used in traditional plastic connector design. The maximum resistance was chosen over the ultimate since in many cases the ultimate load is similar or less than the yield load, due to the nature of the wood-crushing behaviour. As such, designing for the ultimate load may not allow the connector to yield, and thus it would never reach a plastic state. Stiffness, being another important property of the connector in both design philosophies, was also investigated.

3.6.2 Bayesian Linear Regression Analysis

A Bayesian linear regression was conducted in order to develop a design model for the connector's yield and maximum shear resistance. Unlike in classical linear regression, Bayesian regression accounts for the uncertainty in the collected data by formulating the model based on probability distributions rather than point estimates. Thus, the resulting resistance is also given as a probability distribution, allowing for the evaluation of its Cumulative Distribution Function (CDF) in order to determine a 5^{th}-percentile design value. The model may also be implemented in a reliability analysis. The Bayesian linear regression model is given as:

$$R = \theta_1 + \theta_2 d_{rod} + \theta_3 d_{grout} + \theta_4 f_{y/u,s} + \varepsilon \tag{3.7}$$

where: R, d_{rod}, d_{grout}, and $f_{y/u,s}$ have been previously defined. θ_1, θ_2, θ_3, and θ_4 are normally distributed random variables known as the regression coefficients, and ε is a normally distributed random variable, with zero mean, representing the model error. The exclusion of a term for CLT grade is explained in Section 4.7.

This expression can also be written in matrix notation, as follows:

$$\boldsymbol{y} = \boldsymbol{X\theta} + \boldsymbol{\varepsilon} \tag{3.8}$$

where: $\boldsymbol{y}$ is a vector of size n containing the recorded yield or maximum load for each test, $\boldsymbol{X}$ is an n-by-k matrix of regressors in which each row corresponds to the design parameter values for a given test in the order $[1, d_{rod}, d_{grout}, f_{y/u,s}]$, $\boldsymbol{\theta}$ is a vector of size k containing the regression coefficients, and $\boldsymbol{\varepsilon}$ is a vector of size n containing the discrepancy between the model prediction and the observation for each test.

As in classical linear regression,the goal of Bayesian linear regression is to find the values of the regression coefficients that minimize the sum of squared errors. This is achieved by rearranging the above equation for $\boldsymbol{\varepsilon}$ and setting the derivative of the square with respect to $\boldsymbol{\theta}$ equal to zero, as follows:

$$\frac{\partial \|\boldsymbol{y} - \boldsymbol{X}\boldsymbol{\theta}\|^2}{\partial \boldsymbol{\theta}} = 0 \tag{3.9}$$

Solving for $\boldsymbol{\theta}$ yields the ordinary least squares estimates for the regression coefficients, as follows:

$$\hat{\boldsymbol{\theta}} = (\boldsymbol{X}^T\boldsymbol{X})^{-1}\boldsymbol{X}^T\boldsymbol{y} \tag{3.10}$$

The standard error of the model (i.e., the variance of $\boldsymbol{\varepsilon}$) is calculated by:

$$s^2 = \frac{1}{n-k}(\boldsymbol{y} - \boldsymbol{X}\hat{\boldsymbol{\theta}})^T(\boldsymbol{y} - \boldsymbol{X}\hat{\boldsymbol{\theta}}) \tag{3.11}$$

Assuming non-informative locally uniform priors, the posterior distribution for $\boldsymbol{\theta}$ is the multivariate t-distribution, from which the mean $\mu_{\boldsymbol{\theta}}$ and covariance matrix $\boldsymbol{\Sigma}_{\boldsymbol{\theta}\boldsymbol{\theta}}$ are given as follows:

$$\mu_{\boldsymbol{\theta}} = \hat{\boldsymbol{\theta}} \tag{3.12}$$

$$\boldsymbol{\Sigma}_{\boldsymbol{\theta}\boldsymbol{\theta}} = s^2(\boldsymbol{X}^T\boldsymbol{X})^{-1} \tag{3.13}$$

The standard deviations of the regression coefficients are simply the square-root of the values in the diagonal of the covariance matrix.

The coefficients of variation are calculated as usual:

$$COV = \frac{\sigma_{\boldsymbol{\theta}}}{\mu_{\boldsymbol{\theta}}} \tag{3.14}$$

All of the aforementioned calculations were conducted using the "Model Inference" python script prepared by Dr. Terje Haukaas.

With the statistical parameters of the models fully defined, it is possible to determine statistical properties for the resistance itself based on the rules governing the analysis of functions of random variables. Specifically, the mean and standard deviation of the resistance for each combination of design parameters may be determined. From this, the corresponding 5$^{\text{th}}$-percetile value of resistance is determined by evaluating the inverse CDF.

The model for resistance is rewritten as a linear function of random variables:

$$R = \boldsymbol{b}^T \boldsymbol{\theta'} \tag{3.15}$$

where: $\boldsymbol{b} = [1, d_{rod}, d_{grout}, f_{y/u,s}, 1]$ and $\boldsymbol{\theta'} = [\theta_1, \theta_2, \theta_3, \theta_4, \varepsilon]$.

It can be shown that for such a linear function of random variables, the mean and variance of resistance are as follows:

$$\mu_R = \boldsymbol{b}^T \boldsymbol{M}_{\boldsymbol{\theta'}} \tag{3.16}$$

$$\sigma_R^2 = \boldsymbol{b}^T \boldsymbol{\Sigma}_{\boldsymbol{\theta'}\boldsymbol{\theta'}} \boldsymbol{b} \tag{3.17}$$

where: $\boldsymbol{M}_{\boldsymbol{\theta'}}$ is a vector of the mean values of $\boldsymbol{\theta'}$ and $\boldsymbol{\Sigma}_{\boldsymbol{\theta'}\boldsymbol{\theta'}}$ is the covariance matrix, which is simply $\boldsymbol{\Sigma}_{\boldsymbol{\theta\theta}}$ with an extra row and column added containing zeros except for the diagonal, which has a value of s^2.

Therefore, $R \sim N(\mu_R, \sigma_R)$. For each combination of design variables, the inverse CDF of R can be evaluated at 0.05 in order to determine the 5$^{\text{th}}$-percentile resistance. In other words, the 5$^{\text{th}}$-percentile resistance is that load for which there is at most a 5% chance of not being exceeded. The 5$^{\text{th}}$-percentile values determined from this method were compared with those calculated using the typical method of assuming a lognormal distribution.

3.6.3 Reliability Analysis

With the Bayesian linear regression model, a reliability analysis was performed in order to determine an appropriate resistance factor that produces a consistent and reasonable level of safety.

From Section 2.3, the final performance function was defined as:

$$G = R - \phi \frac{R_o}{1.25\gamma + 1.50}(d\gamma + q) \tag{3.18}$$

where: γ is taken to be equal to 0.25 and the statistical information for the demand random variables d and q, derived by Foschi et al. (1989), were previously given in Table 2.1.

For yield resistance F_y and maximum shear resistance F_{max}, Equation 3.18 becomes:

$$G_y = F_y - \phi \frac{F_{y,0.05}}{1.25\gamma + 1.50}(d\gamma + q) \tag{3.19}$$

and

$$G_m = F_{max} - \phi \frac{F_{max,0.05}}{1.25\gamma + 1.50}(d\gamma + q) \tag{3.20}$$

Where: $F_{y,0.05}$ and $F_{max,0.05}$ are the 5$^{\text{th}}$-percentile values of yield and maximum capacity, respectively. All other variables have been previously defined.

The reliability method used for the analysis was FORM and it was run using the Rt software developed by Mahsuli and Haukaas (2013). The analysis was carried out for every combination of design variables, varying the value of phi from 0.5 to 1.0 in increments of 0.1, resulting in a plot of the reliability index β against the resistance factor ϕ.

The flow of data from acquisition to the various software packages used is given in Figure 3.4.

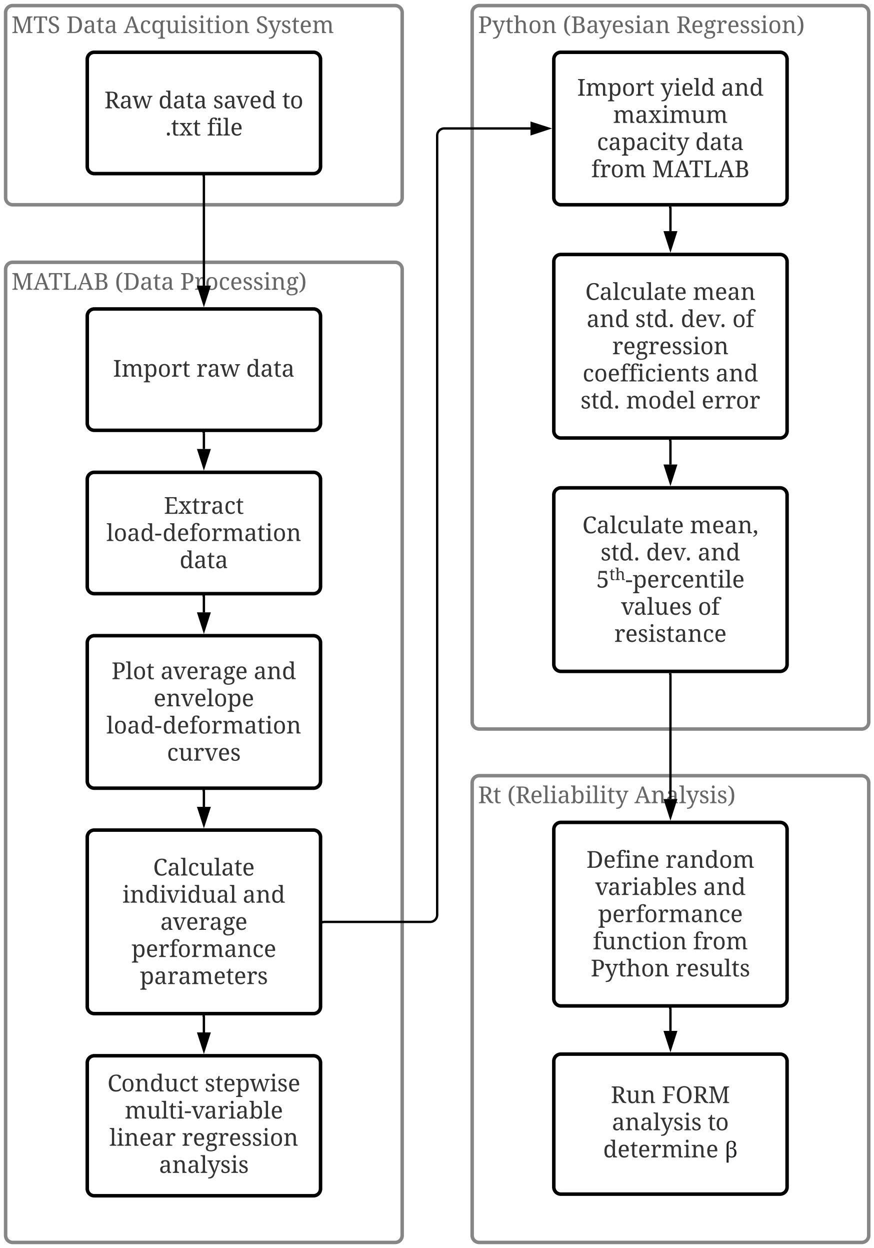

Figure 3.4: Data flow.

Chapter 4

Results and Discussion

This chapter provides a comprehensive review of the behaviour and performance of the proposed shear connector, with in-depth discussion of the experimental results, statistical analysis, and reliability analysis. It begins with a discussion of the failure modes observed as well as the variability in the load-deformation curves for a given specimen. This is followed with a discussion on the load-deformation behaviour and a qualitative assessment of the impact of each design parameter on the performance of the connector. Next, the relevant structural performance parameters are presented and the impact of the design parameters are discussed quantitatively by means of a linear regression analysis. Models for yield and maximum shear resistance are developed using Bayesian linear regression in order to calculate characteristic values. These values are subsequently used to perform a reliability analysis, establishing an appropriate level of safety for the connector.

4.1 Failure Modes

Three distinct failure modes were observed in the tested specimens, governed by wood crushing (mode i), steel hinging (mode ii), and a combination of both (mode iii), as illustrated in Figure 4.1. Table 4.1 gives the failure mode of each specimen type, showing that the majority exhibited mode i failure, while only two exhibited mode ii failure, and seven exhibited mode iii failure.

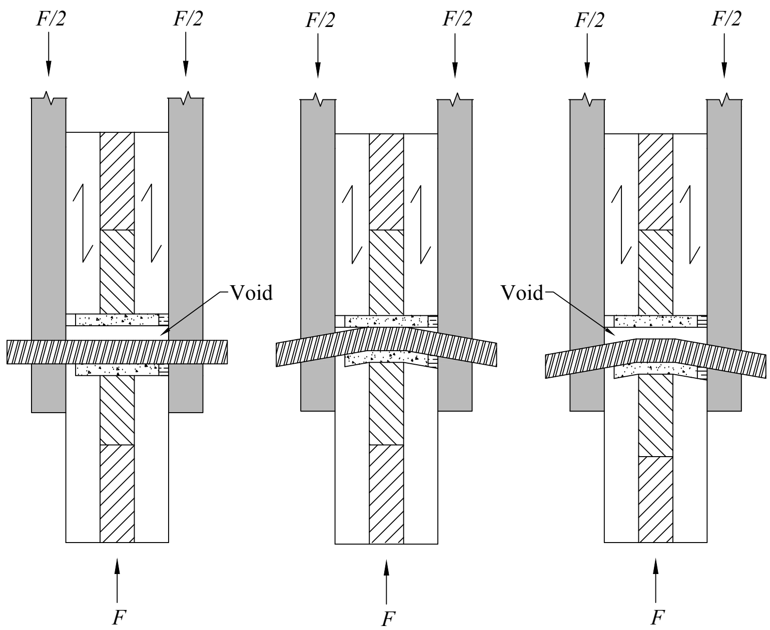

(a) Failure mode i (b) Failure mode ii (c) Failure mode iii

Figure 4.1: Observed failure modes.

Table 4.1: Failure mode of each specimen type.

ID	Rod Dia.	Rod Str.-Class	CLT Grade	Grout Dia.	Fail. Mode
20M-4E-2x	20 mm	4.8	E	2x	iii
20M-4E-3x	20 mm	4.8	E	3x	iii
20M-4E-4x	20 mm	4.8	E	4x	iii
20M-4V-2x	20 mm	4.8	V	2x	iii
20M-4V-3x	20 mm	4.8	V	3x	iii
20M-4V-4x	20 mm	4.8	V	4x	iii
20M-8E-2x	20 mm	8.8	E	2x	i
20M-8E-3x	20 mm	8.8	E	3x	i
20M-8E-4x	20 mm	8.8	E	4x	i
20M-8V-2x	20 mm	8.8	V	2x	i
20M-8V-3x	20 mm	8.8	V	3x	i
20M-8V-4x	20 mm	8.8	V	4x	i
24M-4E-2x	24 mm	4.8	E	2x	i
24M-4E-3x	24 mm	4.8	E	3x	iii
24M-4E-4x	24 mm	4.8	E	4x	ii
24M-4V-2x	24 mm	4.8	V	2x	i
24M-4V-3x	24 mm	4.8	V	3x	i
24M-4V-4x	24 mm	4.8	V	4x	ii
24M-8E-2x	24 mm	8.8	E	2x	i
24M-8E-3x	24 mm	8.8	E	3x	i
24M-8E-4x	24 mm	8.8	E	4x	i

Table 4.1 continued from previous page

ID	Rod Dia.	Rod Str.-Class	CLT Grade	Grout Dia.	Fail. Mode
24M-8V-2x	24 mm	8.8	V	2x	i
24M-8V-3x	24 mm	8.8	V	3x	i
24M-8V-4x	24 mm	8.8	V	4x	i
30M-4E-2x	30 mm	4.8	E	2x	i
30M-4E-3x	30 mm	4.8	E	3x	i
30M-4E-4x	30 mm	4.8	E	4x	i
30M-4V-2x	30 mm	4.8	V	2x	i
30M-4V-3x	30 mm	4.8	V	3x	i
30M-4V-4x	30 mm	4.8	V	4x	i

The corresponding load-deformation behaviour of the three failure modes are characterized by either a decrease in load after the yield point (mode i), an increase in load after the yield point (mode ii), or a plateau after the yield point (mode iii). Figures 4.2, 4.3 and 4.4 show the average and envelope load-deformation curves for each of the tested arrangements, grouped by rod diameter. The area in grey represents the range of recorded load-deformation values bounded by the envelope curves, that is the minimum and maximum curves, serving as a qualitative measure of the variability in the recorded data.

After testing, one sample of each of the arrangements with E grade CLT was selected to be cross-sectioned in order to visually analyze the behaviour of the rod. These cross-sections are also given in the following figures and correspond to one of the three failure modes shown schematically in Figure 4.1.

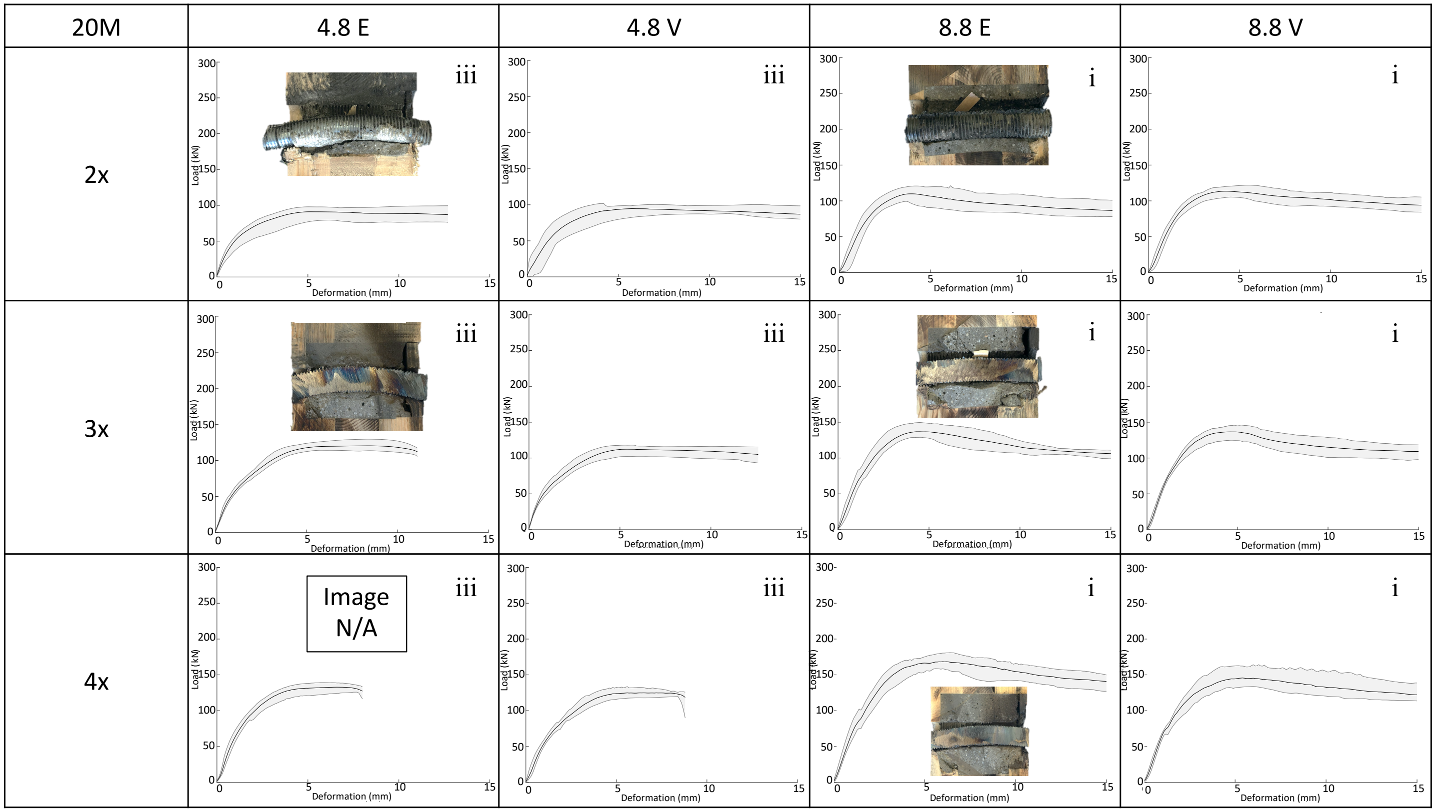

Figure 4.2: Failure modes and corresponding load-deformation curves of specimens with 20M rods.

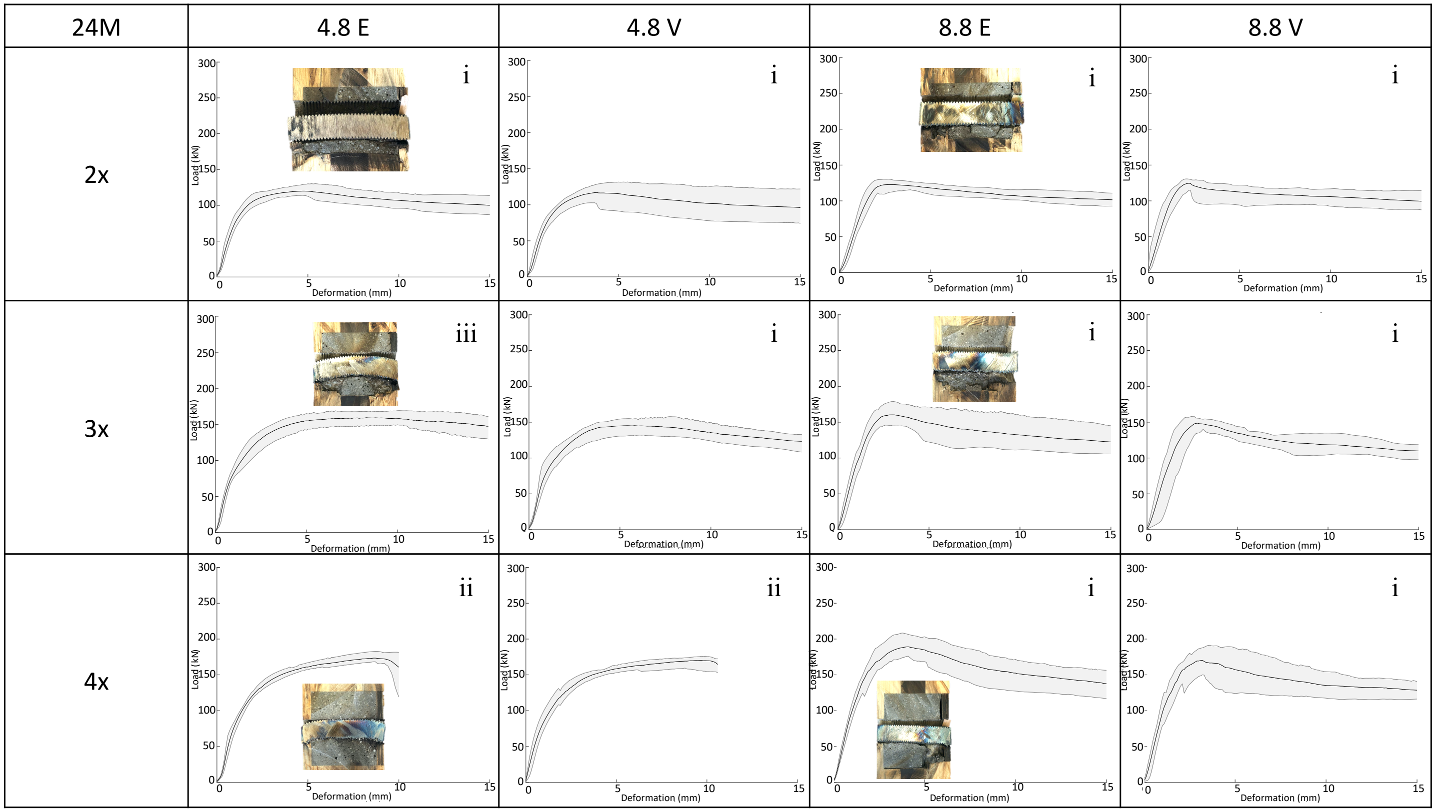

Figure 4.3: Failure modes and corresponding load-deformation curves of specimens with 24M rods.

30M	4.8 E	4.8 V
2x	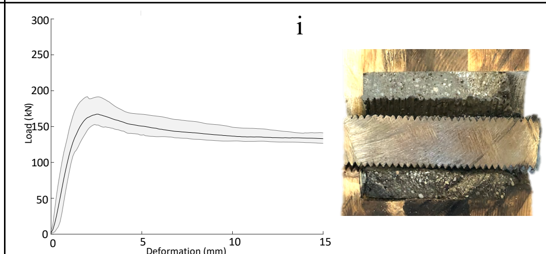	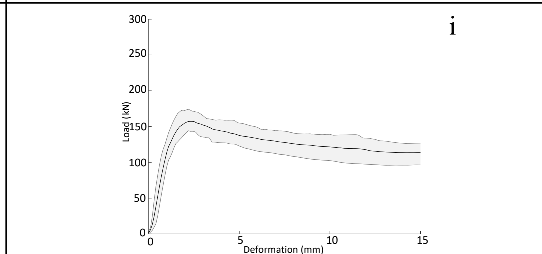
3x	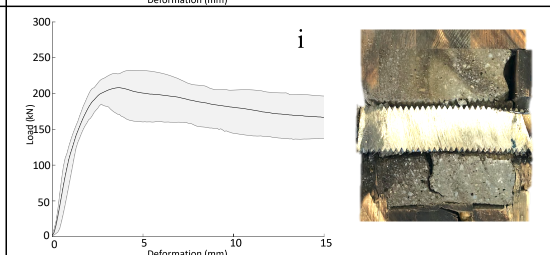	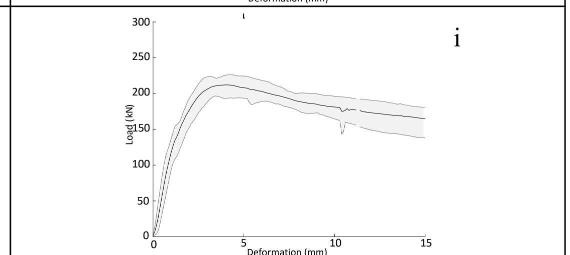
4x	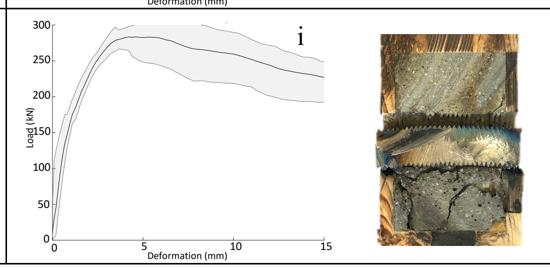	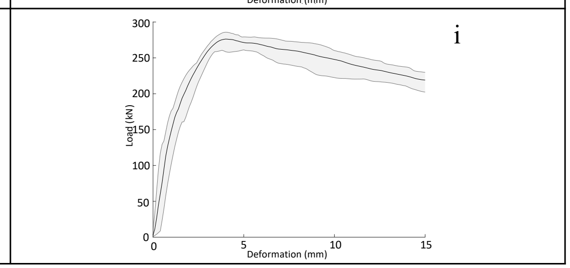

Figure 4.4: Failure modes and corresponding load-deformation curves of specimens with 30M rods.

Referring to the 20M specimens in Figure 4.2, all of those with 4.8 grade steel rods exhibited a plateau after the yield point, indicative of a combination of wood crushing and steel hardening. This behaviour is clearly seen in the cross-sections, which show both bending in the steel rod as well as embedment in the wood. Conversely, specimens with 8.8 grade steel all exhibited a decrease in load after the yield point, indicative of wood crushing solely governing the behaviour. Though some rod bending is visible in the cross-sections, it is much less pronounced than in the specimens with 4.8 grade steel rods, and does not govern the load-deformation behaviour.

For the 24M specimens, given in Figure 4.3, the majority of specimens exhibited a decrease in load after yielding, indicative of pure wood crushing behaviour. The arrangement with 4.8 grade steel, E grade CLT, and a grout diameter three times the rod diameter exhibited a combination behaviour, as can be seen in the cross-section. Both the E grade and V grade CLT specimens with 4.8 grade steel and a grout diameter four times the rod diameter an increase in load after yielding, indicative of strain hardening.

Regardless of CLT grade, all 30M specimens exhibit a decrease in load after yielding, indicative of pure wood crushing, as shown in Figure 4.4. The cross-sections show very little hinging in the rods.

As evidenced by the grey area between the envelope load-deformation curves, the variability appears to increase with increasing rod diameter. Additionally, variability is more pronounced in specimens that exhibited wood crushing over specimens that exhibited combination behaviour and least of all in specimens that exhibited steel hardening. The explanation for this comes down to the variable nature of wood. Unlike steel, whose manufacturing is highly controlled (explaining

Figure 4.5: A specimen with no visible defects.

why the specimens governed by steel hardening show the least variability), wood is a product of nature that often contains any number of defects such as knots, checks, splits, shakes, and even holes. Though these are accounted for in the grading process of the lumber that makes up the CLT panel, the relevance of the grade diminishes as the panel is sectioned off. One specimen may have been cut from a section of panel containing no or few defects (Figure 4.5) while another may have been cut from a section containing multiple defects (Figure 4.6). In fact, this is exactly what was observed during specimen fabrication. Some specimens had defects close to the drill hole, where stress is highest, while others had defects farther away from the hole, where their impact would not be as significant. Additionally, if the specimen was tested with a defect above the hole, it would have no impact as it was not in the load path, whereas a defect below the hole would have an impact. The location

Figure 4.6: A typical defect seen in cut specimens: a hole through the drill hole to the edge of the specimen.

of the drill hole also varied from specimen to specimen, with it sometimes being cleanly in the centre of a board, while at other times it was between two boards or at a finger joint.

The combination of the inherent variability of wood and the random cutting and drilling of the specimens explains why the specimens governed by wood crushing display the most variability and why no noticeable difference is seen between E grade and V grade CLT specimens. That variability increases with increasing rod diameter is explained by the fact that the larger the rod diameter, the more wood is involved in bearing, and there is more likely to be a defect in the load path.

4.2 Qualitative Analysis: Load-Deformation Behaviour

To assess the influence of the geometric design parameters on the behaviour of the shear connector, the average load-deformation curve of each specimen type with one fixed geometric property were plotted on the same chart. First the impact of the grout diameter is assessed by plotting the load-deformation curves for each rod diameter: 20 mm, 24 mm, and 30 mm in Figures 4.7, 4.9 and 4.10, respectively. For the 20M specimens shown in Figure 4.7, the inclusion of a grout layer (broken compared to solid lines) significantly increases the stiffness and maximum load. with particular attention to the CLT grade, only specimens with grout diameters four times the rod diameter display higher capacity for E grade CLT compared to V grade CLT. In general, the grade of the CLT (dark compared to light shade) does not have a great impact on the behaviour. Increasing the grout diameter caused an increase in strength and elastic range. These benefits did not negatively impact the ductility, with the exception of the following three specimens that failed before reaching the target displacement of 15 mm, as indicated by an "x" marker:

- 4.8 steel,grout diameter 4x rod diameter, E grade CLT,
- 4.8 steel,grout diameter 4x rod diameter, V grade CLT,
- 4.8 steel,grout diameter 3x rod diameter, E grade CLT.

None of the specimens with 8.8 grade steel rods failed prematurely, and these were all stronger than their 4.8 grade steel counterparts (orange compared to blue lines). This indicates that the combination of a relatively low-strength and slender rod with a large grout diameter causes local stresses exceeding the rod's shear capacity. An example of this shear failure can be seen in Figure 4.8.

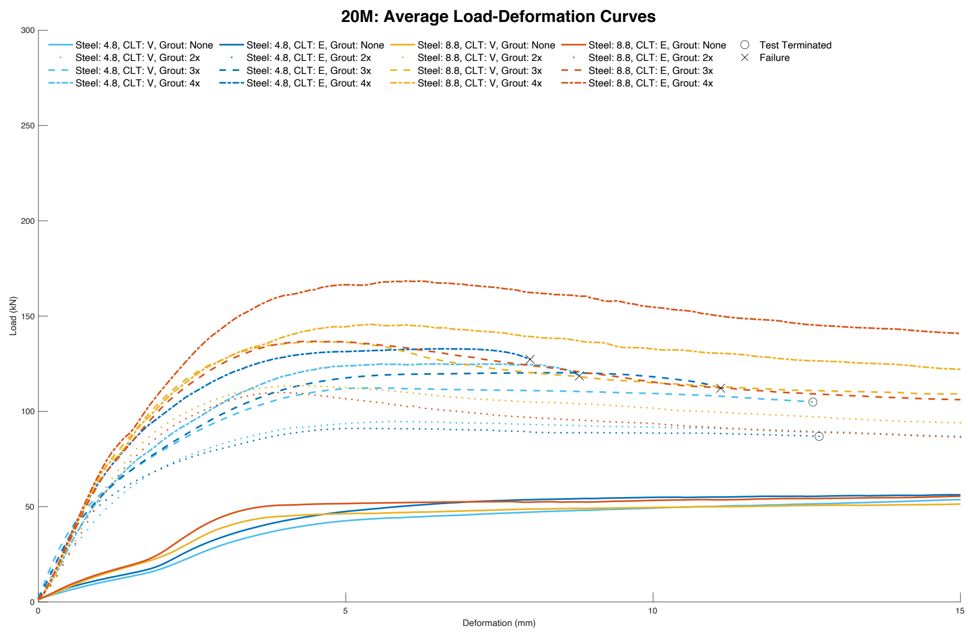

Figure 4.7: Load-deformation behaviour of specimens with 20M rods.

Focusing now on specimens with 24M steel rods, Figure 4.9 shows a similar relationship between design properties and load-deformation behaviour as previously discussed for 20M specimens. Again, an increase in load and elastic range is associated with an increasing grout diameter. Also observed again is greater load for 8.8 grade steel specimens over 4.8 grade steel specimens. Importantly, there is a much more prominent and discernible yield point for specimens with 8.8 grade steel. While specimens with 4.8 grade steel tend to have a smooth and shallow transition from elastic to plastic behaviour, those with 8.8 grade steel exhibit more of a sharp transition, which makes identifying the yield point much easier.

Again, the specimens with the lower-strength rods and the thickest grout layers failed prematurely, though these are also the only specimens which exhibited true strain-hardening and therefore an increase in load after the yield point.

Figure 4.8: Shear failure of specimen with weak/slender rod and large grout diameter.

Lastly, Figure 4.10 shows the load-deformation curves for specimens with 30M rods, with a remarkable increase in strength and stiffness when a grout layer is included and no specimens failing prematurely.

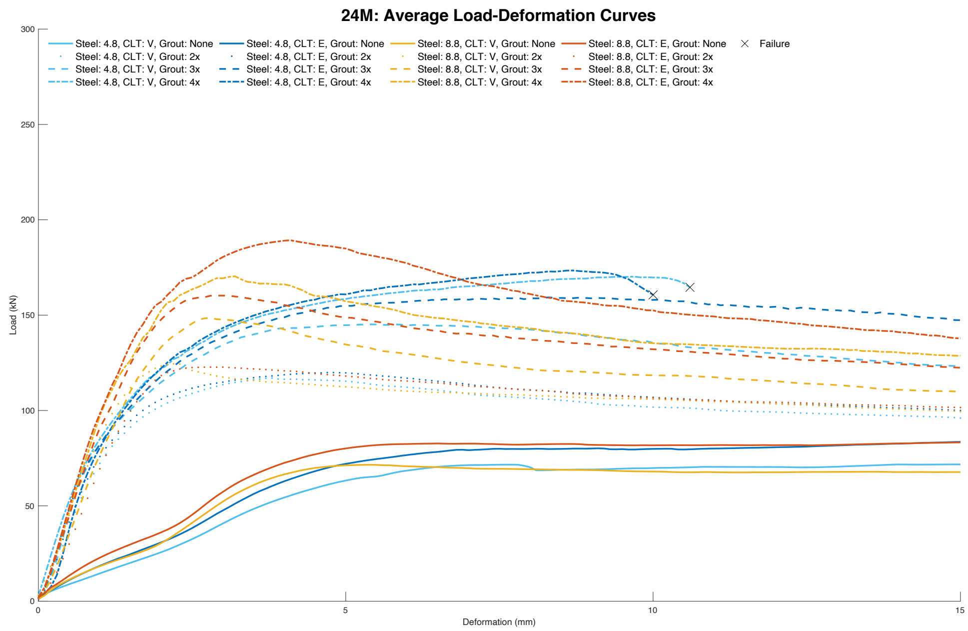

Figure 4.9: Load-deformation behaviour of specimens with 24M rods.

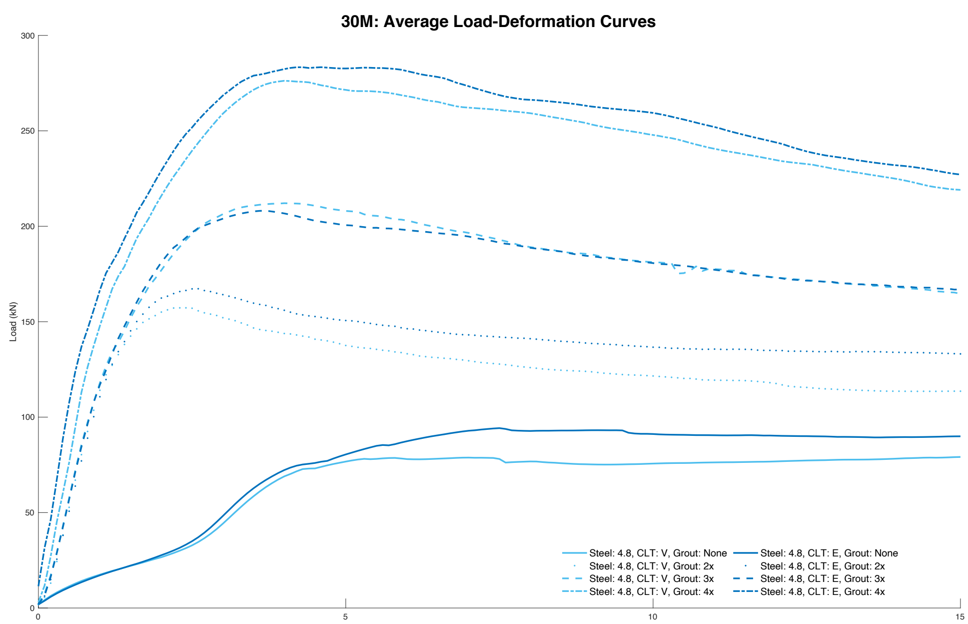

Figure 4.10: Load-deformation behaviour of specimens with 30M rods.

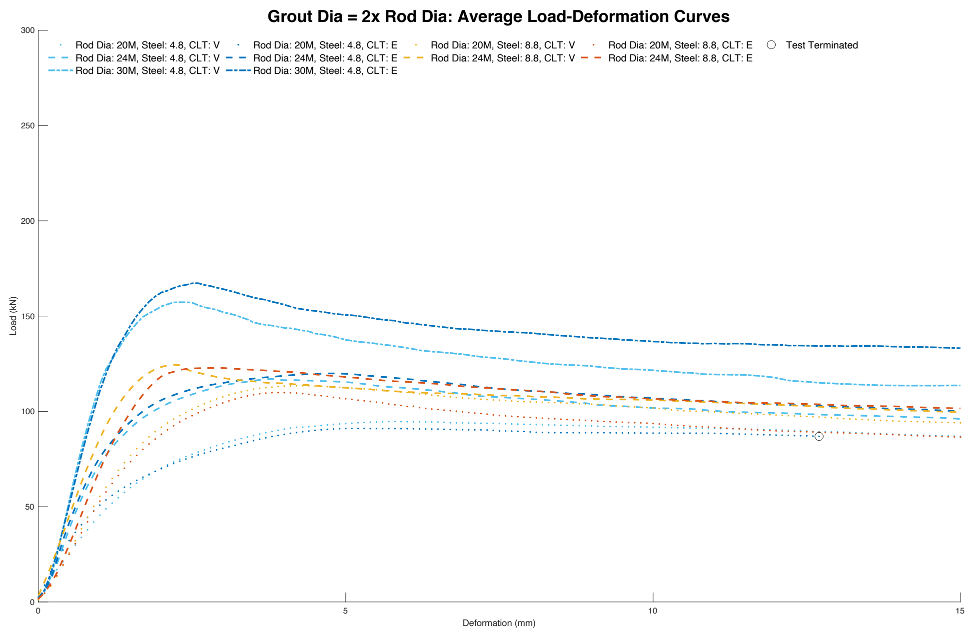

Figure 4.11: Load-deformation behaviour of specimens with grout diameter 2x rod diameter.

To assess the influence of the rod diameter, the load-deformation curves are plotted for each grout diameter: 2x, 3x, and 4x, as shown in Figures 4.11, 4.12 and 4.13, respectively. In all three cases, there is an increase in maximum load with increasing rod diameter. An increase in stiffness with increasing rod diameter is also observed, which was not observed in the previous plots in which grout diameter was varied for each rod diameter. This indicates that the stiffness of the connector is mainly governed by the rod diameter. It is also observed that there is a negligible impact from the CLT grade and clearer yield points associated with stronger steel rods.

A detailed look at the previous six load-deformation curves reveals the following:

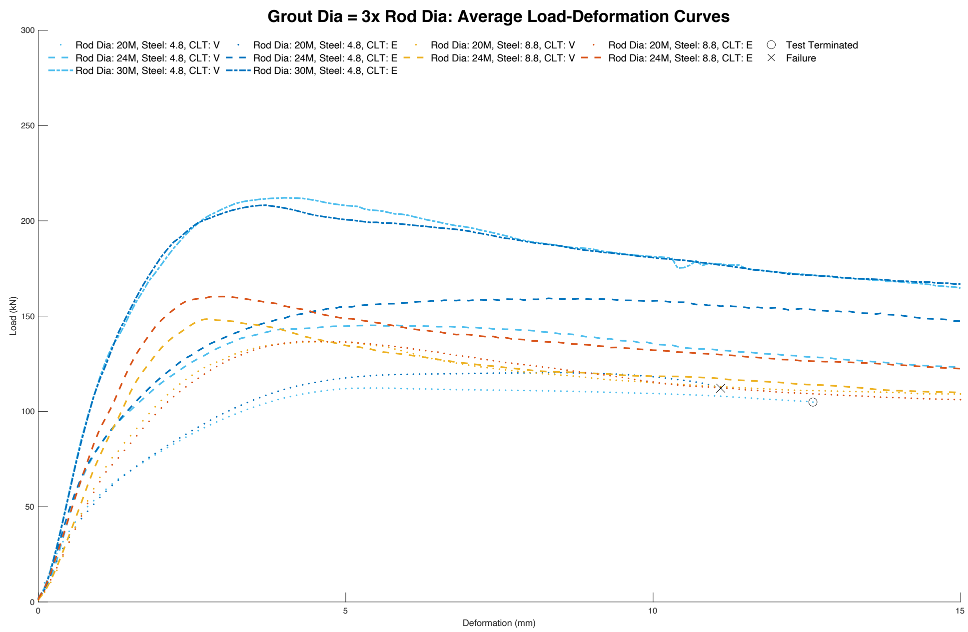

Figure 4.12: Load-deformation behaviour of specimens with grout diameter 3x rod diameter.

- The majority of specimens showed a decrease in load after yielding, indicative of predominantly wood crushing behaviour,
- The combination of a low-strength and slender rod with a thick grout layer leads to shear failure of the rod,
- All specimens, even those that failed before the target displacement, developed significant plastic behaviour after yielding,
- The grade of CLT does not have a significant impact on capacity or stiffness,
- The inclusion of a grout layer of any size significantly increases capacity and stiffness
- Yield capacity increases as a function of rod and grout diameter,

- Stiffness increases primarily with rod diameter.

The load-deformation curves for each of the tested specimens are available in Appendix C.

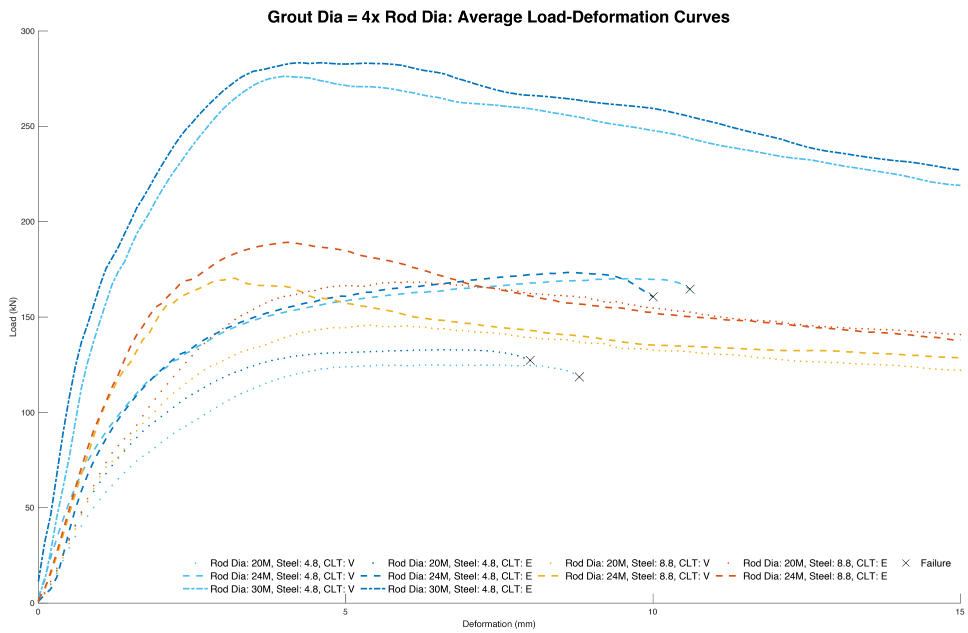

Figure 4.13: Load-deformation behaviour of specimens with grout diameter 4x rod diameter.

4.3 Structural Performance Parameters

Tables 4.2, 4.3, 4.4, 4.5 and 4.6 summarize the maximum load F_{max}, ultimate load F_u, yield load F_y, elastic limit F_e, and stiffness k for each specimen type, including the mean value, coefficient of variation, and 5$^{\text{th}}$-percentile value, where relevant.

Focusing first on rod diameter, there is a clear increase in all performance parameters as the rod diameter increases. Increasing the rod diameter from 20 mm to 24 mm results in an increase in all performance parameters, though the magnitude of this increase is more pronounced in specimens with strength-class 4.8 rods compared to those with strength-class 8.8 rods. In the former case, the maximum and ultimate load increase on average about 30%, whereas in the latter case, the increase is roughly half of that. For yield load, the increase is 38% for 4.8 rods and 26% for 8.8 rods. For stiffness, the increase is 73% for 4.8 rods and 43% for 8.8 rods. Only for the elastic limit is the increase similar between 4.8 and 8.8 rods, being 33% and 37%, respectively.

Considering now the difference between 30M rods and 24M rods, comparisons can only be made for strength-class 4.8 rods since no strength-class 8.8 30M rods were tested. In this case, there is a 46% increase in maximum load, 40% increase in ultimate load, a 65% increase in yield load and elastic limit, and a 70% increase in stiffness. This confirms that rod diameter is a primary determinant of structural performance of the connector, though more so for strength-class 4.8 rods than 8.8 rods.

Looking now at the grout diameter, the increase in load and stiffness from no grout to a grout layer of diameter twice the rod diameter is remarkable. Both maximum and yield load increase by roughly 75% with ultimate load increasing by 52% and elastic limit increasing by 105%. Most notably, stiffness increases anywhere from 375% to 1290%. This immediately shows the benefit of the grout layer and suggests that a high-capacity and stiff connector is possible with only a small grout layer. Increasing the grout diameter from 2x to 3x results in a 15 to 26% increase in load parameters. Stiffness, however, only increases roughly 7% and even decreases in some cases. Increasing from a grout diameter of 3x to 4x, the load parameters increases 11 to 18% and stiffness again increases slightly in some cases and decreases in others. This confirms that the load parameters of the connector are proportional to the thickness of the grout layer. As for the stiffness, it increases drastically when a grout layer is added but does not change significantly as the thickness of the grout layer increases.

Considering the strength-class of the steel rod, differences are apparent between 20M rods and 24M rods. For the former, the increase in rod strength-class causes a 20% increase in maximum load and a 33% increase in yield load and elastic limit. For the latter however, only an increase in yield load and elastic limit is observed (21% and 37%, respectively), while maximum load is nearly unaffected. What's more is that the stiffness of the 24M rods generally decreases with increased rod strength-class. Therefore it may be suggested that for 24M rods, the use of 8.8 strength-class steel rods is not economical.

Lastly, the impact of CLT grade is assessed. As has already been noticed in the load-deformation curves, this does not appear to have a noticeable impact on the specimen behaviour. This is true of the performance parameters as well, with E grade CLT specimens only increasing in load parameters by roughly 4%, and actually decreasing in some cases, compared to specimens with V grade CLT.

Once again, the variability in the results is of interest, and this is quantified by the coefficients of variation (COVs) for the load parameters and stiffness. For the load parameters, the COV is almost always below 10%, indicating a satisfactory level of variability between replicates. For stiffness however, the COV is often greater than 10%. This may be explained by the fact that stiffness is a relatively sensitive measurement, depending on both load and deformation.

The last row in the tables presents the loss of strength *LoS*, a measure of the decrease in strength between the maximum load and the ultimate load, as defined by Equation 3.1. For specimens without grout, this value tends to be small or zero as these specimens mainly exhibit an increase in load after yielding (strain-hardening). For the specimens with grout, the *LoS* corresponds to the failure mode. Those specimens that exhibited a decrease in load after yielding (failure mode i) have a large *LoS*, as high as 20%, which is the maximum possible value since ultimate load was defined as the greater of the final recorded load and 80% of the maximum load. Those specimens that exhibited an increase in load after yielding (failure mode ii) should have *LoS* values of zero. However, they have values of 18.6% and 15.2%. This is because the Matlab code captures a small portion of the sudden drop in load at failure, establishing a slightly underestimated ultimate load, resulting in a non-zero *LoS*. Lastly, specimens that exhibited a plateau after yielding (failure mode iii) have *LoS* values ranging from 7.5% to 17.7%, indicating that wood crushing was still the predominant failure mechanism, resulting in an overall decrease in load.

Table 4.2: Structural performance parameters for specimens with 20M 4.8 strength-class rods.

Rod Diameter		20M							
Steel Strength-Class		4.8							
CLT Grade		E				V			
Grout Diameter		N/A	2x	3x	4x	N/A	2x	3x	4x
Failure Mode			iii	iii	iii		iii	iii	iii
F_{max}	Mean (kN)	56.9	92.0	120.8	134.5	53.7	97.6	112.9	127.1
	COV (%)	4.2	8.0	4.0	3.7	7.0	4.2	5.5	3.1
	5^{th}-perc. (kN)	48.6	76.2	107.9	120.1	42.9	87.1	99.3	113.5
F_u	Mean (kN)	56.3	85.1	102.5	114.6	53.7	86.9	101.9	104.6
	COV (%)	3.5	8.6	3.8	5.0	7.0	6.8	9.1	3.3
	5^{th}-perc. (kN)	48.0	70.2	91.6	102.3	42.9	74.7	82.8	93.5
F_y	Mean (kN)	52.0	74.6	93.4	108.2	44.7	76.4	87.1	98.1
	COV (%)	3.8	10.0	6.3	3.9	1.5	12.9	5.7	8.3
	5^{th}-perc. (kN)	44.4	58.0	81.4	96.6	38.2	56.0	76.7	81.3
F_e	Mean (kN)	24.7	42.6	52.4	60.0	24.2	46.4	48.6	55.6
	COV (%)	5.8	7.8	4.9	2.8	5.2	18.2	6.3	4.1
	5^{th}-perc. (kN)	20.5	35.4	46.7	53.6	20.5	32.0	42.1	49.7
k	Mean (kN/mm)	9.1	55.5	56.1	75.9	8.6	55.5	60.5	59.6
	COV (%)	5.0	18.6	11.6	14.6	2.3	20.2	11.7	5.9
LoS (%)		1.2	7.5	15.2	14.7	0.0	10.9	9.7	17.7

Table 4.3: Structural performance parameters for specimens with 20M 8.8 strength-class rods.

Rod Diameter		20M							
Steel Strength-Class		8.8							
CLT Grade		E				V			
Grout Diameter		N/A	2x	3x	4x	N/A	2x	3x	4x
Failure Mode			i	i	i		i	i	i
F_{max}	Mean (kN)	55.5	111.4	138.3	172.5	51.5	114.1	137.6	147.4
	COV (%)	3.2	8.5	4.8	4.4	9.4	5.2	5.4	8.6
	5^{th}-perc. (kN)	47.4	91.6	123.5	154.0	38.3	101.2	121.5	121.3
F_u	Mean (kN)	55.5	89.7	111.1	141.1	51.4	95.0	111.4	123.7
	COV (%)	3.2	8.9	4.2	5.4	9.4	8.1	5.9	7.0
	5^{th}-perc. (kN)	47.4	73.2	99.2	124.5	38.2	78.7	97.1	105.6
F_y	Mean (kN)	52.0	99.5	121.9	145.6	46.6	103.0	122.7	120.7
	COV (%)	4.5	8.2	7.0	6.4	7.6	6.2	5.8	11.9
	5^{th}-perc. (kN)	44.4	82.6	104.5	125.4	36.4	89.4	107.3	91.2
F_e	Mean (kN)	25.7	58.5	69.0	81.1	25.4	57.6	69.6	71.8
	COV (%)	6.0	11.1	11.0	7.2	9.7	4.9	6.5	10.3
	5^{th}-perc. (kN)	21.2	44.8	54.1	68.6	18.5	51.4	60.1	56.7
k	Mean (kN/mm)	11.2	61.7	68.1	70.8	11.2	64.5	72.8	74.7
	COV (%)	2.5	8.2	10.8	12.0	18.7	9.6	4.7	6.7
LoS (%)		0.0	19.4	19.7	18.2	0.1	16.8	19.1	16.1

Table 4.4: Structural performance parameters for specimens with 24M 4.8 strength-class rods.

Rod Diameter		24M							
Steel Strength-Class		4.8							
CLT Grade		E				V			
Grout Diameter		N/A	2x	3x	4x	N/A	2x	3x	4x
Failure Mode			i	iii	ii		i	i	ii
F_{max}	Mean (kN)	84.9	121.7	162.2	174.9	74.5	118.8	147.9	172.5
	COV (%)	5.3	5.2	4.1	2.9	6.3	8.8	6.2	3.2
	5^{th}-perc. (kN)	71.8	108.3	144.9	156.3	61.0	97.0	128.2	154.1
F_u	Mean (kN)	83.5	102.4	147.4	142.4	71.7	100.3	123.6	146.3
	COV (%)	3.4	7.4	8.5	3.5	12.0	13.1	6.5	4.3
	5^{th}-perc. (kN)	71.3	86.6	121.3	127.2	48.3	74.3	106.2	130.6
F_y	Mean (kN)	77.5	109.5	128.6	131.7	71.5	107.5	124.5	136.2
	COV (%)	7.7	5.3	8.4	5.4	7.2	6.6	6.7	5.8
	5^{th}-perc. (kN)	60.5	97.0	105.2	116.7	57.0	92.1	106.3	119.7
F_e	Mean (kN)	49.0	56.7	70.8	77.5	35.8	58.2	68.1	76.2
	COV (%)	39.0	8.2	5.1	10.3	9.4	13.9	8.3	6.3
	5^{th}-perc. (kN)	15.0	47.3	62.9	62.0	26.4	42.6	55.9	66.2
k	Mean (kN/mm)	14.0	105.8	104.7	114.3	11.5	94.3	106.7	96.4
	COV (%)	21.3	22.2	7.4	22.5	7.9	8.9	21.1	19.6
LoS (%)		1.6	15.8	9.1	18.6	3.7	15.6	16.4	15.2

Table 4.5: Structural performance parameters for specimens with 24M 8.8 strength-class rods.

Rod Diameter		24M							
Steel Strength-Class		8.8							
CLT Grade		E				V			
Grout Diameter		none	2x	3x	4x	none	2x	3x	4x
Failure Mode			i	i	i		i	i	i
F_{max}	Mean (kN)	83.8	126.0	163.7	192.4	71.8	125.7	151.6	177.2
	COV (%)	6.3	4.4	7.0	5.7	3.5	4.4	3.9	7.8
	5^{th}-perc. (kN)	68.6	111.9	139.8	169.3	61.3	112.2	135.4	147.7
F_u	Mean (kN)	83.3	104.8	131.6	153.9	67.7	103.3	121.2	141.7
	COV (%)	5.7	4.9	6.7	5.7	7.9	6.9	3.9	7.8
	5^{th}-perc. (kN)	69.5	93.1	113.1	135.5	52.7	88.2	108.3	118.1
F_y	Mean (kN)	81.5	124.4	160.5	177.0	70.3	120.9	148.9	167.2
	COV (%)	8.6	5.7	7.6	7.4	3.9	8.7	4.8	11.6
	5^{th}-perc. (kN)	61.9	108.1	135.3	149.6	60.0	97.7	132.9	126.0
F_e	Mean (kN)	43.9	92.9	89.1	98.0	34.4	85.5	86.9	102.0
	COV (%)	21.9	12.3	12.5	12.5	6.7	8.0	7.2	18.9
	5^{th}-perc. (kN)	21.6	68.8	67.9	73.7	27.9	71.0	73.7	64.4
k	Mean (kN/mm)	16.6	78.4	102.3	111.3	13.6	92.8	94.6	109.6
	COV (%)	9.2	22.0	14.2	9.4	9.5	13.4	17.8	9.5
LoS (%)		0.5	16.8	19.6	20.0	5.7	17.8	20.0	20.0

Table 4.6: Structural performance parameters for specimens with 30M 4.8 strength-class rods.

Rod Diameter		30M							
Steel Strength-Class		4.8							
CLT Grade		E				V			
Grout Diameter		N/A	2x	3x	4x	N/A	2x	3x	4x
Failure Mode			i	i	i		i	i	i
F_{max}	Mean (kN)	95.8	169.8	212.1	289.6	81.6	160.3	213.7	278.3
	COV (%)	4.9	7.5	7.6	6.3	16.6	7.3	5.3	3.0
	5^{th}-perc. (kN)	81.8	143.8	178.0	249.4	48.6	135.9	189.1	247.5
F_u	Mean (kN)	90.0	138.0	173.7	234.6	79.1	128.2	171.9	224.1
	COV (%)	7.0	6.7	9.6	5.8	19.3	7.3	5.5	3.4
	5^{th}-perc. (kN)	72.1	118.8	139.4	203.9	43.8	108.7	151.3	199.2
F_y	Mean (kN)	93.2	167.6	205.0	259.1	76.3	157.7	205.6	246.6
	COV (%)	2.4	7.6	7.3	6.4	22.0	6.8	6.3	5.1
	5^{th}-perc. (kN)	79.6	141.6	173.5	221.9	38.9	135.0	178.3	217.7
F_e	Mean (kN)	41.5	95.6	117.3	127.1	36.6	95.4	114.4	120.0
	COV (%)	5.5	14.4	12.8	2.7	13.5	25.4	10.8	6.5
	5^{th}-perc. (kN)	34.7	68.1	87.3	113.0	24.1	54.8	89.3	102.8
k	Mean (kN/mm)	12.8	150.3	147.1	213.3	11.1	154.8	144.1	243.2
	COV (%)	3.9	16.5	18.5	19.7	17.8	20.8	13.3	36.9
LoS (%)		6.1	18.8	18.1	19.0	3.0	20.0	19.6	19.5

The variability in the performance parameters is assessed by producing box-plots for the maximum loads, yield loads, and stiffness datasets in Figures 4.14, 4.15 and 4.16, respectively. Each figure contains a box-plot for each rod diameter with the data grouped by grout diameter. Blue boxes represent E grade CLT while orange boxes represent V grade CLT. Additionally, solid boxes represent 4.8 strength-class steel while dotted boxes represent 8.8 strength-class steel.

As has already been observed, the variability in the performance parameters generally increases with increasing rod and grout diameter, this being attributed to the corresponding inclusion of more wood in the bearing mechanism and therefore potentially more defects. Comparing CLT grades, there does not appear to be a clear relationship between grade and variability in the performance parameters. In some cases E grade specimens show more variability, in some cases V grade specimens show more variability, but in general they show a similar level of variability. Considering the steel strength-class, between 4.8 and 8.8, specimens with 8.8 strength-class steel tend to show slightly more variability in loads. This may be explained by the fact that these rods tend to bend less and therefore transfer more force into the wood, which has been established as the main source of variability in the connector.

In general, the 30M specimens show the most variability in load and stiffness for all grout diameters, steel strength-classes, and CLT grades. Such variability would lead to overly conservative design values, rendering the use of 30M rods uneconomical. From a variability perspective, the 20M and 24M specimens are the most appropriate for design.

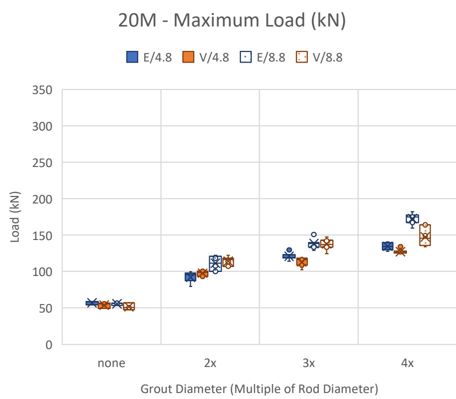

(a) 20M

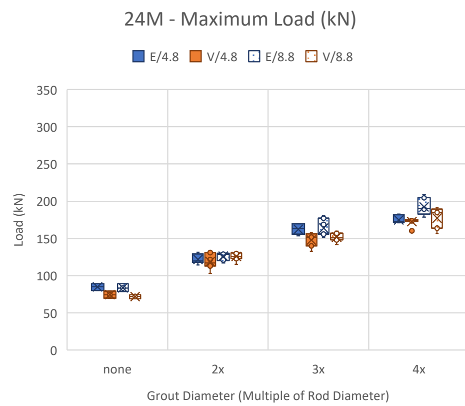

(b) 24M

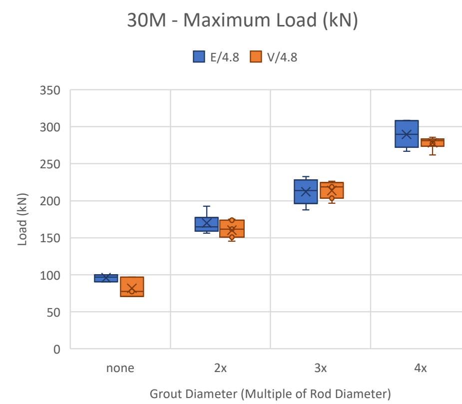

(c) 30M

Figure 4.14: Box plots for maximum load.

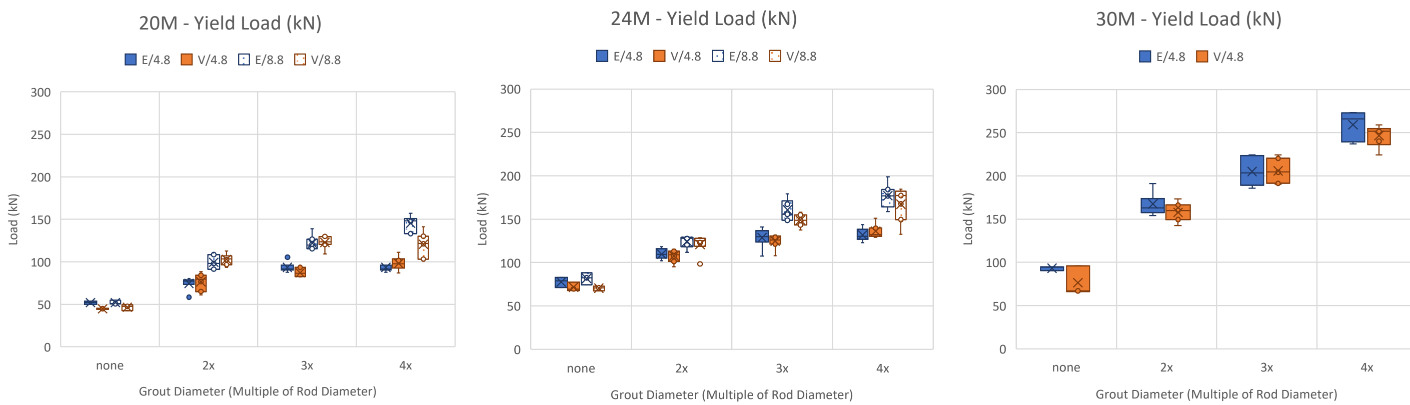

(a) 20M **(b)** 24M **(c)** 30M

Figure 4.15: Box plots for yield load.

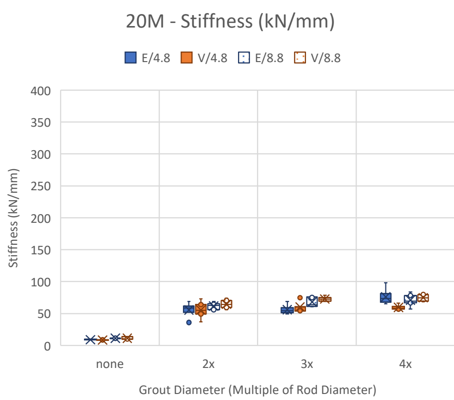

(a) 20M

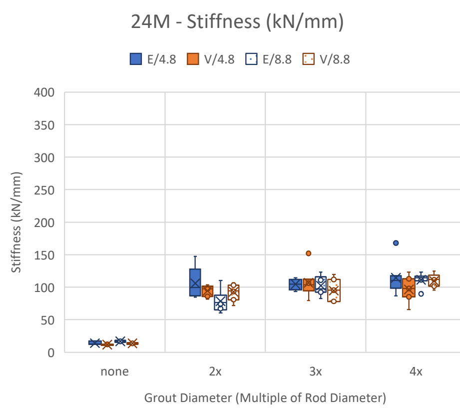

(b) 24M

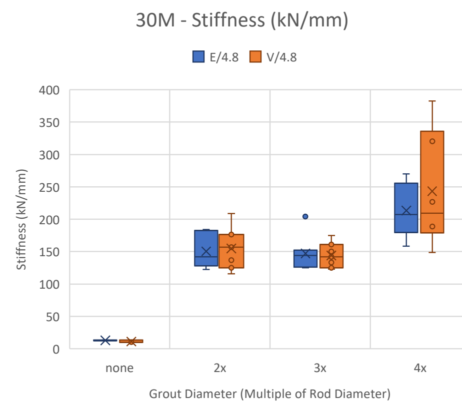

(c) 30M

Figure 4.16: Box plots for stiffness.

4.4 Ductility

Though this connector is intended to be capacity-protected and remain elastic, it is desired that it still remain useful for traditional connector design, by which the connector itself is designed to deform plastically. To this end, the increased capacity and stiffness should not result in a significant decrease in ductility, as compared to typical dowel-type fasteners.

Table 4.7: Ductility classifications according to Smith et al. (2006).

Classification	Average Ductility Ratio D_{av}
Brittle	$D_{av} \leq 2$
Low-Ductility	$2 < D_{av} \leq 4$
Moderate-Ductility	$4 < D_{av} \leq 6$
High-Ductility	$D_{av} > 6$

The ductility of the connector is assessed according to the criteria put forth by Smith et al. (2006), as summarized in Table 4.7. The average ductility ratio and corresponding ductility classification for each specimen type is given in Table 4.8. The table mostly shows moderate ductility across specimen types. The only specimen type that displays consistently low ductility are the 24M specimens with 8.8 strength-class steel and V grade CLT. Interestingly, even those specimens that failed before the target displacement (see Section 4.2) mostly classify as moderately ductile. These results are promising and indicate that the connector may be applied in traditional design procedures that call for plastic deformation in the connector. However, cyclic testing would need to be conducted on the specimens to accurately assess their true ductility.

Table 4.8: Ductility of each specimen type.

Rod Dia.	Rod Strength-Class	CLT Grade	Grout Dia.	D_{av}	Ductility
20 mm	4.8	E	2x	6.36	High
			3x	6.28	High
			4x	4.50	Moderate
		V	2x	6.13	High
			3x	3.66	Low
			4x	4.07	Moderate
	8.8	E	2x	4.86	Moderate
			3x	5.51	Moderate
			4x	4.61	Moderate
		V	2x	4.83	Moderate
			3x	4.75	Moderate
			4x	5.47	Moderate
24 mm	4.8	E	2x	5.80	Moderate
			3x	5.30	Moderate
			4x	6.14	High
		V	2x	6.23	High
			3x	4.82	Moderate
			4x	4.61	Moderate
	8.8	E	2x	4.50	Moderate
			3x	4.78	Moderate
			4x	3.51	Low
		V	2x	3.22	Low
			3x	3.65	Low
			4x	2.88	Low
30 mm	4.8	E	2x	4.38	Moderate
			3x	3.20	Low
			4x	4.35	Moderate
		V	2x	4.36	Moderate
			3x	4.97	Moderate
			4x	5.23	Moderate

4.5 Equivalent Bearing Block Stress

The equivalent bearing block stress in the CLT was calculated assuming a bearing area as shown in Figure 4.17. The equivalent bearing stress is calculated as follows:

$$\sigma_b = \frac{F_{max}}{Dt_b} \tag{4.1}$$

Where: σ_b is the equivalent bearing stress, F_{max} is the mean maximum load of the arrangement in kN, D is the grout diameter in mm, and t_b is the bearing length of the rod in mm.

Table 4.9 gives the bearing stress for each arrangement. The values range from 18.7 MPa to 33.3 MPa and generally decrease with increasing grout diameter. Equation 4.1 assumes a uniform distribution of load on the bearing area, but in reality the load is not distributed uniformly as part of the load is transferred into the rod in bending. Therefore, specimens that exhibit little to no steel hinging (failure mode i) tend to have higher bearing stresses than those that exhibit some bending (failure mode ii and iii). This is readily observed by comparing the bearing stresses for the 20M specimens with 4.8 strength-class rods with those with 8.8 strength-class rods. Those with 4.8 strength-class rods exhibit wood crushing and steel hinging (failure mode iii) and thus have lower bearing stresses than those with 8.8 strength-class rods, which primarily exhibit wood crushing (failure mode i).

Table 4.9: Bearing stresses.

Rod Dia.	Rod Str.-Class	CLT Grade	Grout Dia.	σ_b (MPa)	Failure Mode
20 mm	4.8	E	2x	27.1	iii
			3x	23.7	iii
			4x	19.8	iii
		V	2x	28.7	iii
			3x	22.1	iii
			4x	18.7	iii
	8.8	E	2x	32.8	i
			3x	27.1	i
			4x	25.4	i
		V	2x	33.6	i
			3x	27.0	i
			4x	21.7	i
24 mm	4.8	E	2x	29.8	i
			3x	26.5	iii
			4x	21.4	ii
		V	2x	29.1	i
			3x	24.2	i
			4x	21.1	ii
	8.8	E	2x	30.9	i
			3x	26.8	i
			4x	23.6	i
		V	2x	30.8	i
			3x	24.8	i
			4x	21.7	i
30 mm	4.8	E	2x	33.3	i
			3x	27.7	i
			4x	28.4	i
		V	2x	31.4	i
			3x	27.9	i
			4x	27.3	i

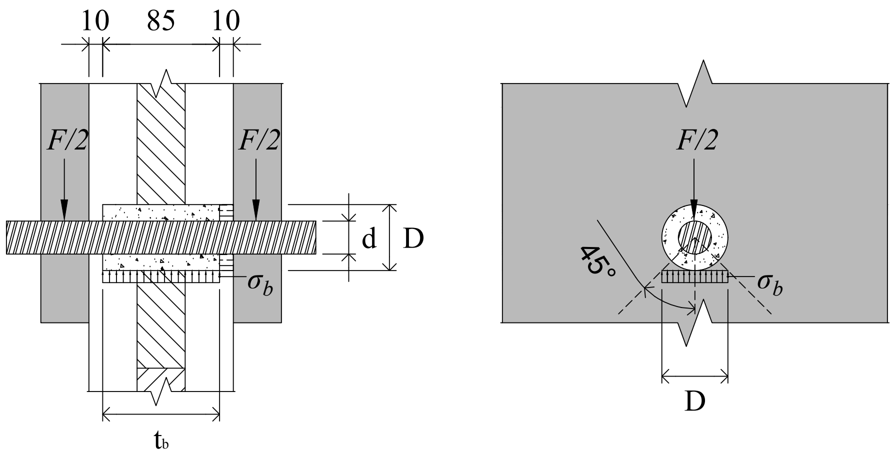

(a) Frontal view (b) Lateral view

Figure 4.17: Applied load and bearing area.

4.6 Quantitative Analysis: Linear Regression

The linear regression analysis, presented in Section 3.6.1, was first conducted on the specimens without grout. Though only three replicates of each specimen type were tested, which is too small a sample size to produce significant results, this analysis serves as a general point of comparison for the specimens with grout.

The results of the regression analyses for specimens without grout are given in Table 4.10. For both yield resistance and maximum shear resistance, the stepwise multi-variable linear regression identified only rod diameter and CLT grade as significant, with steel strength-class being left out. The overall R-squared values for the two models were found to be 0.756 and 0.778, respectively, indicating a good fit. Looking closer at the semi-partial correlation coefficients reveals that the vast majority of the model R-squared comes from the rod diameter, with sr^2 values of 0.676 and 0.699 for yield resistance and maximum shear resistance, respectively.

The sr^2 values for CLT grade are 0.079 in both cases. This indicates that about 70% of the variance in the yield and maximum load data is explained by the rod diameter, while only about 8% is explained by the CLT grade.

Considering the stiffness of the connector without grout, Table 4.10 shows that steel-strength class is a significant variable, with a similar sr^2 value as rod diameter of roughly 26%. Again, CLT grade contributes less, at only 9%. It is important to note here that the R-squared value for the model is only 0.481, which indicates that this model is not a strong fit. This is likely a result of the small sample size of three, as previously mentioned.

Focusing now on the specimens with grout, the results of the regression analyses are given in Table 4.11. For yield and maximum shear resistance, it can be seen that all four independent variables are deemed significant and included in the regression models. In both cases, the model explains almost 90% of the variance in the dependent variable. From the sr^2 values it can be seen that the impact of rod and grout diameter are inverted for yield and maximum shear resistance. In the former case, the rod diameter explains more variance than the grout diameter (32% compared to 18%), whereas in the latter case, the opposite is true (15% compared to 34%). This indicates that rod diameter has the biggest impact in the elastic range, but after yielding it is the grout diameter which becomes more important. Steel strength-class contributes about 6.5% in the case of yield resistance and only about 1.4% in the case of maximum shear resistance. In both cases, though deemed significant by its p-value, the CLT grade contributes less than 1% to explaining the variance in the dependent variable. It is therefore concluded that CLT grade is not a significant predictor of yield or maximum load for specimens with grout.

For the stiffness of specimens with grout, Table 4.11 shows that the primary contributing variable is rod diameter, explaining about 37% of the variance, with a small contribution from grout diameter, explaining about 5.3% of the variance.

The regression analyses confirm the observations made from the load-deformation curves in Section 4.2. Specifically, it is shown that yield and maximum shear resistance are primarily governed by rod and grout diameter. As has already been observed, the contribution of CLT grade is minimal and is therefore not considered in the following analyses. Lastly, stiffness depends primarily on rod diameter, with a small contribution from grout diameter.

Table 4.10: Linear regression results for specimens without grout.

Value	Statistic	Model	Rod Diameter	Steel Class	CLT Grade
Yield Load	p-value	5.5×10^{-9}	2.94×10^{-9}	N/A	0.006
	R^2 / sr^2	0.756	0.676	N/A	0.079
Max Load	p-value	1.49×10^{-9}	7.85×10^{-10}	N/A	0.004
	R^2 / sr^2	0.778	0.699	N/A	0.079
Stiffness	p-value	5.91×10^{-4}	1.45×10^{-3}	9.39×10^{-4}	0.043
	R^2 / sr^2	0.481	0.253	0.278	0.090

Table 4.11: Linear regression results for specimens with grout.

Value	Statistic	Model	Rod Diameter	Grout Diameter	Steel Class	CLT Grade
Yield Load	p-value	3.84×10^{-98}	2.95×10^{-63}	1.48×10^{-45}	3.20×10^{-23}	0.007
	R^2 / sr^2	0.896	0.316	0.177	0.065	0.004
Max Load	p-value	4.86×10^{-98}	1.20×10^{-40}	1.10×10^{-65}	3.54×10^{-7}	0.001
	R^2 / sr^2	0.896	0.148	0.341	0.014	0.005
Stiffness	p-value	1.40×10^{-56}	6.55×10^{-39}	4.06×10^{-9}	N/A	N/A
	R^2 / sr^2	0.717	0.371	0.053	N/A	N/A

4.7 Bayesian Linear Regression

The previous linear regression analysis served to identify quantitatively which parameters contributed to the yield resistance, maximum shear resistance, and stiffness of the connector. It was decided that the CLT grade was not a significant determinant of any of the performance parameters investigated. Removing CLT grade as a variable essentially causes each specimen type to now consist of fourteen replicates rather than seven.

As discussed in Section 3.6.2, a Bayesian linear regression analysis was used to build a model for yield and maximum shear resistance in the form of:

$$R = \theta_1 + \theta_2 d_{rod} + \theta_3 d_{grout} + \theta_4 f_{y/u,s} + \varepsilon \tag{4.2}$$

The standard error of the model was determined to be $s^2 = 2.21 \times 10^8$ for yield load and $s^2 = 2.28 \times 10^8$ for maximum load. The mean $\hat{\theta}$ and standard deviation $\Sigma_{\theta\theta}$ of the regression coefficients were calculated in Python according to Equation 3.10 and Equation 3.13, respectively. The statistical properties of the Bayesian regression coefficients are given in Table 4.12. The coefficients of variation are all within an acceptable range below 10%, except for that of θ_4 for maximum load. This corresponds to steel strength-class, and has already been shown in Section 4.6, this is not a strong predictor of maximum load, with a sr^2 value of only 0.014. However, it is still a significant variable and, for the sake of consistency, it was chosen to leave this in the model.

With the statistical properties of the correlation coefficients defined, the mean and standard deviation of the yield resistance (μ_{F_y} and σ_{F_y}) and maximum shear resistance ($\mu_{F_{max}}$ and $\sigma_{F_{max}}$) for each combination of design variables were determined.

Table 4.12: Statistical properties of Bayesian regression coefficients.

Resistance	Regression Coeff.	Dist. Type	Mean	COV
Yield Load	θ_1	Normal	-2.02×10^5	5.65%
	θ_2	Normal	8310	4.10%
	θ_3	Normal	978	5.47%
	θ_4	Normal	122	9.02%
Maximum Load	θ_1	Normal	-1.02×10^5	10.01%
	θ_2	Normal	5710	6.05%
	θ_3	Normal	1370	3.97%
	θ_4	Normal	37.1	19.51%

With these values, the inverse CDF was evaluated at 0.05 in order to calculate the 5^{th}-percentile resistance of each arrangement. The results are given in Table 4.13 for yield resistance and Table 4.14 for maximum shear resistance. It is noted that the standard deviation, calculated as the square root of the variance given in Equation 3.17, is approximately 15 kN for each arrangement. This is due to the fact that the contribution of the model standard error s^2 far outweighs the contribution of the other values in the covariance matrix $\mathbf{\Sigma}_{\boldsymbol{\theta}'\boldsymbol{\theta}'}$, resulting in a near-constant standard deviation regardless of arrangement.

The 5^{th}-percentile values determined from this method were compared with those calculated assuming a lognormal distribution. These are not the same 5^{th}-percentile values presented in the tables in Section 3.4, as these are grouped by CLT grade. In order to be compared with the values calculated from the Bayesian model, the 5^{th}-percentile values were recalculated assuming a lognormal distribution without considering CLT grade as a variable, therefore considering 14 replicates rather than 7. It is observed that the results of the two analyses are sometimes similar and sometimes differ by up to 20 kN, in favour of one analysis or the other.

Table 4.13: Bayesian model for yield resistance.

d_{rod} (mm)	d_{grout} (mm)	f_{ys} (MPa)	μ_{F_y} (kN)	σ_{F_y} (kN)	$F_{y,0.05}$ (kN)
20	40	528.6	67.5	15.0	42.7
	60		87.0	15.0	62.3
	80		106.6	15.0	81.8
	40	733.5	92.4	15.0	67.7
	60		112.0	15.0	87.4
	80		131.5	15.0	106.9
24	48	528.6	108.5	15.0	83.9
	72		132.0	14.9	107.4
	96		155.4	15.0	130.8
	48	733.5	133.5	15.0	108.8
	72		157.0	15.0	132.3
	96		180.4	15.0	155.7
30	60	528.6	170.1	15.1	145.3
	90		199.4	15.0	174.7
	120		228.8	15.1	203.9

The differences are likely due to the fundamental differences between the two methods. In the lognormal method, the 5$^{\text{th}}$-percentile value is determined by fitting a lognormal distribution to the results of the 14 replicates. In the Bayesian method, a single model consisting of normally distributed random variables is developed based on all of the test data. The 5$^{\text{th}}$-percentile value is determined by inputting the specific combination of design parameters of interest and evaluating the inverse CDF of the resulting random variable for resistance.

Due to the variability in 5$^{\text{th}}$-percentile values obtained by these two methods, they are compared by plotting the empirical CDFs for yield and maximum resistance along with the fitted lognormal and Bayesian normal distributions, as shown in Figures 4.18, 4.19 and 4.20. From these plots, it is clear that the lognormal

Table 4.14: Bayesian model for maximum shear resistance.

d_{rod} (mm)	d_{grout} (mm)	f_{us} (MPa)	$\mu_{F_{max}}$ (kN)	$\sigma_{F_{max}}$ (kN)	$F_{max,0.05}$ (kN)
20	40	562.4	87.9	15.3	62.8
	60		115.2	15.2	90.2
	80		142.5	15.3	117.4
	40	878.3	99.6	15.2	74.6
	60		126.9	15.2	101.9
	80		154.3	15.2	129.2
24	48	562.4	121.7	15.2	96.7
	72		154.5	15.2	129.5
	96		187.2	15.2	162.2
	48	878.3	133.4	15.3	108.3
	72		166.2	15.2	141.2
	96		199.0	15.3	173.9
30	60	562.4	172.4	15.3	147.2
	90		213.3	15.2	188.3
	120		254.3	15.3	229.1

distribution is a much more accurate fit than the normal distribution obtained from the Bayesian regression. This latter analysis was conducted over the entire data set, rather than on each design arrangement separately. This, combined with the assumption of normally distributed regression coefficients, results in the model poorly fitting the test values at small and large values. Therefore, it was chosen to use the lognormal distributions and correpsonding 5$^{\text{th}}$-percentile values in the following reliability analysis.

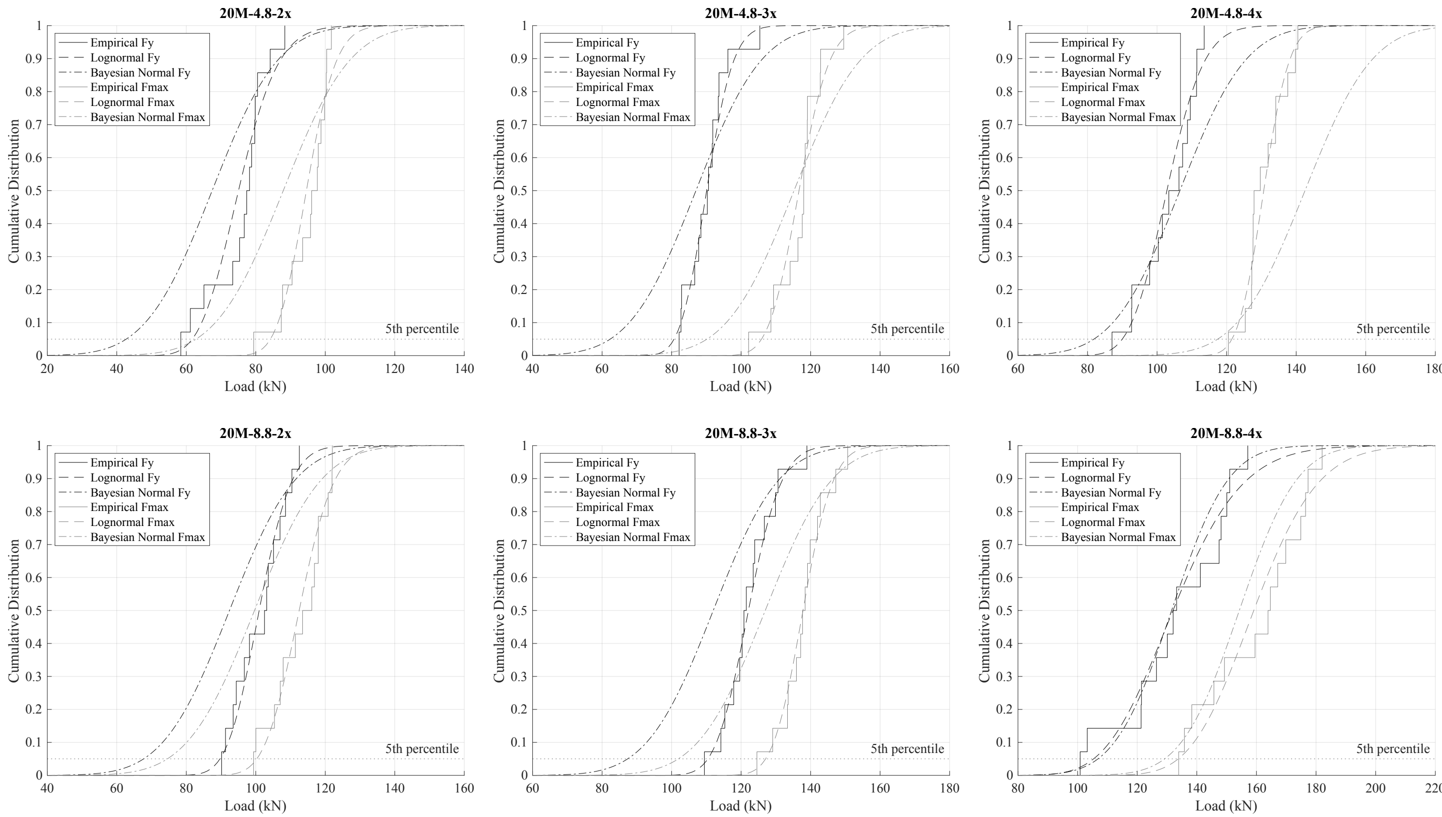

Figure 4.18: CDFs for specimens with 20M rods.

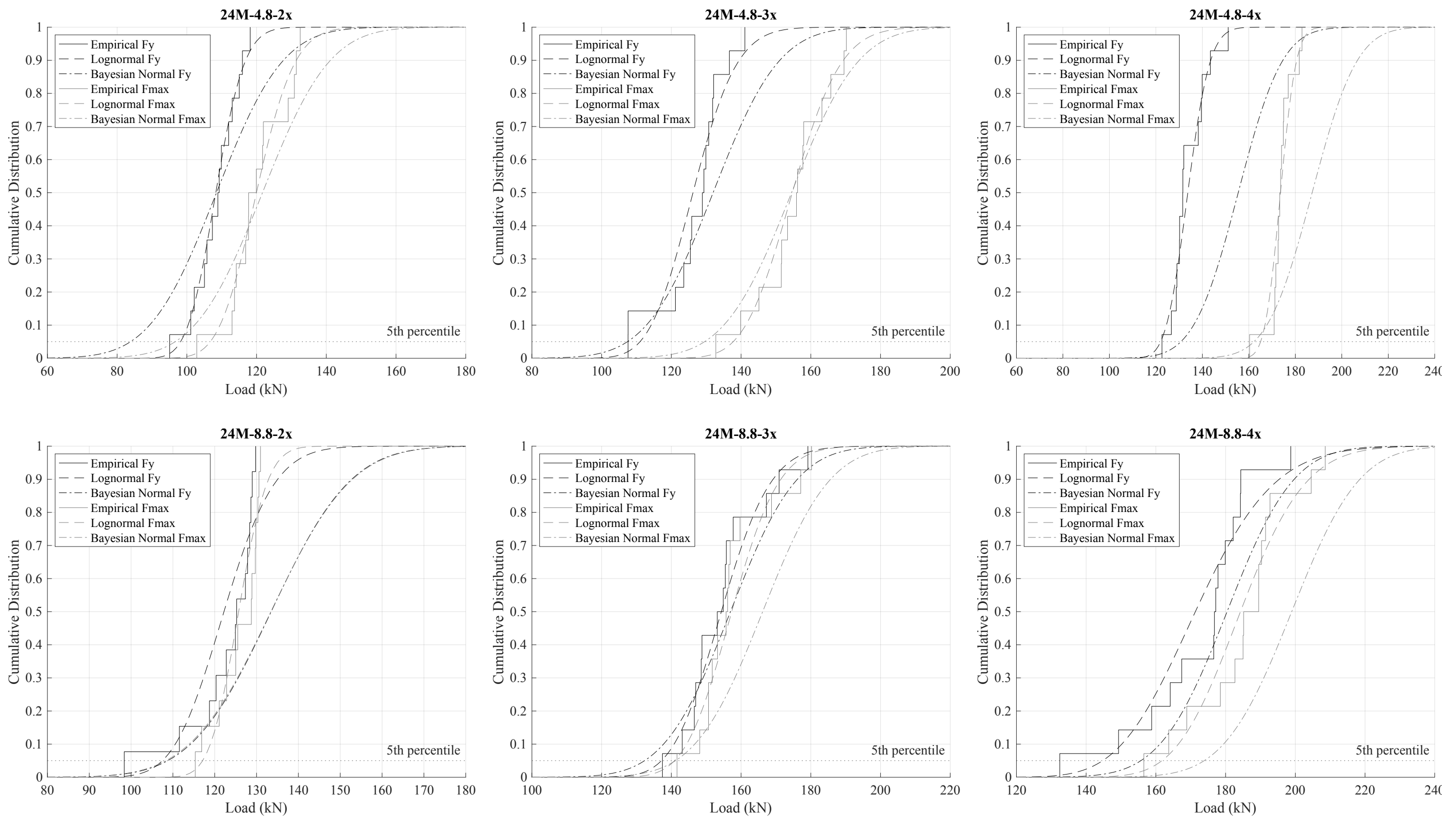

Figure 4.19: CDFs for specimens with 24M rods.

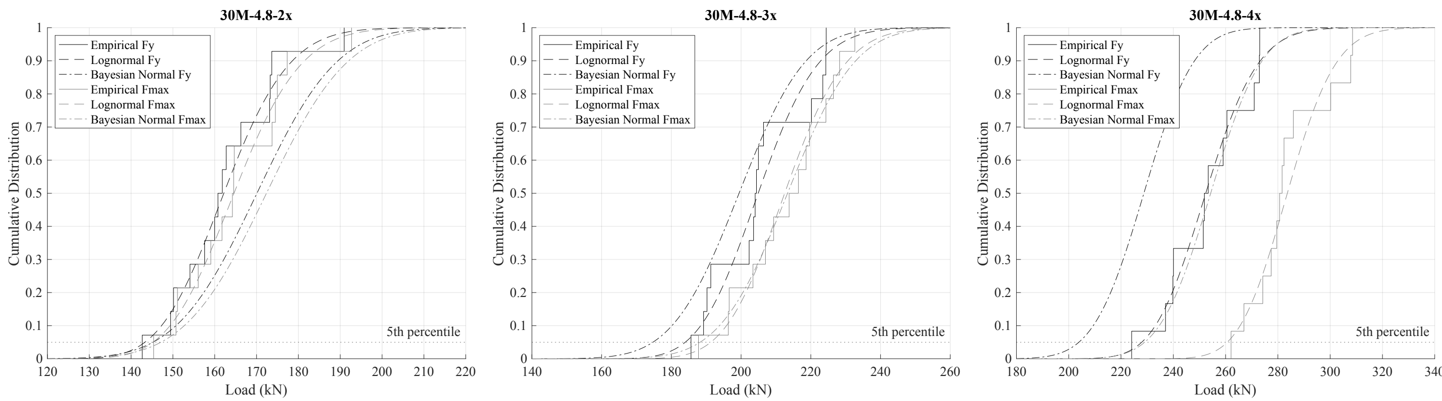

Figure 4.20: CDFs for specimens with 30M rods.

Table 4.15: Comparison of 5th-percentile values.

d_{rod} (mm)	d_{grout} (mm)	f_{ys} (MPa)	$F_{y,0.05}$ Lognormal	$F_{y,0.05}$ Bayesian	$F_{max,0.05}$ Lognormal	$F_{max,0.05}$ Bayesian
20	40	528.6	59.3	42.7	82.2	62.8
	60		78.9	62.3	103.8	90.2
	80		87.5	81.8	119.7	117.4
	40	733.5	87.5	67.7	97.9	74.6
	60		108.1	87.4	124.9	101.9
	80		100.5	106.9	129.0	129.2
24	48	528.6	96.3	83.9	104.2	96.7
	72		108.1	107.4	134.5	129.5
	96		119.8	130.8	163.4	162.2
	48	733.5	104.5	108.8	115.3	108.3
	72		133.8	132.3	137.7	141.2
	96		139.7	155.7	157.4	173.9
30	60	528.6	139.7	145.3	141.5	147.2
	90		179.9	174.7	187.2	188.3
	120		222.6	203.9	255.6	229.1

4.8 Reliability Analysis

The goal of the reliability analysis is to establish a resistance factor ϕ that corresponds to an appropriate reliability index β. A reliability index is considered appropriate if it is similar to those currently in use in codes and if it is relatively consistent across different combinations of design variables. As discussed in Section 2.3, a target reliability of approximately 3.5 is desired.

The performance functions for the reliability analysis have been previously established as:

$$G_y = F_y - \phi \frac{F_{y,0.05}}{1.25\gamma + 1.50}(d\gamma + q) \tag{4.3}$$

and

$$G_{max} = F_{max} - \phi \frac{F_{max,0.05}}{1.25\gamma + 1.50}(d\gamma + q) \tag{4.4}$$

The lognormal distributions for F_y and F_{max} were defined by their average and standard deviation and the distributions for d and q were defined by Foschi et al. (1989), as summarized in Table 2.1. The values for the characteristic yield and maximum shear resistance were taken from Table 4.15 from the columns titled "Lognormal."

The plots drawn from the reliability analyses are given in Figure 4.21 and Figure 4.22 for yield resistance and maximum shear resistance, respectively. Each point represents the β value for a given set of design variables.

From Table 4.16 and Table 4.17, it can be seen that a ϕ value of 0.8 results in an average β of approximately 3.5. This is not only the target reliability index previously established, but a ϕ of 0.8 is the same resistance factor stipulated in CSA-O86 for dowel-type fasteners failing in yielding, further substantiating this result. Not only does this mean that the connector has a similar safety level as existing connectors, but has a consistent level of safety for all combinations of tested design variables.

Table 4.16: Results of the reliability analysis for yield resistance.

Rod Dia.	Steel Str.-Class	Grout Dia.	$F_{y,0.05}$ (kN)	ϕ 0.5	0.6	0.7	0.8	0.9	1
20 mm	4.8	2x	59.3	5.35	4.68	4.13	3.66	3.24	2.86
		3x	78.9	5.32	4.60	4.01	3.51	3.06	2.66
		4x	87.5	5.37	4.66	4.08	3.57	3.13	2.73
	8.8	2x	87.5	5.34	4.63	4.04	3.53	3.09	2.69
		3x	108.1	5.31	4.59	4.00	3.49	3.04	2.63
		4x	100.5	5.38	4.73	4.19	3.72	3.31	2.94
24 mm	4.8	2x	96.3	5.32	4.59	3.99	3.48	3.03	2.62
		3x	108.1	5.37	4.66	4.07	3.57	3.12	2.72
		4x	119.8	5.29	4.57	3.97	3.46	3.01	2.60
	8.8	2x	104.5	5.39	4.67	4.09	3.58	3.14	2.74
		3x	133.8	5.33	4.62	4.03	3.53	3.08	2.68
		4x	139.7	5.41	4.72	4.14	3.66	3.22	2.83
30 mm	4.8	2x	139.7	5.34	4.63	4.04	3.54	3.10	2.70
		3x	179.9	5.33	4.61	4.01	3.51	3.06	2.65
		4x	222.6	5.33	4.61	4.01	3.50	3.05	2.65
			Average	**5.34**	**4.64**	**4.05**	**3.55**	**3.11**	**2.71**

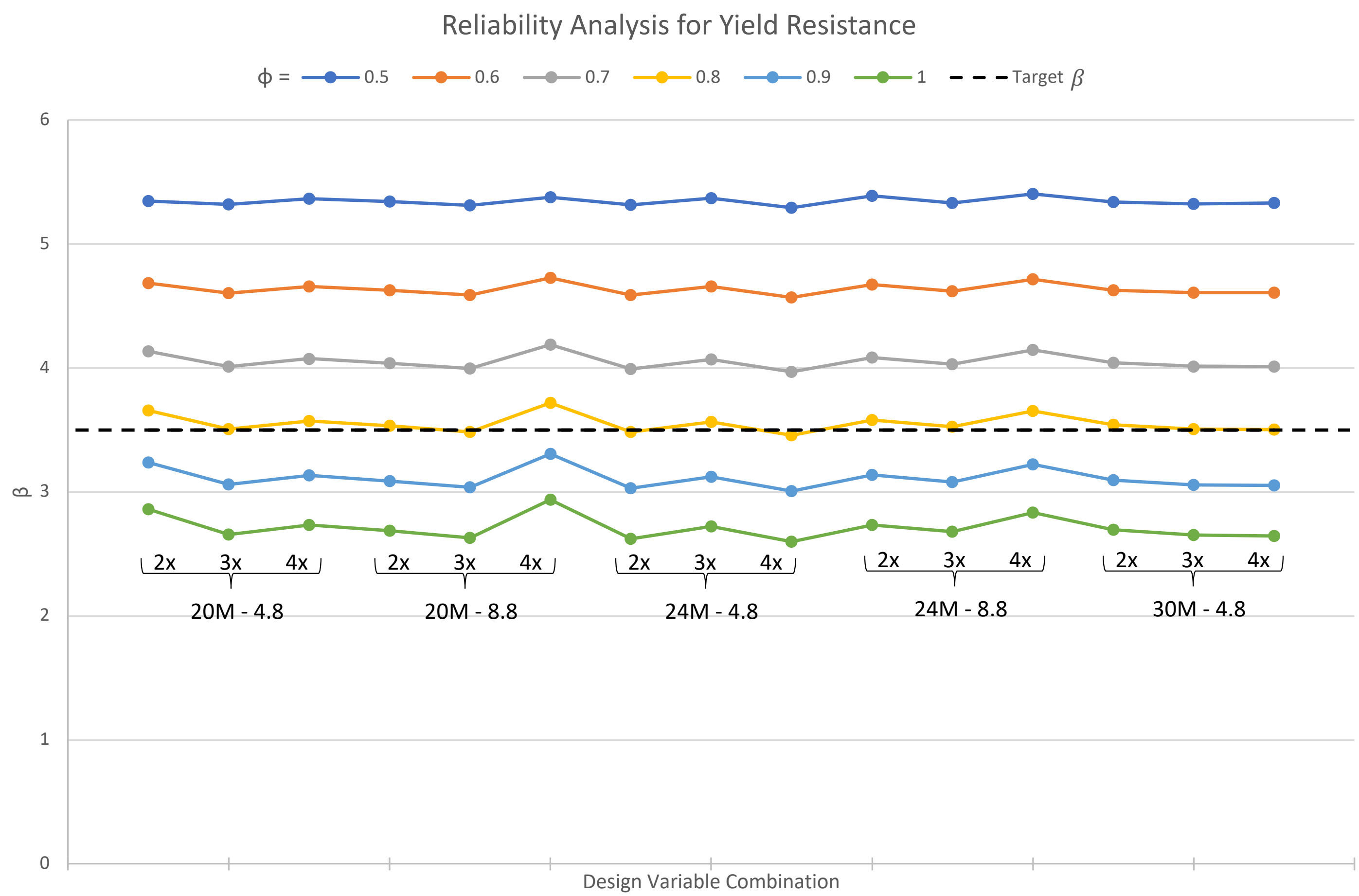

Figure 4.21: $\phi - \beta$ relationship for yield resistance.

Table 4.17: Results of the reliability analysis for maximum shear resistance.

Rod Dia.	Steel Str.-Class	Grout Dia.	$F_{max,0.05}$ (kN)	ϕ 0.5	0.6	0.7	0.8	0.9	1
20 mm	4.8	2x	82.2	5.35	4.64	4.04	3.54	3.09	2.69
		3x	103.8	5.31	4.59	3.99	3.48	3.03	2.62
		4x	119.7	5.26	4.52	3.92	3.40	2.95	2.53
	8.8	2x	97.9	5.34	4.63	4.03	3.53	3.08	2.68
		3x	124.9	5.28	4.55	3.95	3.43	2.98	2.57
		4x	129.0	5.38	4.70	4.13	3.65	3.22	2.83
24 mm	4.8	2x	104.2	5.34	4.63	4.04	3.53	3.09	2.68
		3x	134.5	5.35	4.63	4.04	3.53	3.09	2.68
		4x	163.4	5.19	4.45	3.85	3.33	2.87	2.45
	8.8	2x	115.3	5.26	4.52	3.92	3.40	2.95	2.53
		3x	137.7	5.32	4.60	4.01	3.51	3.06	2.66
		4x	157.4	5.36	4.65	4.07	3.57	3.12	2.72
30 mm	4.8	2x	141.5	5.34	4.63	4.05	3.55	3.10	2.70
		3x	187.2	5.33	4.61	4.01	3.50	3.05	2.65
		4x	255.6	5.29	4.56	3.96	3.45	2.99	2.58
			Average	**5.31**	**4.59**	**4.00**	**3.49**	**3.04**	**2.64**

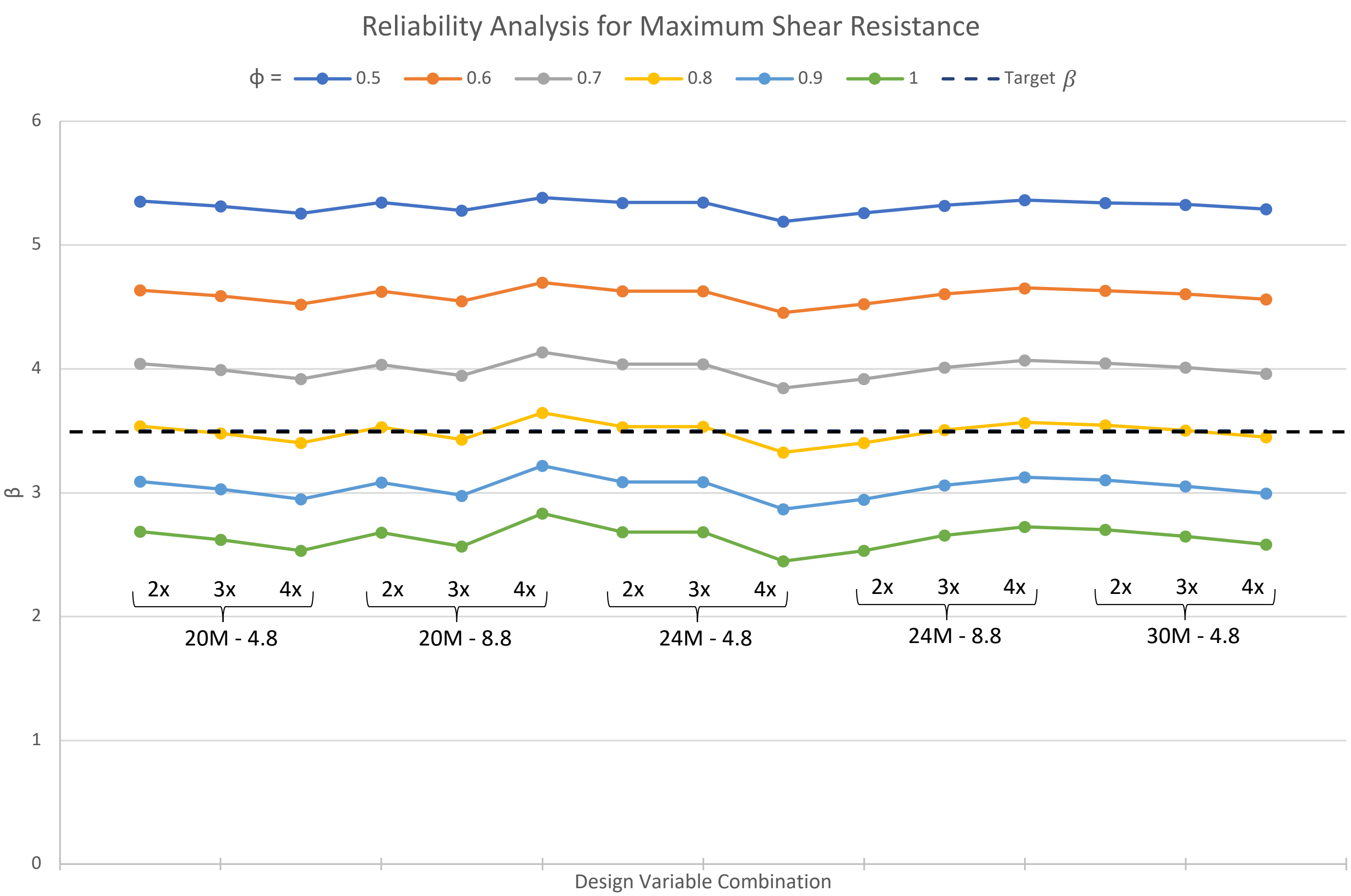

Figure 4.22: $\phi - \beta$ relationship for maximum shear resistance.

Chapter 5

Conclusions, Limitations, and Future Work

This chapter provides a summary of the work completed and puts forth the primary conclusions of the thesis as well as recommendations for future work.

5.1 Summary and Conclusions

In this thesis, a novel type of shear connector for tall mass timber buildings was developed and tested. The intended application of the connector was in forming hybrid timber-steel floor or shearwall systems, in which the connectors are designed to remain elastic, resulting in no damage to the wood and allowing for deconstruction and potential reuse. The connector consisted of a threaded rod embedded in CLT and surrounded by a layer of epoxy-based grout. Various combinations of rod diameter, grout diameter, rod strength-class, and CLT grade were tested. Monotonic tests were conducted in a double-shear configuration on single-rod specimens in order to determine the mechanical properties of the connectors. The failure modes and load-deformation behaviour of the specimens were assessed and statistical analyses were conducted to quantify the impact of each design variable on the structural performance of the connector. Finally, a reliability analysis was carried out to establish a resistance factor for the connector and ensure a similar level of safety as with existing dowel-type connectors.

Before testing and determining structural performance, the first part of the objective of this thesis was to develop the connector. This included selecting geometric constraints, acquiring materials, and fabricating the specimens. Though this portion of the research does not result in any quantifiable conclusions, it did provide valuable insight into the feasibility of the connector. Respecting codified limitations on bolt edge spacing, connectors of a reasonable size were developed for various combinations of design variables. The materials used in the connector were all acquired locally from manufacturers in British Columbia and required no custom or specialized manufacturing. All of the materials were processed using typical equipment that most fabricators would have in-house. The fabrication of the specimens themselves was done by the author and one other graduate student in batches of 30 to 45 specimens at a time. The biggest challenge in fabrication was working within the hardening time of the grout mixture, though at no point did the grout harden to such an extent that fabrication had to be halted before completion. Though working in-situ is more complicated than working in a lab, it is feasible to suggest that pouring the grout could be done on-site by a team of two or three fabricators. However, the fabrication process lends itself more toward off-site prefabrication in a controlled environment. At a large scale, the process may even be automated.

Focusing on the results of the testing program, the structural performance of the connector was assessed. First, it has been shown that the grout-reinforced connector offers significantly higher stiffness and load-carrying capacity as compared to typical dowel-type connectors. These are both desirable properties in capacity-protected connectors. Importantly, the increase in these values does not come at the expense of ductility, which is vital in the typical design of timber connectors in which they are designed to deform plastically. In general, the grout-reinforced connector has been shown to be moderately ductile, even considering those specimens that failed before the target displacement. Thus, this connector is suitable for both capacity-design and traditional design scenarios.

The load-deformation curves showed that the specimens generally exhibited either a primarily wood-crushing behaviour (characterized by a decrease in capacity after yielding) or a behaviour combining wood-crushing and steel hinging (characterized by a plateau after yielding). In general, the larger the rod and grout diameter, the more pronounced the wood-crushing behaviour became. Regardless of post-yield behaviour, the majority of specimens did not fail before the 15 mm target displacement, save for those with a slender rod combined with a thick grout layer.

From both visual observations of the load-deformation curves as well as a linear regression analysis, it was determined that the grade of CLT was not a significant contributor to the connector's load-carrying capacity. It has been suggested that the random sectioning of the CLT panels and the resulting random distribution of defects in the load-path essentially obscure any fundamental differences between E grade and V grade CLT. This, however, is not necessarily true at the system scale, and only applies to the small-scale samples tested here.

As for the other design variables, it was concluded that the yield resistance of the shear connector was primarily determined by rod diameter, with some influence from grout diameter, and a small influence from the rod's steel strength-class. Maximum shear resistance, on the other hand, was primarily determined by grout diameter, then to a lesser extent, by rod diameter. Stiffness was primarily a function of rod diameter.

Models for yield resistance and maximum shear resistance were developed by means of a Bayesian linear regression analysis. However, these were shown not be as good a fit as a lognormal distribution fit to each design arrangement. The resulting lognormal distributions and corresponding 5th-percentile values were implemented in a reliability analysis using FORM. From these analyses, it has been concluded that a resistance factor of $\phi = 0.8$ is appropriate for use for both yield and maximum shear resistance. Not only does this provide a similar level of safety across combinations of design variables, but also provides a similar level of reliability as with typical dowel-type connectors.

5.2 Design Recommendations

For application in capacity-design, all of the tested combinations of design parameters are appropriate as they all exhibit high yield resistance and stiffness. Connection design consists of selecting a combination of design variables with sufficient 5th-percentile yield resistance and then designing the connected energy dissipating device to yield before this load is reached, ensuring the connector itself remains elastic.

For use as a traditional plastic fastener, it is suggested to avoid combinations involving low-strength steel rods with very thick grout layers. Specifically 20M and 24M strength-class 4.8 rods with a grout diameter four times the rod diameter should be avoided. Since yield resistance and stiffness are mainly governed by rod diameter, it is suggested to first select rod diameter to satisfy serviceability criteria. Since maximum shear resistance is mainly governed by grout diameter, the ultimate limit state criteria may then be satisfied by then selecting an appropriate grout diameter.

The 5th-percentile values for yield and maximum shear resistance have been presented as design values. These are only applicable to the specific combinations of design parameters tested in this campaign and only under monotonic short-term loading. More testing as well as mechanics-based modelling is required to produce more generalized results for use in practice.

5.3 Recommendations for Future Work

Though over 200 tests were conducted on 30 different types of specimens, the experimental program had its limitations in terms of both design and procedure. First of all, because the design models are empirical, they are only valid for connectors with combinations of design variables tested. Mechanics-based or finite element modelling would be required to develop reliable design equations for grout-reinforced connectors outside the scope of this study.

In terms of specimens, they were all fabricated from 3-ply panels CLT of similar densities. Further testing would be required to assess the impact of connector thickness and wood density on the performance. Similarly, all specimens had rods installed perpendicular to their face, whereas it may be of interest to investigate different angles of insertion, as has been done for self-tapping screws (Loss et al., 2018), both in terms of constructability and performance.

The testing program was limited in that it consisted only of monotonic tests. To develop a better understanding of the dynamic behaviour and energy-dissipation potential of the connector, cyclic testing should be conducted. Additionally, specimens were only tested in the direction of the grain of the CLT outer layers, whereas testing perpendicular to the grain and possibly at intermediate angles would be required to develop design equations incorporating the direction of load.

Due to the nature of the test setup, specimens were restricted from exhibiting brittle wood failure modes, like those specified for dowel-type connectors in CSA Group (2014*a*). In order to assess potential brittle failure modes, specimens would need to be tested in a pull-out configuration rather than a push-out configuration.

Finally, only single-rod specimens were tested. Future work should test full-scale systems of multiple connectors to assess any potential group effect, load-sharing characteristics, or potential brittle failure modes such as group tear-out.

The research presented in this thesis serves as the inauguration of a larger research project with the aim of developing a robust understanding of this connector and systems that are made up of these connectors, leading to design equations for inclusion in the Canadian standard for wood design, CSA-O86. As such, there remains much work to be done to achieve this final goal. The results of this preliminary study are to inform future work in this large-scale research project.

Specifically, future work will include cyclic testing of test specimens as well as full-scale testing of structural systems including hybrid CLT-steel floors and CLT shear walls. In addition to more testing, mechanics-based and finite element modelling will be undertaken in order to develop general design equations for the connector. Additionally, further reliability analyses may be conducted considering different live loads to ensure that 0.8 is an appropriate resistance factor for this connector for various load combinations.

Bibliography

Andersen, M. and Høier, M. (2016), Glued-in rods in cross laminated timber, Master's thesis, Aarhus University, Aarhus,Denmark. → page 24

ANSI/APA PRG 320 (2012), Standard for Performance-Rated Cross-Laminated Timber, Standard, APA - The Engineered Wood Association, Tacoma, WA. → page 30

APA PR-L314 (2021), Structurlam crosslam, Product report, APA - The Engineered Wood Association, Tacoma, WA. → page 30

Arup (2019), *Rethinking Timber Buildings*, Arup, London. → pages 1, 2, 5

ASTM D5764 (2018), Standard Test Method for Evaluating Dowel-Bearing Strength of Wood and Wood-Based Products, Standard, ASTM International, West Conshohocken, PA. → pages 39, 40, 43

ASTM E8/E8M (2021), Test Methods for Tension Testing of Metallic Materials, Standard, ASTM International, West Conshohocken, PA. → page 32

Azinović, B., Serrano, E., Kramar, M. and Pazlar, T. (2018), 'Experimental investigation of the axial strength of glued-in rods in cross laminated timber', *Materials and Structures* **51**(6), 143. → page 24

Blaß, H. J. and Sandhaas, C. (2017), *Timber Engineering - Principles for Design*, KIT Scientific Publishing, Karlsruhe, Germany. → pages 19, 20

Breneman, S., Timmers, M. and Richardson, D. (2019), Tall Wood Buildings in the 2021 IBC Up to 18 Stories of Mass Timber, Report, WoodWorks. → page 8

Canadian Wood Council (2004), Energy and the Environment in Residential Construction, No. 1, Canadian Wood Council, Ottawa, ON. → page 3

CSA Group (2014*a*), *CSA O86-14: Engineering Design in Wood*, CSA Group, Mississauga, ON. → pages 10, 17, 110

CSA Group (2014*b*), *CSA S16-14: Design of Steel Structures*, CSA Group, Mississauga, ON. → page 38

CSA SP S408-1981 (1981), Guide for the development of limit states design, Special publication, CSA - Canadian Standards Association, Rexdale, ON. → page 28

Cuerrier-Auclair, S. (2020), *Design Guide for Timber-Concrete Composite Floors in Canada*, FP Innovations, Pointe-Claire, QC. → page 23

Davis, T. J. and Claisse, P. A. (2001), 'Resin-injected dowel joints in glulam and structural timber composites', *Construction and Building Materials* **15**(4), 157–167. → pages 24, 31

Dujic, B., Aicher, S. and Zarnic, R. (2006), Testing of wooden wall panels applying realistic boundary conditions, *in* 'Proceedings of the 9th World Conference on Timber Engineering', Portland, Oregon. → page 10

Earle, J., Ergun, D. and Gorgolewski, M. (2014), 'Barriers for Deconstruction and Reuse/Recycling of Construction Materials in Canada', p. 18. → pages 5, 6

Ehlbeck, J. and Larsen, H. J. (1993), Eurocode 5 - Design of timber structures: Joints, *in* 'Proceedings of the International Workshop on Wood Connectors', Forest Products Society, Madison, WI, pp. 9–23. → page 22

EN 12512 (2001), Timber structures - Test methods - Cyclic testing of joints made with mechanical fasteners, Technical Report Standard, European Committee for Standardization (CEN), Brussels, Belgium. → page 44

EN 1995-1-1 (2004), *Eurocode 5: Design of timber structures - Part 1-1: General - Common rules and rules for buildings*, European Committee for Standardization (CEN), Brussels, Belgium. → page 22

EN 26891 (1991), Timber structures – Joints made with mechanical fasteners – General principles for the determination of strength and deformation characteristics, Standard, European Committee for Standardization (CEN), Brussels, Belgium. → page 43

EN 383 (2007), Timber structures – Test methods - Determination of embedding strength and foundation values for dowel type fasteners, Standard, European Committee for Standardization (CEN), Brussels, Belgium. → page 37

FAO (2016), *Global forest resources assessment 2015: how are the world's forests changing?*, 2nd edn, Food and Agriculture Organization of the United Nations, Rome. → page 3

Foschi, R., Folz, B. and Yao, F. (1989), Reliability-Based Design of Wood Structures, Technical Report 34, University of British Columbia, Vancouver. → pages 25, 27, 28, 52, 100

Gavric, I., Fragiacomo, M., Popovski, M. and Ceccotti, A. (2014), Behaviour of Cross-Laminated Timber Panels under Cyclic Loads, *in* S. Aicher, H.-W. Reinhardt and H. Garrecht, eds, 'Materials and Joints in Timber Structures', Springer Netherlands, Dordrecht, pp. 689–702. → page 10

Guy, B. and McLendon, S. (2000), Building Deconstruction: Reuse and Recycling of Building Materials, Report to the Florida Department of Environmental Protection, Powell Center for Construction and Environment, University of Florida, Gainesville. → page 6

Guy, B., Shell, S. and Esherick, H. (2006), Design For Deconstruction and Materials Reuse, *in* 'Proceedings of the CIB Task Group 39', Vol. 4, pp. 189–209. → pages 5, 6

Hart-Smith, L. J. (1985), 'Bonded-bolted composite joints', *Journal of Aircraft* **22**(11), 993–1000. → page 24

Hunger, F., Stepinac, M., Rajčić, V. and van de Kuilen, J.-W. G. (2016), 'Pull-compression tests on glued-in metric thread rods parallel to grain in glulam and laminated veneer lumber of different timber species', *European Journal of Wood and Wood Products* **74**(3), 379–391. → page 24

IPCC (2007), *Climate change 2007: Mitigation of Climate Change: Contribution of Working Group III to the Fourth Assessment Report of the Intergovernmental Panel on Climate Change*, Cambridge University Press, New York. → page 4

Johansen, K. W. (1949), 'Theory or timber connections', *International Association for Bridge and Structural Engineering* **9**, 249–262. → page 15

Karacabeyli, E. and Gagnon, S., eds (2019), *Canadian CLT Handbook*, 2019 edn, FPInnovations, Pointe-Claire, QC. → page 11

Kennedy, S., Salenikovich, A., Munoz, W., Mohammad, M. and Sattler, D. (2014), Design Equations for Embedment Strength of Wood For Threaded Fasteners in the Canadian Timber Design Code, *in* 'Proceedings of the 13th World Conference on Timber Engineering', Quebec City. → page 17

Larsen, H. J. (1973), The Yield Load of Bolted and Nailed Joints, *in* 'Proceedings of the International Union of Forestry Research Organization', Cape Town, South Africa. → page 16

Loss, C., Hossain, A. and Tannert, T. (2018), 'Simple cross-laminated timber shear connections with spatially arranged screws', *Engineering Structures* **173**, 340–356. → page 109

Loss, C., Piazza, M. and Zandonini, R. (2016), 'Connections for steel–timber hybrid prefabricated buildings. Part I: Experimental tests', *Construction and Building Materials* **122**, 781–795. → page 23

Mahsuli, M. and Haukaas, T. (2013), 'Computer Program for Multimodel Reliability and Optimization Analysis', *Journal of Computing in Civil Engineering* **27**(1), 87–98. → page 53

Massé, D. I. and Salinas, J. J. (1989), 'Structural reliability of nailed connections', *Canadian Agricultural Engineering* **31**, 195–203. → page 28

Michael Green Architecture (2020), *The Case For Tall Wood Buildings*, 2nd edn, Blurb, Vancouver. → pages 2, 5

naturally:wood (2016), 'Brock Commons Tall Wood Building Factsheet'. → page 22

Popovski, M., Schneider, J. and Schweinsteiger, M. (2010), Lateral Load Resistance of Cross-Laminated Wood Panels, *in* 'Proceedings of the 11th World Conference on Timber Engineering', Riva del Garda, Italy. → page 10

Riberholt, H. (1986), Glued bolts in glulam, *in* 'Proceedings of the 19th Conference of the CIB Working Commission W18 - Timber Structures', Florence, Italy. → page 24

Richardson, A., ed. (2013), *Reuse of Materials and Byproducts in Construction*, Green Energy and Technology, Springer, London. → page 6

Ringhofer, A., Brandner, R. and Blaß, H. J. (2017), Design Approaches for Dowel-Type Connections in CLT Structures and their Verification, *in* R. Brandner, A. Ringhofer and P. Dietsch, eds, 'Proceedings of the Conference of COST Action FP1402: International Conference on Connections in Timber Engineering – From Research to Standards', Graz, pp. 80–111. → page 17

Rodd, P. D., Hilson, B. O. and Spriggs, R. A. (1989), Resin injected mechanically fastened timber joints, *in* 'Proceedings of the 2nd Pacific Timber Engineering Conference', Auckland. → page 24

Röck, M., Saade, M. R. M., Balouktsi, M., Rasmussen, F. N., Birgisdottir, H., Frischknecht, R., Habert, G., Lützkendorf, T. and Passer, A. (2020), 'Embodied

GHG emissions of buildings – The hidden challenge for effective climate change mitigation', *Applied Energy* **258**, 114107. → page 3

Schober, K.-U. and Tannert, T. (2016), 'Hybrid connections for timber structures', *European Journal of Wood and Wood Products* **74**(3), 369–377. → pages 22, 23

Smith, I., Asiz, A., Snow, M. and Chui, Y. H. (2006), Possible Canadian/ISO approach to deriving design values from test data, *in* 'Proceedings of the 39th CIB-W18 Meeting', Florence. → pages xi, 44, 84

Smith, I. and Snow, M. A. (2008), 'Timber: An ancient construction material with a bright future', *The Forestry Chronicle* **84**(4), 504–510. → page 2

Soltis, L. A., Hubbard, F. K. and Wilkinson, T. L. (1986), 'Bearing Strength of Bolted Timber Joints', *Journal of Structural Engineering* **112**(9), 2141–2154. → page 16

Sorensen, J. (2019), '2020 NBCC code brings new era for Canadian wood construction', *Journal of Commerce* . → page 7

Steiger, R., Gehri, E. and Widmann, R. (2007), 'Pull-out strength of axially loaded steel rods bonded in glulam parallel to the grain', *Materials and Structures* **40**(1), 69–78. → page 24

Structurlam (2016), 'CrossLam CLT Design Guide v2.0 - Canada'. → page 30

Tannert, T. (2016), 'Improved performance of reinforced rounded dovetail joints', *Construction and Building Materials* **118**, 262–267. → page 23

Townsend, P. K. and Buchanan, A. H. (1990), Steel dowels epoxy bonded in glue laminated timber, Technical report, University of Canterbury, Department of Civil Engineering. → page 24

Trayer, G. W. (1932), *The bearing strength of wood under bolts*, Technical Bulletin No. 332, U.S. Dept of Agriculture. → page 15

Uibel, T. and Blaß, H. J. (2006), Load Carrying Capacity of Joints with Dowel Type Fasteners in Solid Wood Panels, *in* R. Görlacher, ed., 'Proceedings of the 39th CIB-W18 Meeting', Florence, p. 11. → pages 16, 17

United Nations Human Settlements Programme (2015), Housing at the Centre of the New Urban Agenda, Technical report, United Nations Human Settlements Programme, Nairobi. → page 3

Whale, L. R. J., Smith, I. and Larsen, H. J. (1987), Design of nailed and bolted joints proposals for the revision of existing formulae in draft Eurocode 5 and the CIB code, *in* CIB-W18, ed., 'Proceedings of the 20th CIB-W18 Meeting', Dublin, Ireland. → pages 16, 17

Ximenes, F. d. A., George, B. H., Cowie, A., Williams, J. and Kelly, G. (2012), 'Greenhouse Gas Balance of Native Forests in New South Wales, Australia', *Forests* **3**(3), 653–683. → pages 4, 5

Xu, Z., Smyth, C. E., Lemprière, T. C., Rampley, G. J. and Kurz, W. A. (2018), 'Climate change mitigation strategies in the forest sector: biophysical impacts and economic implications in British Columbia, Canada', *Mitigation and Adaptation Strategies for Global Change* **23**(2), 257–290. → page 4

Yeboah, D., Taylor, S., McPolin, D., Gilfillan, R. and Gilbert, S. (2011), 'Behaviour of joints with bonded-in steel bars loaded parallel to the grain of timber elements', *Construction and Building Materials* **25**(5), 2312–2317. → page 24

Appendix A

Fabrication Drawings

Test Apparatus

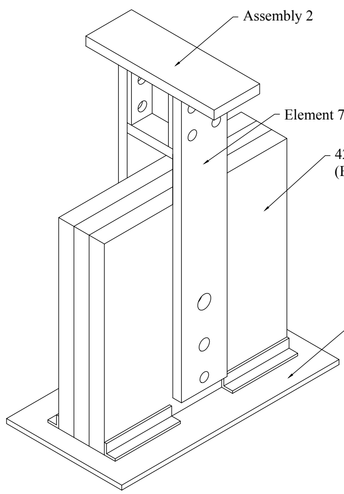

Assembly 1

Platform

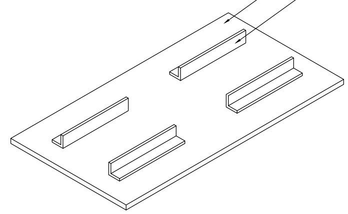

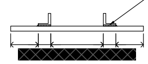

FRONT VIEW

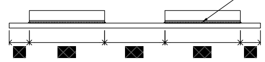

SIDE VIEW

Element 1

Rectangular plate 500x265x10

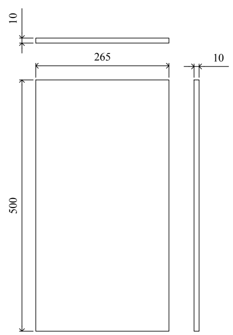

Element 2 (x4)

Angle 25x25x5

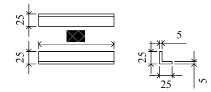

Element 7 (x2)

Loading Arm

Rectangular plate 600x105x20

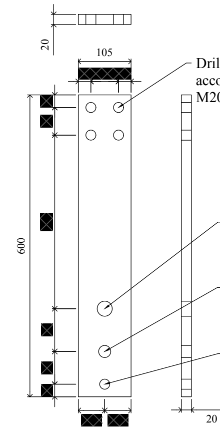

Notes:

Material Schedule

LIST OF ELEMENTS	Dimensions [mm x mm]	Thickness [mm]	Material	Quantity
Assembly 1				
Element 1, rectangular plate	500x265	10	G40.21 300W	1
Element 2, angle 25x25x5, [redacted]			G40.21 300W	4
Assembly 2				
Element 3, rectangular plate	105x105	10	G40.21 300W	2
Element 4, rectangular plate	105x85	10	G40.21 300W	1
Element 5, rectangular plate	105x105	20	G40.21 300W	1
Element 6, rectangular plate	295x105	20	G40.21 300W	1
Element 7				
Element 7, rectangular plate	600x105	20	G40.21 300W	2
Hardware				
M20 bolts, 50 mm length			A325	8
M20 nuts			A563 C	8
M20 washers conforming to ASTM F436				16

Assembly 2

Loading Box

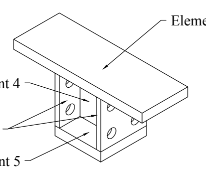

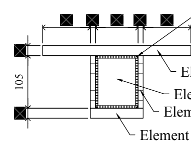

FRONT VIEW

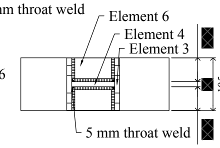

BOTTOM VIEW
(W/O ELEMENT 5)

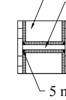

TOP VIEW
(W/O ELEMENT 6)

Element 3 (x2)

Rectangular plate 105x105x10

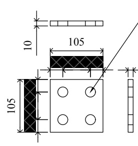

Element 4

Rectangular plate 105x85x10

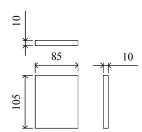

Element 5

Rectangular plate 105x105x20

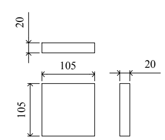

Element 6

Rectangular plate 295x105x20

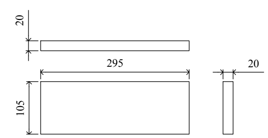

REV:	DESCRIPTION:	BY:	DATE:
A	FOR FABRICATION	SS	12/09/2020

UBC

Deconstructable Hybrid Connections for Prefabricated Mass Timber Buildings
PI Dr. Cristiano Loss
RA Samuel Shulman
Sustainable Engineered Structural Solutions Laboratory
Department of Wood Science
University of British Columbia

TITLE: TEST APPARATUS

SCALE AT A1:	DATE:	DRAWN:	CHECKED:
1:5	12/09/2020	SS	CL
PROJECT NO:	DRAWING NO:		REVISION:
SS-1	1		A

Material Schedule

LIST OF ELEMENTS	Diameter [mm]	Length [mm]	Material	Quantity
CLT Specimens	See CLT Specimen Table			
Threaded Steel Rods	20	250	4.8	90
	20	250	8.8	90
	24	250	4.8	90
	24	250	8.8	90
	30	250	4.8	90
	30	250	8.8	90
Hilti CB-G EG Epoxy Grout	59 lb. bucket			14
Sika UHPC Grout				TBD
Wooden Ring	40 o.d. / 20 i.d.	10	Wood	56
	60 o.d. / 20 i.d.	10	Wood	56
	80 o.d. / 20 i.d.	10	Wood	56
	48 o.d. / 24 i.d.	10	Wood	56
	72 o.d. / 24 i.d.	10	Wood	56
	96 o.d. / 24 i.d. .	10	Wood	56
	60 o.d. / 30 i.d.	10	Wood	56
	90 o.d. / 30 i.d.	10	Wood	56
	120 o.d. / 30 i.d.	10	Wood	56
Wooden Rails	72.5 x 50 x Length TBD		Wood	2
Paper Tape				
Paper Towel				
Compressed Air				
Steel Rod Cleaning/Degreasing Solvent				

CLT Specimens

SPECIMENS	b [mm]	D [mm]	d [mm]	Grade	Quantity
TYPE A: 280x280x105					
A1-E	280	40	20	E	28
A1-V	280	40	20	V	28
A2-E	280	60	20	E	28
A2-V	280	60	20	V	28
A3-E	280	80	20	E	28
A3-V	280	80	20	V	28
TYPE B: 340x340x105					
B1-E	340	48	24	E	28
B1-V	340	48	24	V	28
B2-E	340	72	24	E	28
B2-V	340	72	24	V	28
B3-E	340	96	24	E	28
B3-V	340	96	24	V	28
TYPE C: 420x420x105					
C1-E	420	60	30	E	28
C1-V	420	60	30	V	28
C2-E	420	90	30	E	28
C2-V	420	90	30	V	28
C3-E	420	120	30	E	28
C3-V	420	120	30	V	28

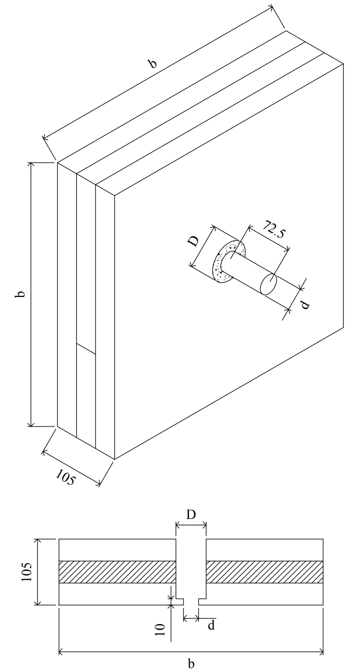

Scale 1:4

Specimen Fabrication Procedure

1) Clean/degrease rod with solvent and clean hole in CLT with compressed air.

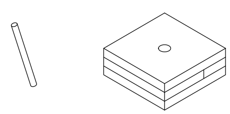

2) Place CLT specimen on wooden rails such that the face with the smaller diameter hole is facing down.

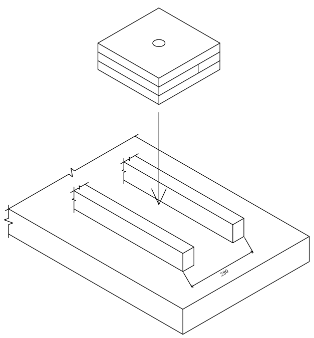

3) Place rod through hole in CLT until it rests on the top of the work surface.

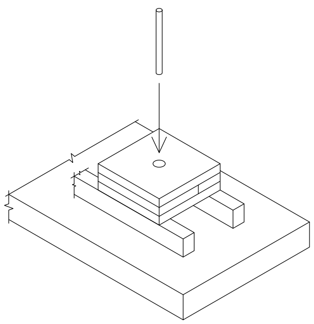

4) Fill gap between rod and CLT with grout.

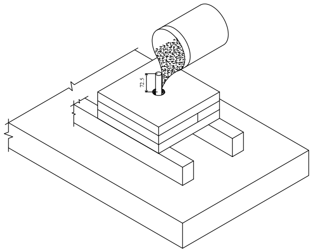

5) Place wooden ring around rod and press it down until it is flush with the CLT face. Let cure for at least 2 hours before moving to long-term storage for at least 7 days.

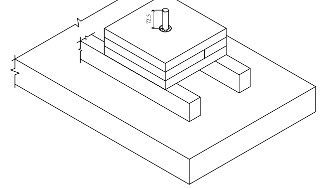

Scale 1:10

Notes:

REV:	DESCRIPTION:	BY:	DATE:
A	FOR FABRICATION	SS	23/09/2020

Deconstructable Hybrid Connections for Prefabricated Mass Timber Buildings
PI Dr. Cristiano Loss
RA Samuel Shulman
Sustainable Engineered Structural Solutions Laboratory
Department of Wood Science
University of British Columbia

TITLE: SPECIMEN FABRICATION

SCALE AT A1:	DATE:	DRAWN:	CHECKED:
VAR.	23/09/2020	SS	CL

PROJECT NO:	DRAWING NO:	REVISION:
SS-1	2	A

PRODUCED BY AN AUTODESK STUDENT VERSION
PRODUCED BY AN AUTODESK STUDENT VERSION

CLT Specimens

SPECIMENS	b [mm]	D [mm]	d [mm]	Grade	Quantity
TYPE A: 280x280x105					
A1-E	280	40	20	E	28
A1-V	280	40	20	V	28
A2-E	280	60	20	E	28
A2-V	280	60	20	V	28
A3-E	280	80	20	E	28
A3-V	280	80	20	V	28
TYPE B: 340x340x105					
B1-E	340	48	24	E	28
B1-V	340	48	24	V	28
B2-E	340	72	24	E	28
B2-V	340	72	24	V	28
B3-E	340	96	24	E	28
B3-V	340	96	24	V	28
TYPE C: 420x420x105					
C1-E	420	60	30	E	28
C1-V	420	60	30	V	28
C2-E	420	90	30	E	28
C2-V	420	90	30	V	28
C3-E	420	120	30	E	28
C3-V	420	120	30	V	28

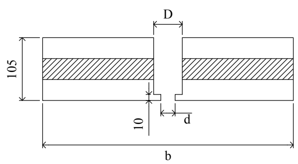

TYPE A: 280x280x105

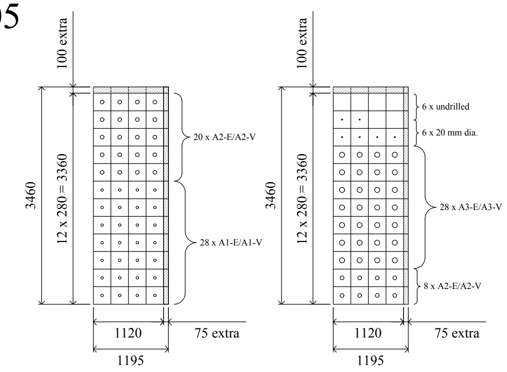

(a) CLT Panel A1(E) & A1(V)

(b) CLT Panel A2(E) & A2(V)

TYPE B: 340x340x105

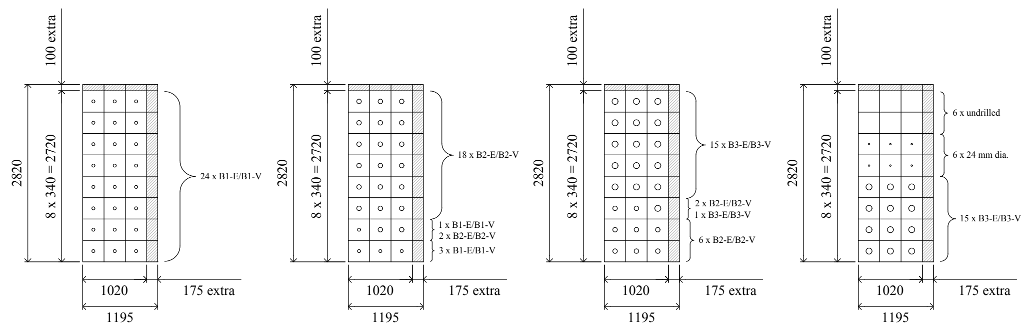

(c) CLT Panel B1(E) & B1(V)

(d) CLT Panel B2(E) & B2(V)

(e) CLT Panel B3(E) & B3(V)

(f) CLT Panel B4(E) & B4(V)

TYPE C: 420x420x105

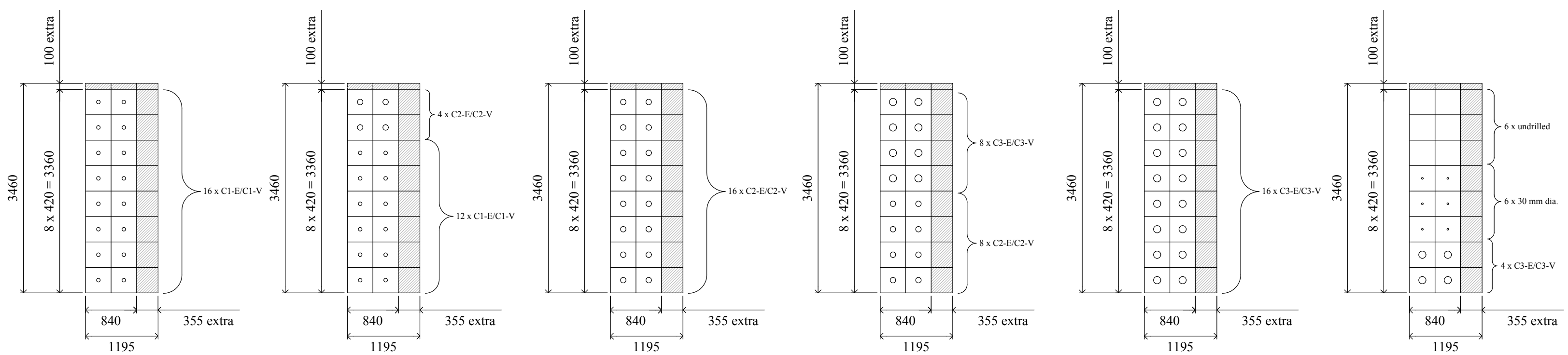

(g) CLT Panel C1(E) & C1(V)

(h) CLT Panel C2(E) & C2(V)

(h) CLT Panel C3(E) & C3(V)

(j) CLT Panel C4(E) & C4(V)

(j) CLT Panel C5(E) & C5(V)

(k) CLT Panel C6(E) & C6(V)

Notes:

REV:	DESCRIPTION:	BY:	DATE:
A	FOR FABRICATION	SS	24/09/2020

Deconstructable Hybrid Connections for Prefabricated Mass Timber Buildings

PI Dr. Cristiano Loss
RA Samuel Shulman

Sustainable Engineered Structural Solutions Laboratory
Department of Wood Science
University of British Columbia

TITLE: CLT DRILLING PATTERNS

SCALE AT A1:	DATE:	DRAWN:	CHECKED:
1:40	24/09/2020	SS	CL
PROJECT NO:	DRAWING NO:		REVISION:
SS-1	3		A

PRODUCED BY AN AUTODESK STUDENT VERSION
PRODUCED BY AN AUTODESK STUDENT VERSION
PRODUCED BY AN AUTODESK STUDENT VERSION

Appendix B

Specimen Fabrication Procedure

Figure B.1: CLT panel in Hundegger.

Figure B.2: CLT cut and drilled into specimens.

Figure B.3: Labelled Specimens.

Figure B.4: Cutting steel rods into four equal lengths of 250 mm.

Figure B.5: Plywood rings in the laser cutter.

Figure B.6: Specimens with rods inserted, ready for grout.

Figure B.7: Mixing grout.

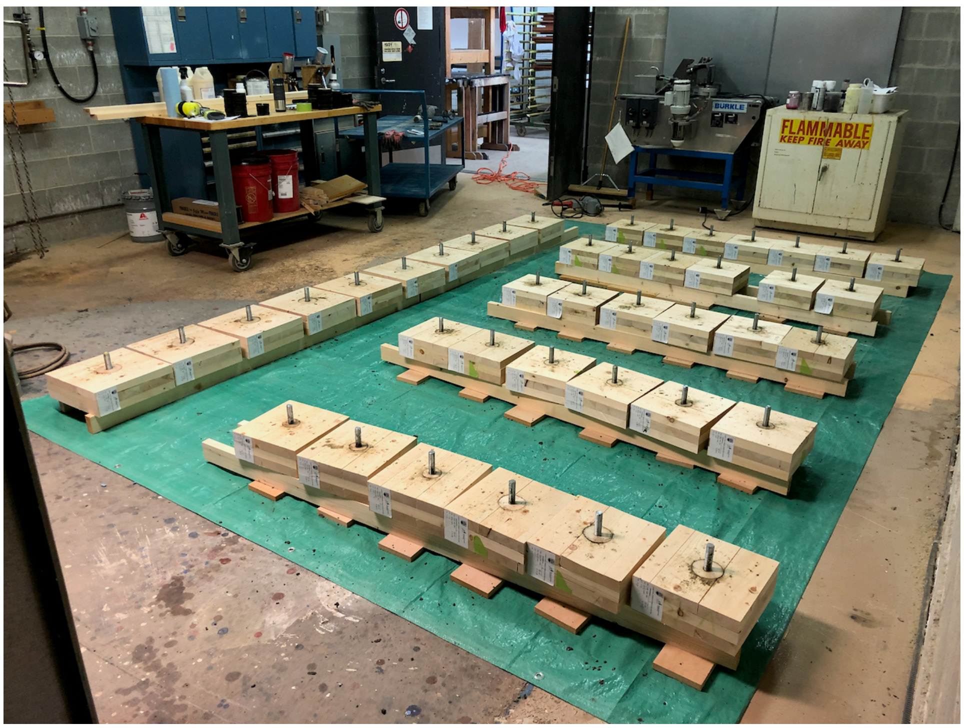

Figure B.8: Specimens curing after grout fill and placement of rings.

Appendix C

Load-Deformation Curves

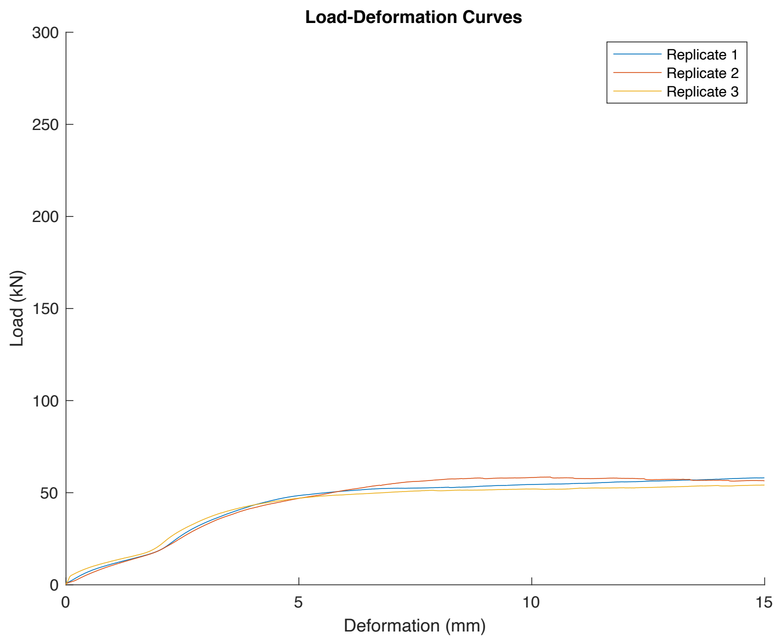

Figure C.1: d = 20M, 4.8 steel, E CLT, no grout

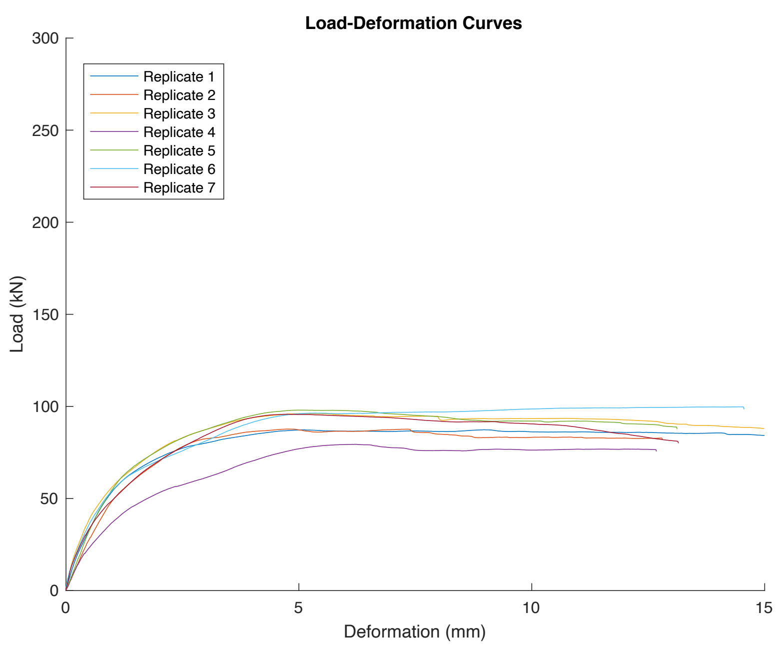

Figure C.2: d = 20M, 4.8 steel, E CLT, D = 2d

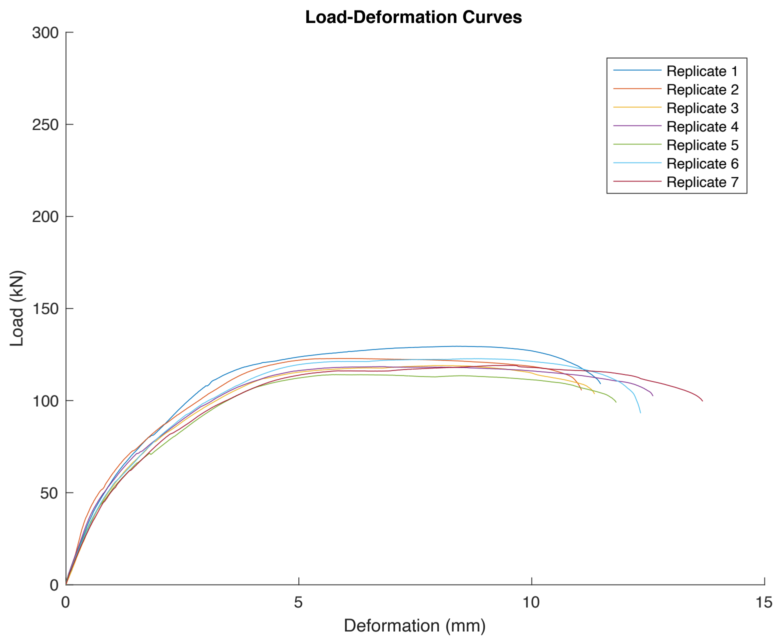

Figure C.3: d = 20M, 4.8 steel, E CLT, D = 3d

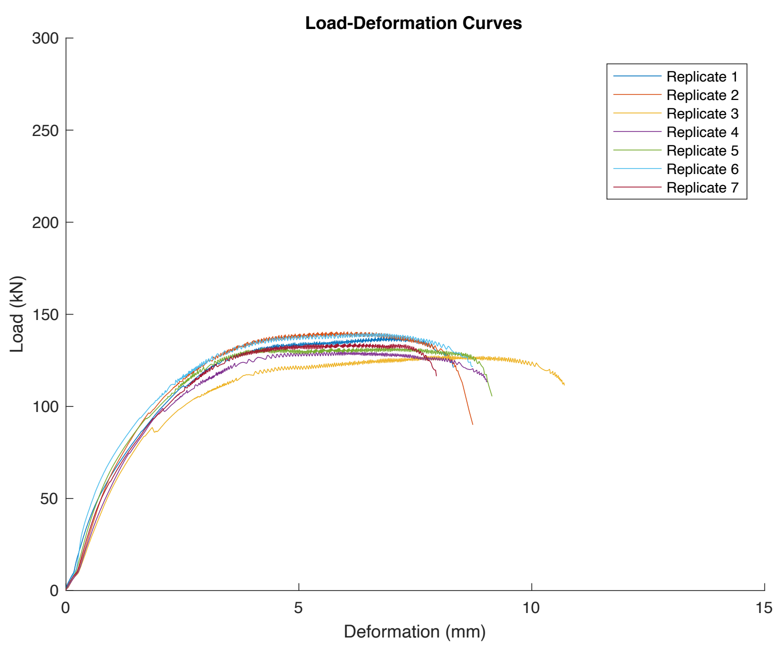

Figure C.4: d = 20M, 4.8 steel, E CLT, D = 4d

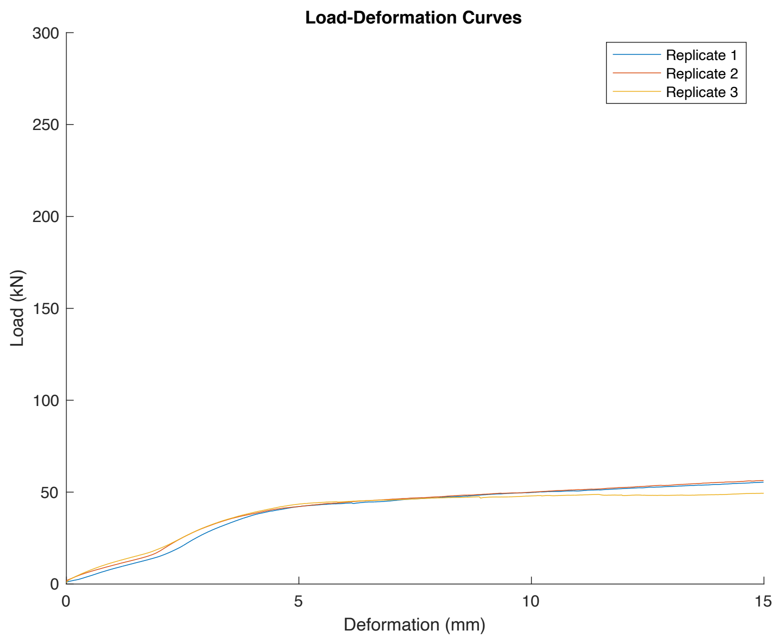

Figure C.5: d = 20M, 4.8 steel, V CLT, no grout

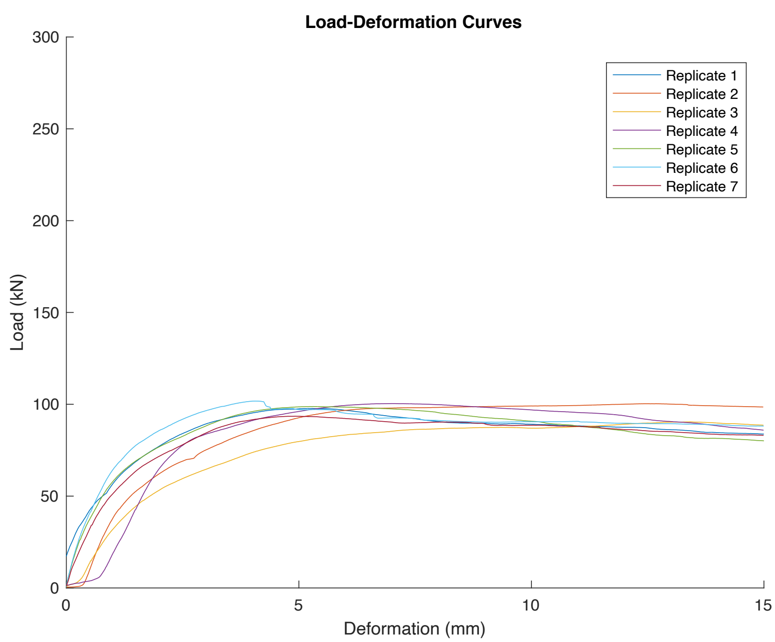

Figure C.6: d = 20M, 4.8 steel, V CLT, D = 2d

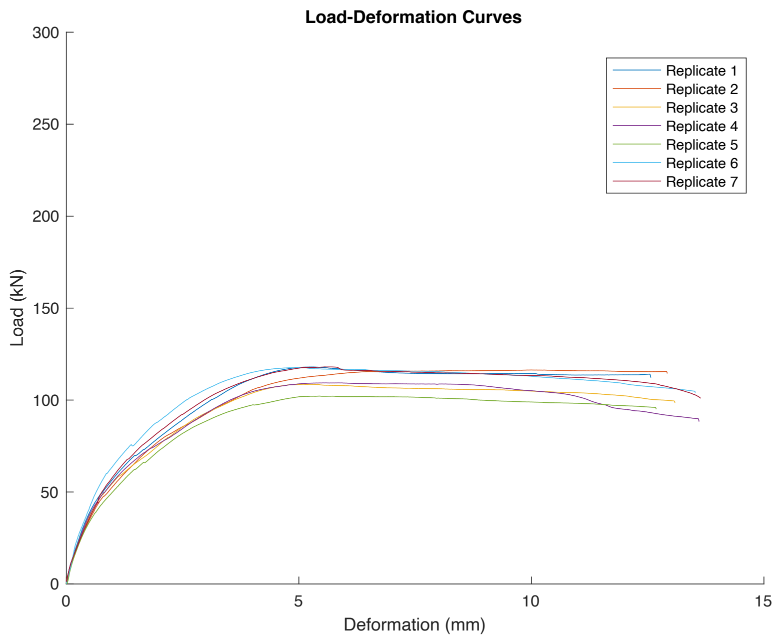

Figure C.7: d = 20M, 4.8 steel, V CLT, D = 3d

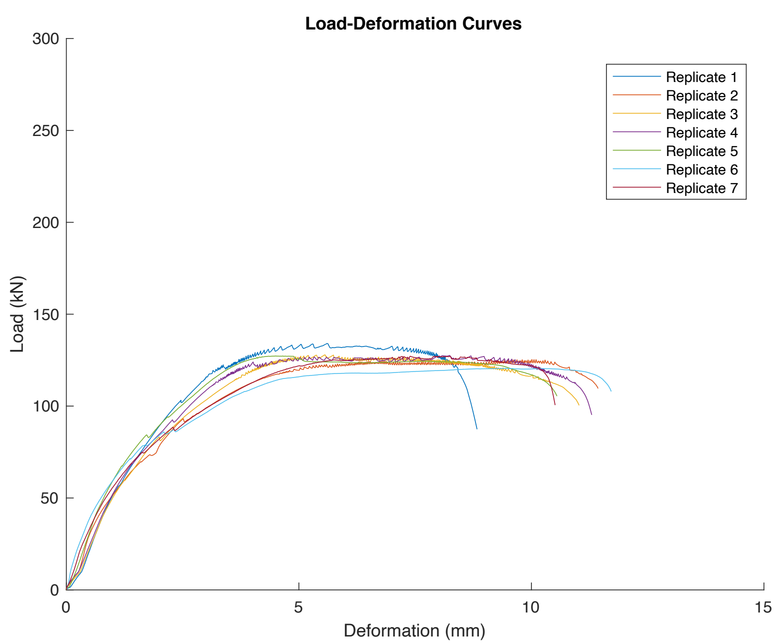

Figure C.8: d = 20M, 4.8 steel, V CLT, D = 4d

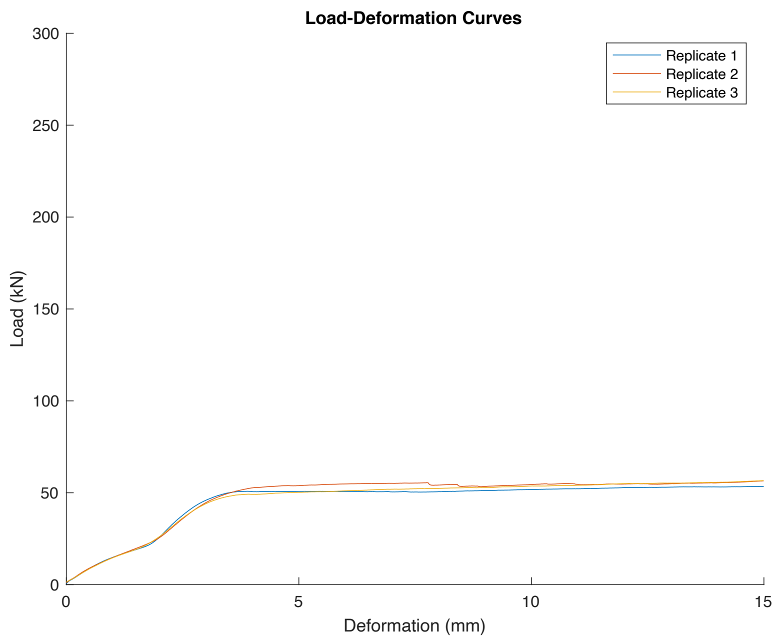

Figure C.9: d = 20M, 8.8 steel, E CLT, no grout

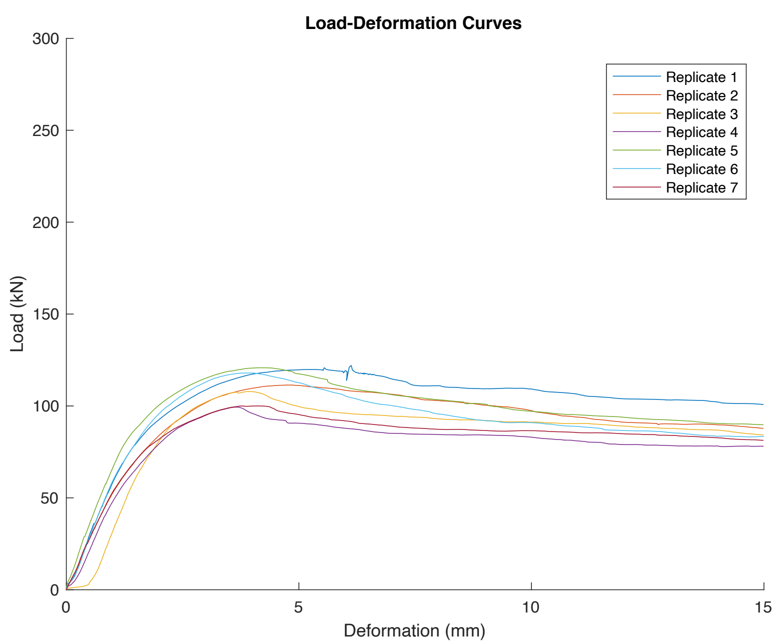

Figure C.10: d = 20M, 8.8 steel, E CLT, D = 2d

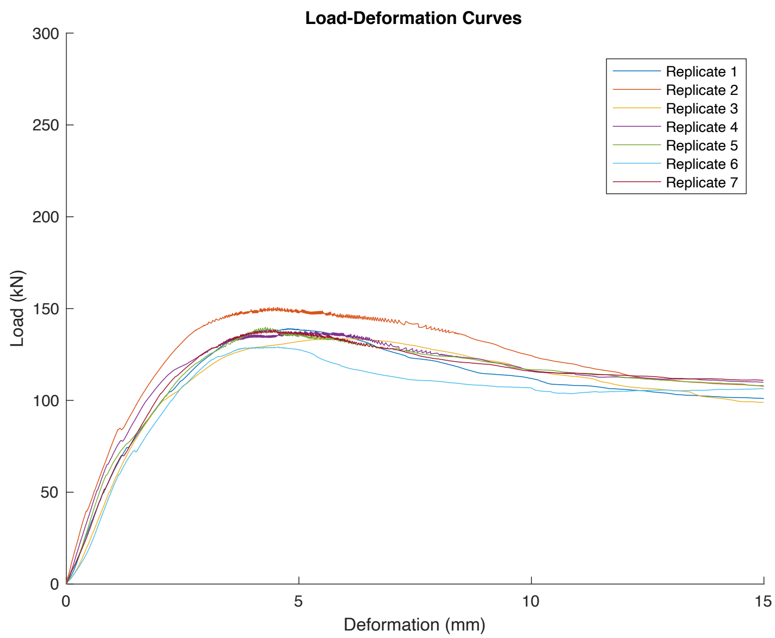

Figure C.11: d = 20M, 8.8 steel, E CLT, D = 3d

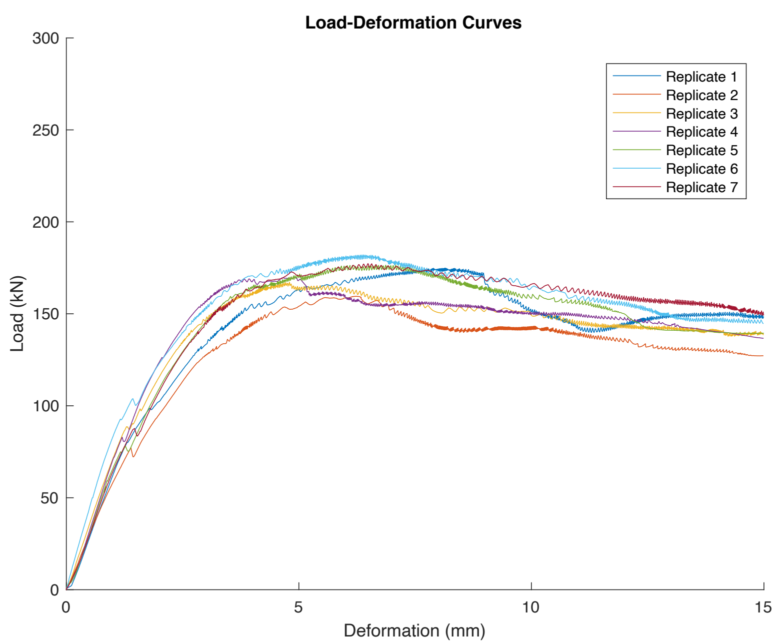

Figure C.12: d = 20M, 8.8 steel, E CLT, D = 4d

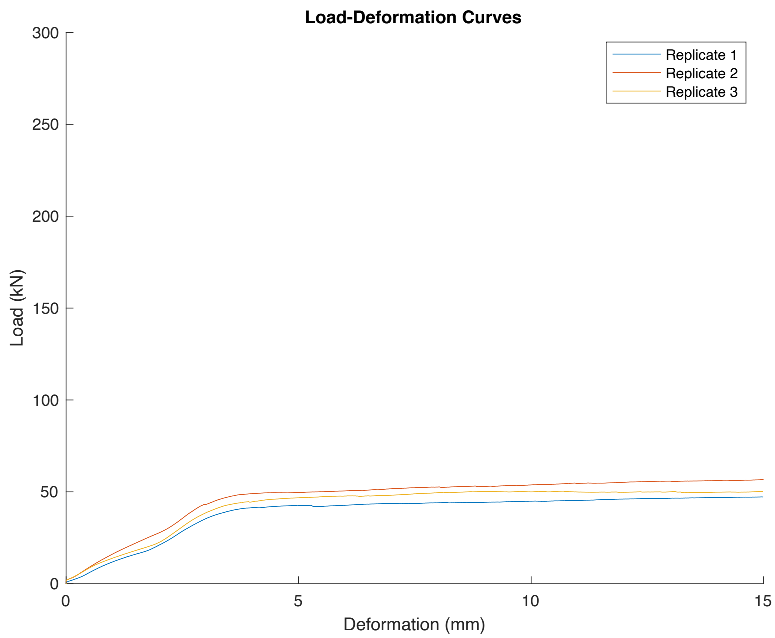

Figure C.13: d = 20M, 8.8 steel, V CLT, no grout

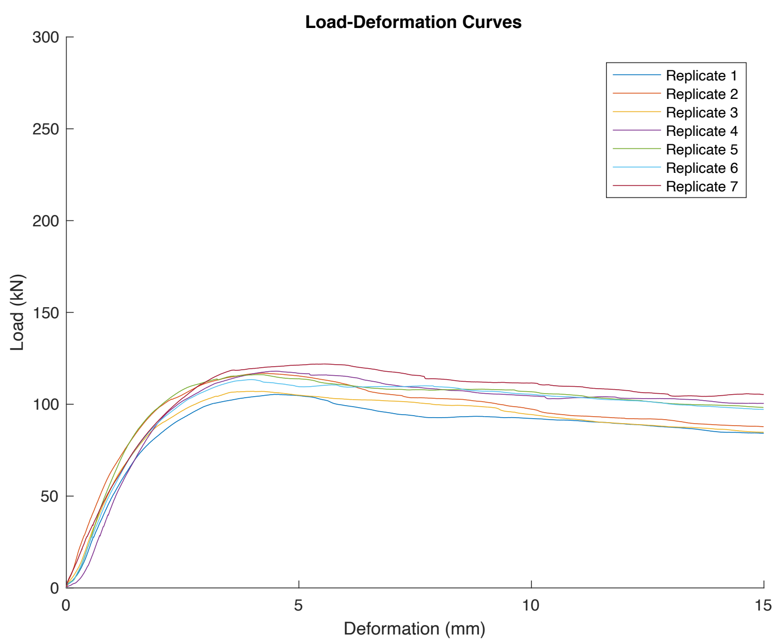

Figure C.14: d = 20M, 8.8 steel, V CLT, D = 2d

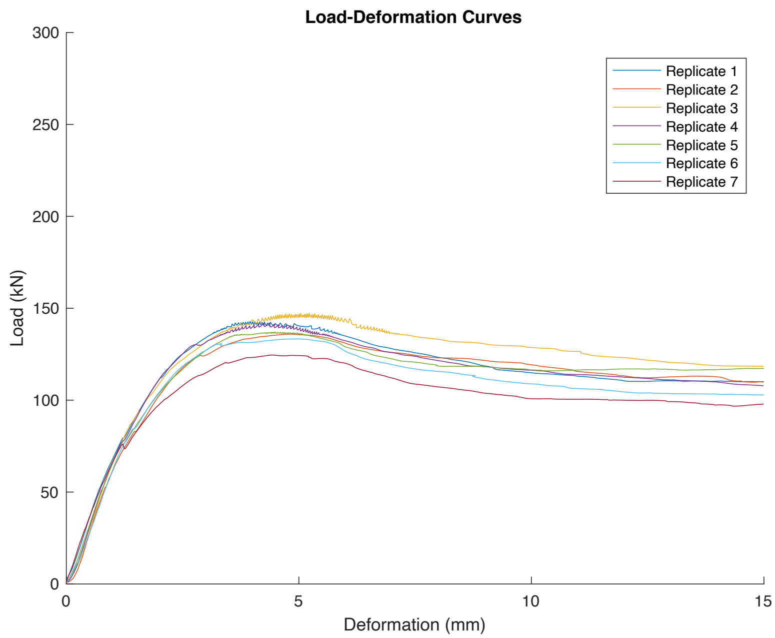

Figure C.15: d = 20M, 8.8 steel, V CLT, D = 3d

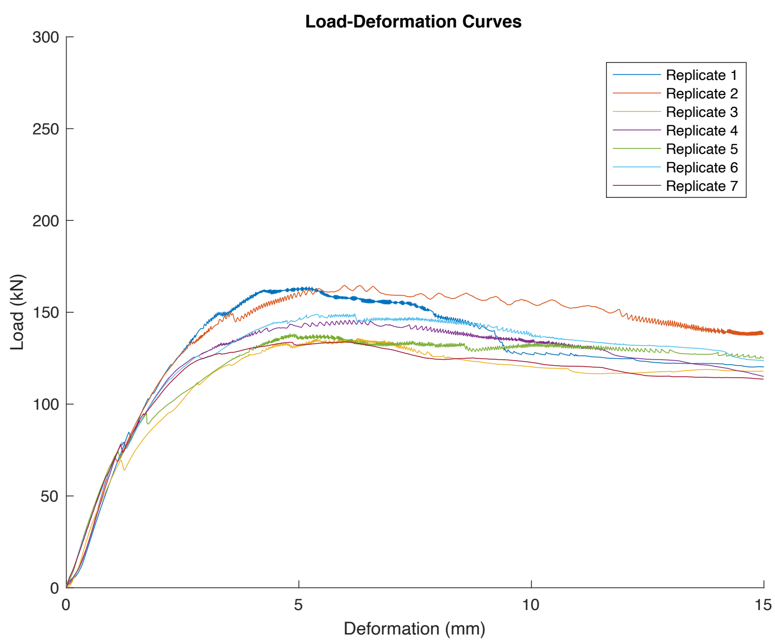

Figure C.16: d = 20M, 8.8 steel, V CLT, D = 4d

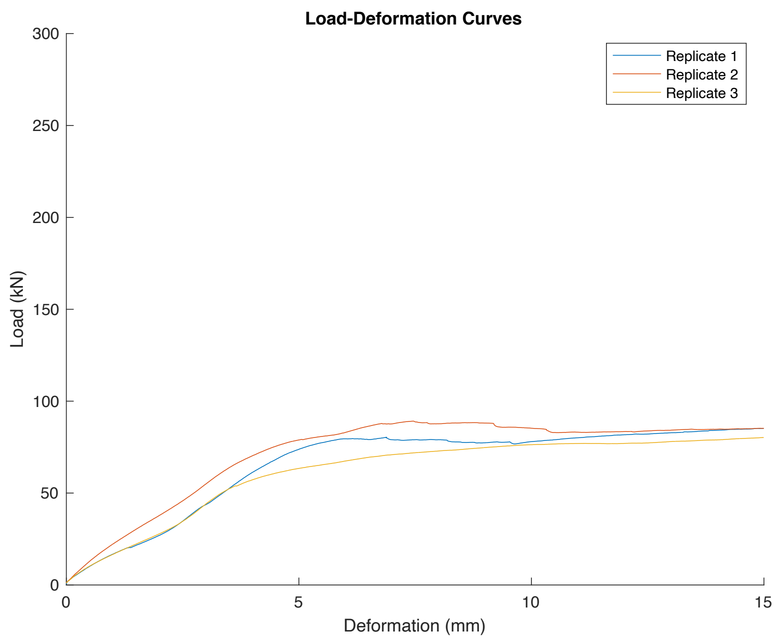

Figure C.17: d = 24M, 4.8 steel, E CLT, no grout

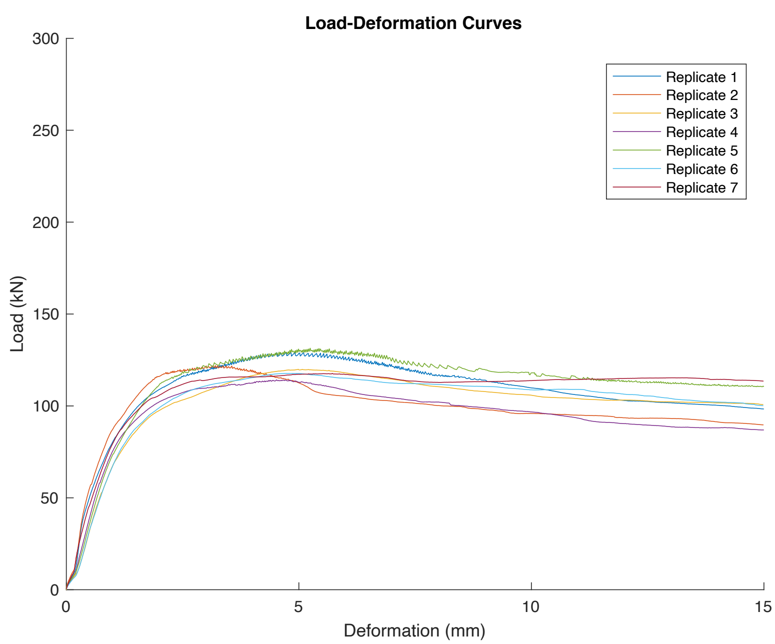

Figure C.18: d = 24M, 4.8 steel, E CLT, D = 2d

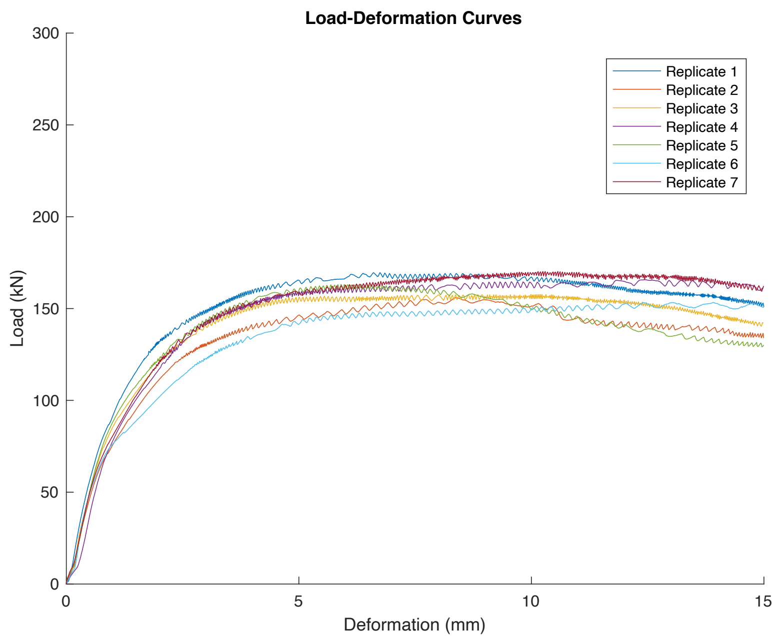

Figure C.19: d = 24M, 4.8 steel, E CLT, D = 3d

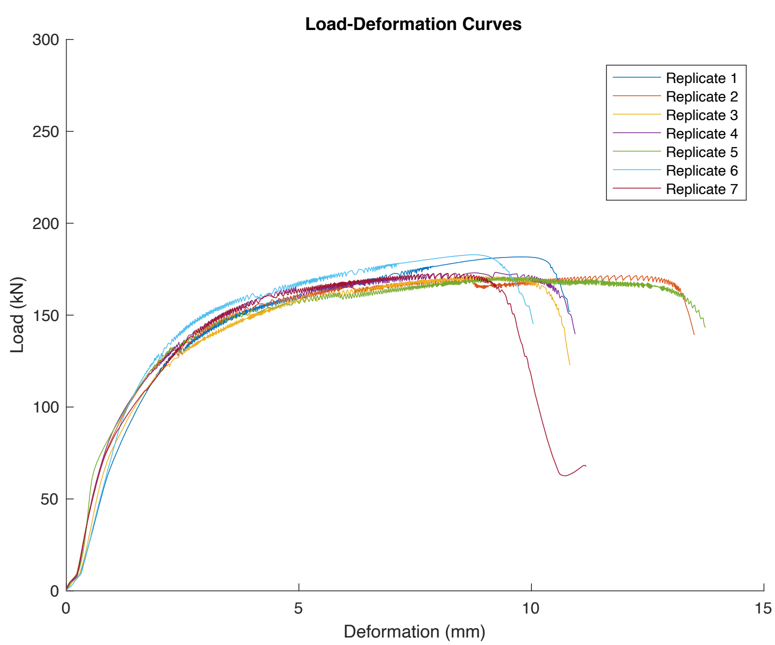

Figure C.20: d = 24M, 4.8 steel, E CLT, D = 4d

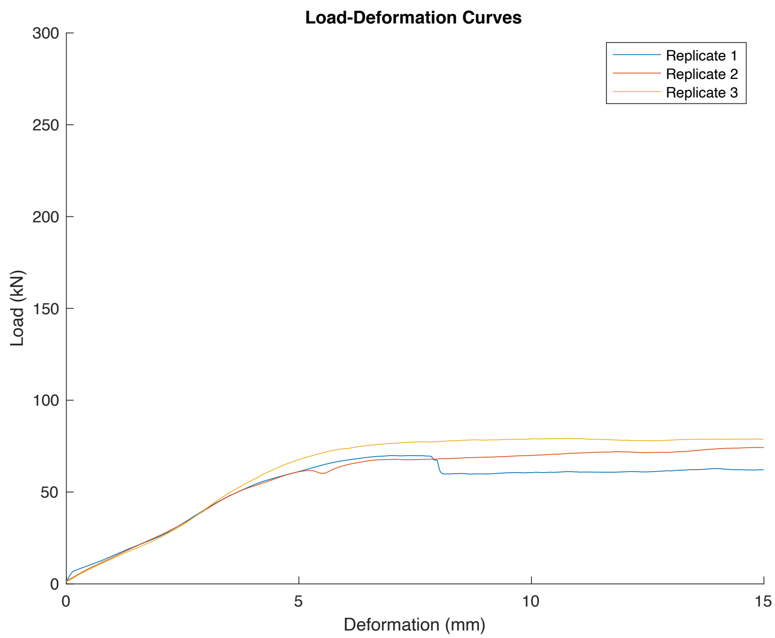

Figure C.21: d = 24M, 4.8 steel, V CLT, no grout

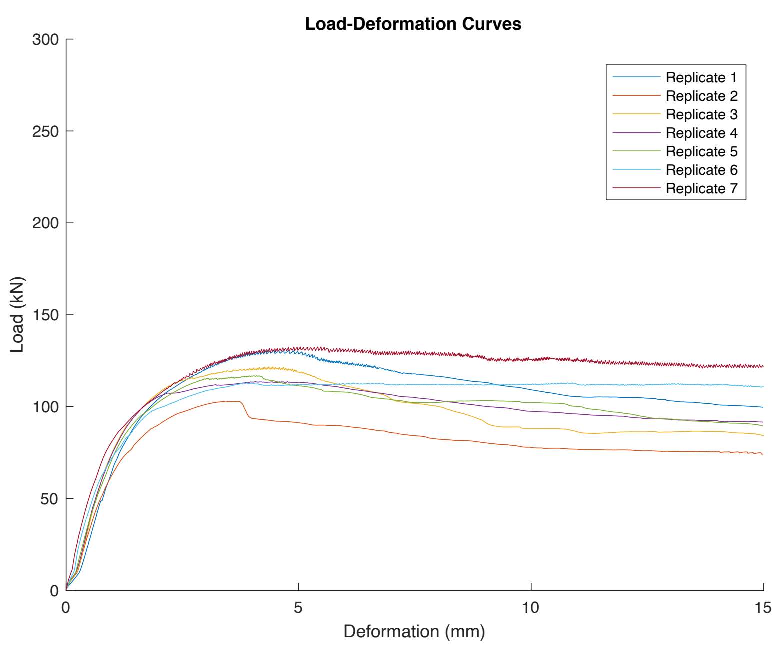

Figure C.22: d = 24M, 4.8 steel, V CLT, D = 2d

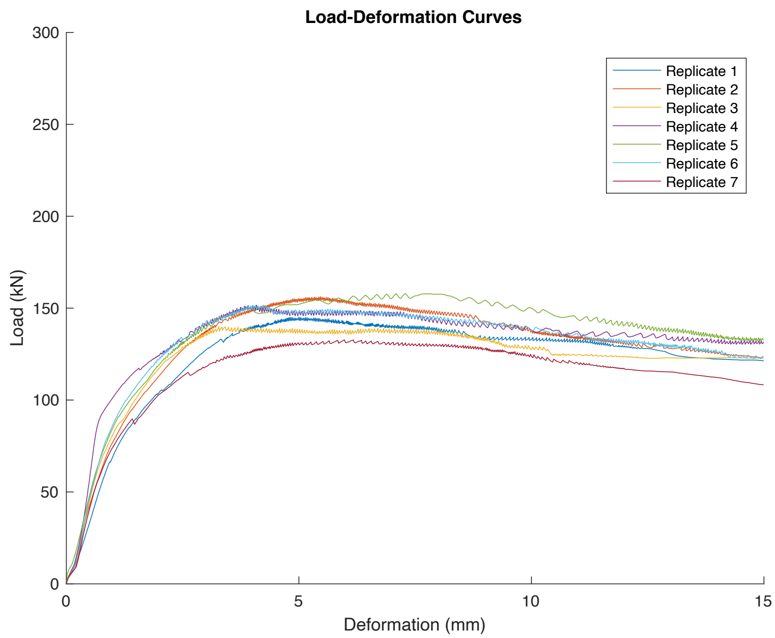

Figure C.23: d = 24M, 4.8 steel, V CLT, D = 3d

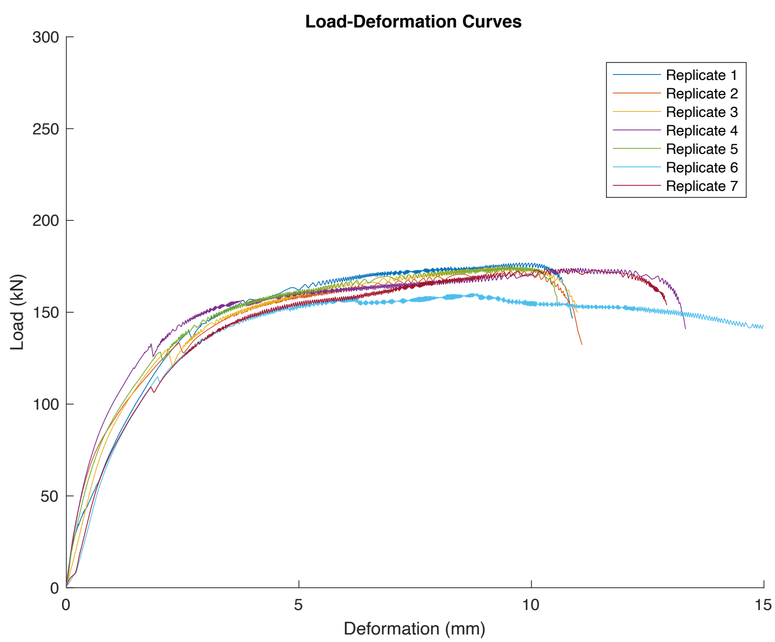

Figure C.24: d = 24M, 4.8 steel, V CLT, D = 4d

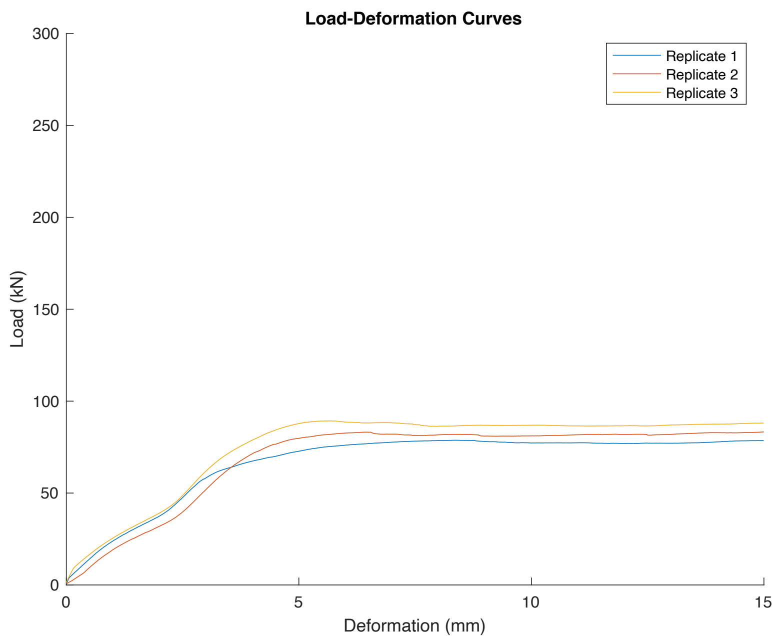

Figure C.25: d = 24M, 8.8 steel, E CLT, no grout

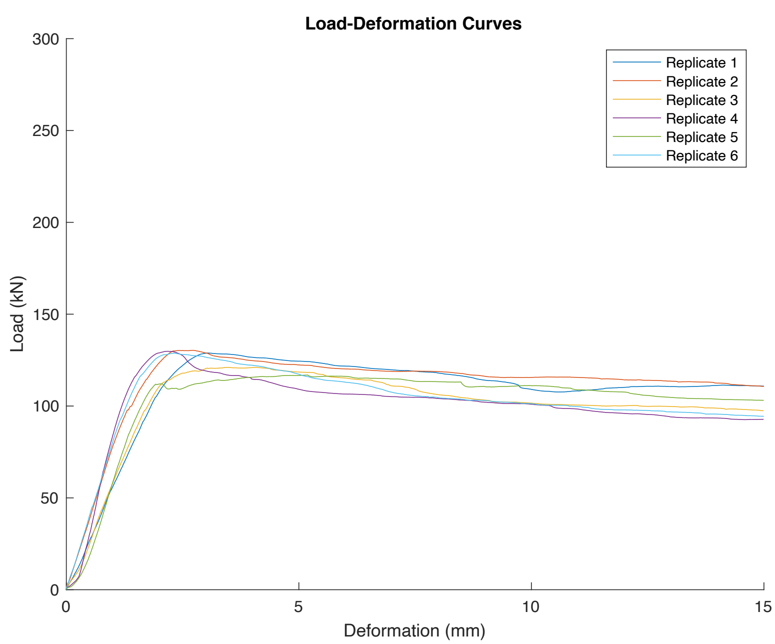

Figure C.26: d = 24M, 8.8 steel, E CLT, D = 2d

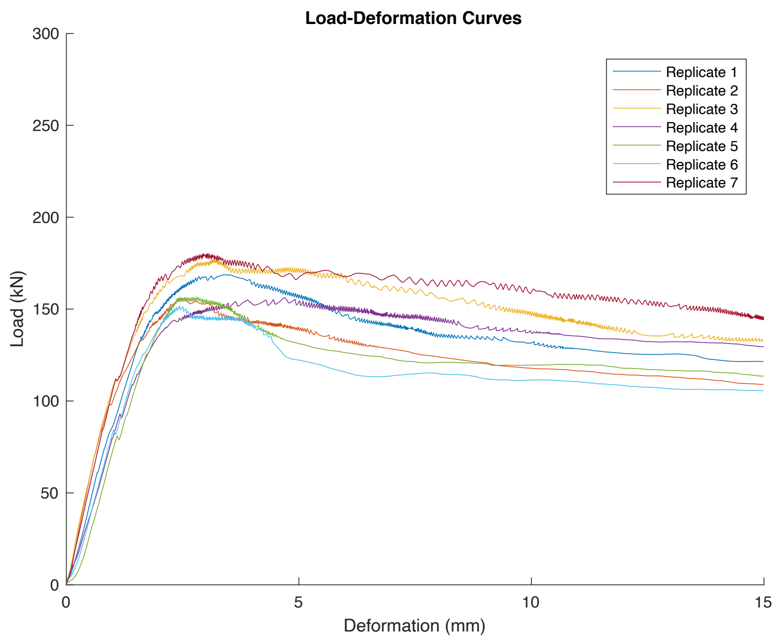

Figure C.27: d = 24M, 8.8 steel, E CLT, D = 3d

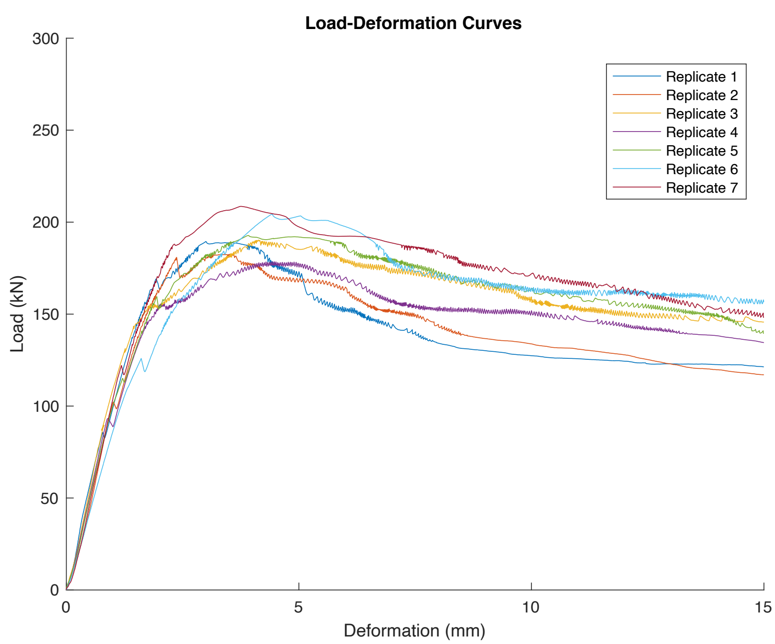

Figure C.28: d = 24M, 8.8 steel, E CLT, D = 4d

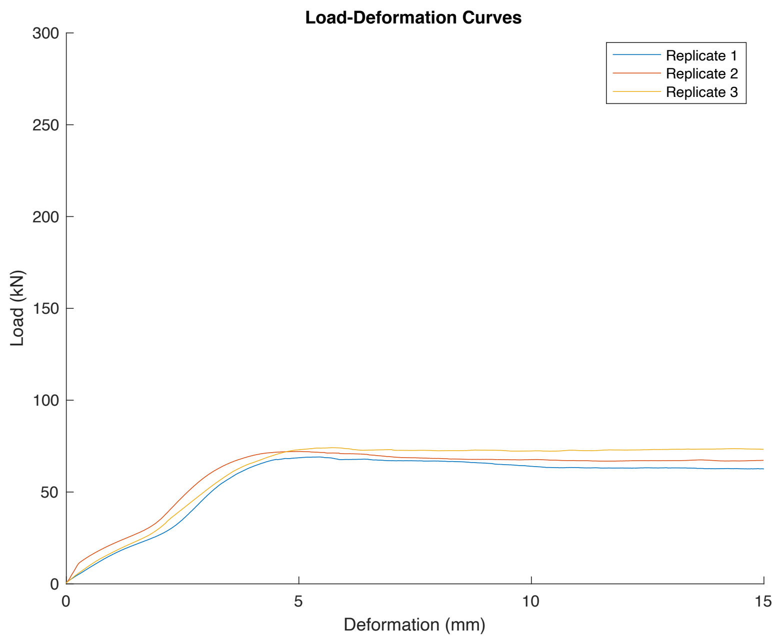

Figure C.29: d = 24M, 8.8 steel, V CLT, no grout

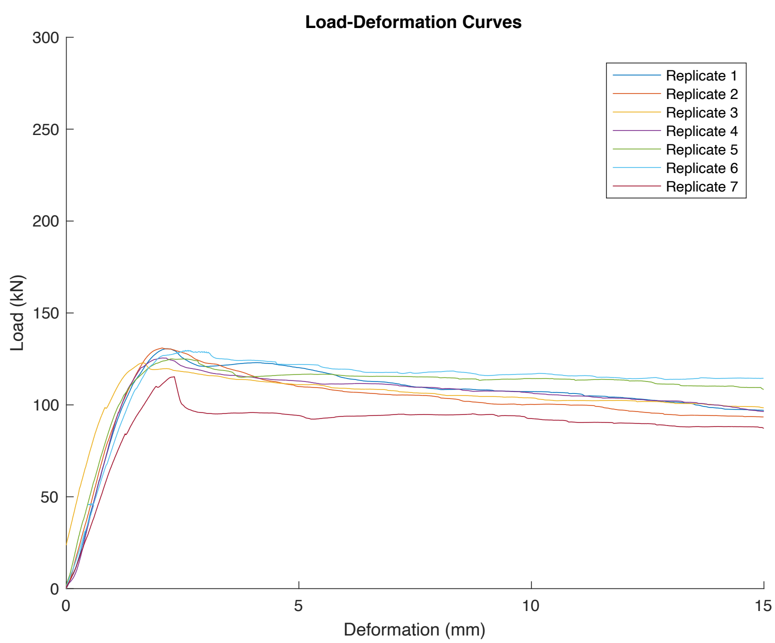

Figure C.30: d = 24M, 8.8 steel, V CLT, D = 2d

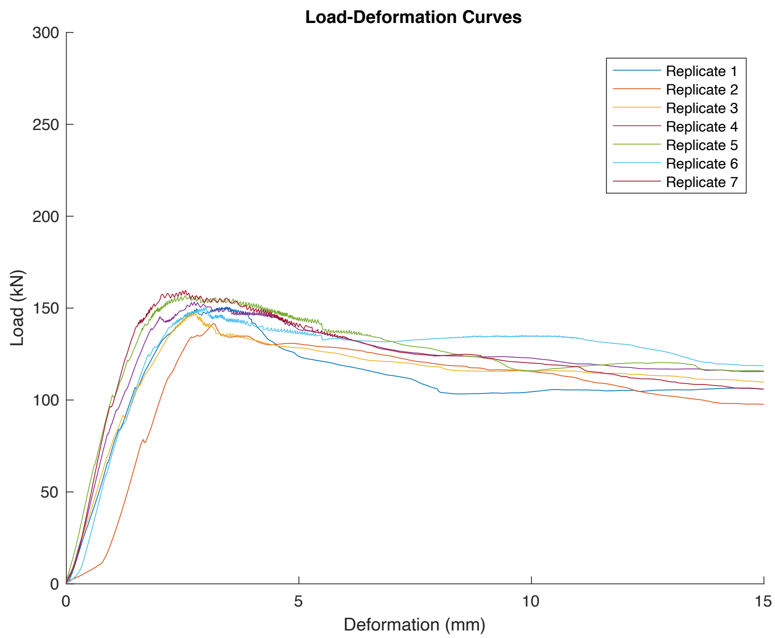

Figure C.31: d = 24M, 8.8 steel, V CLT, D = 3d

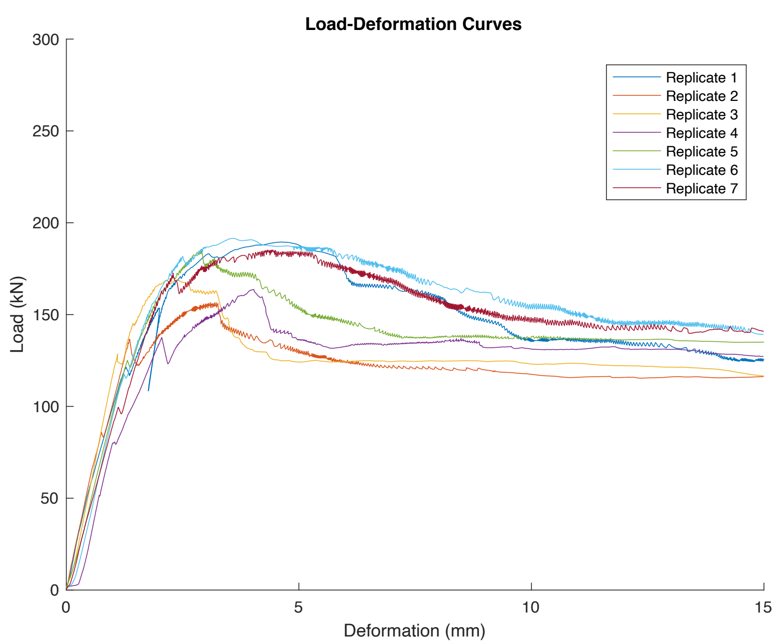

Figure C.32: d = 24M, 8.8 steel, V CLT, D = 4d

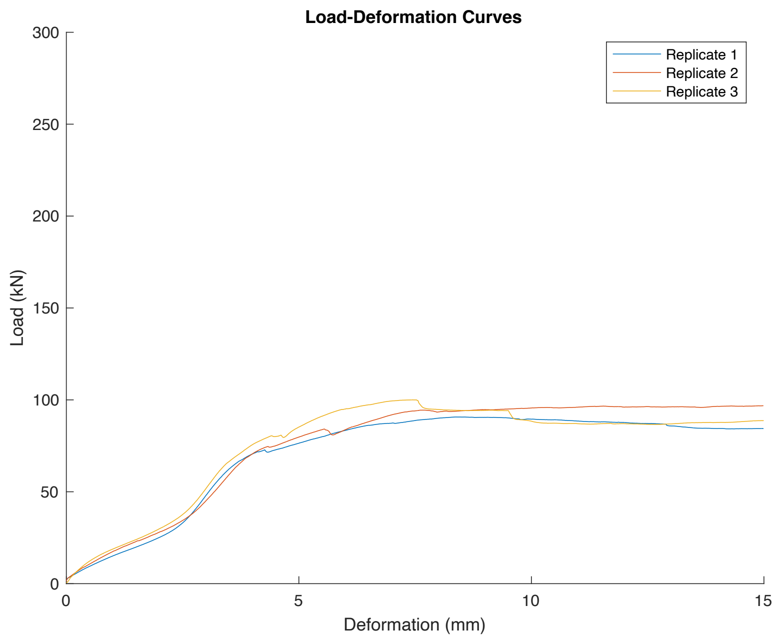

Figure C.33: d = 30M, 4.8 steel, E CLT, no grout

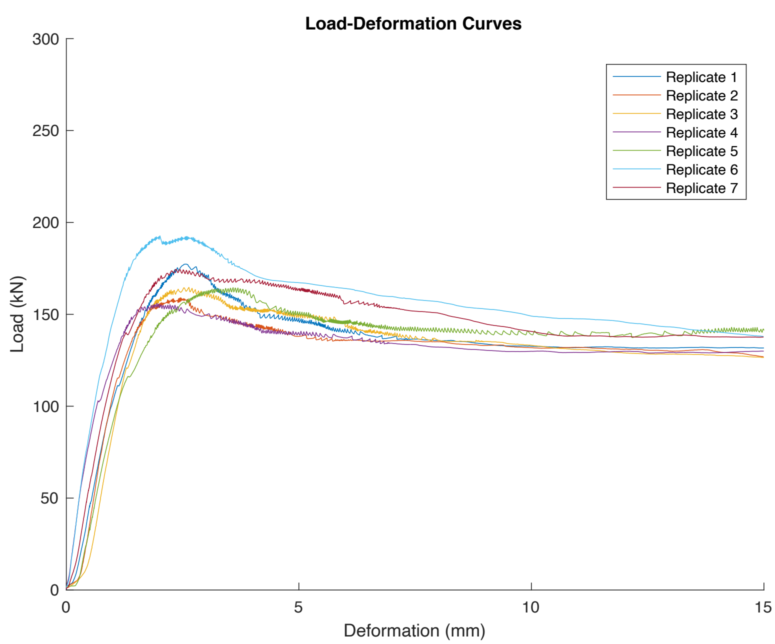

Figure C.34: d = 30M, 4.8 steel, E CLT, D = 2d

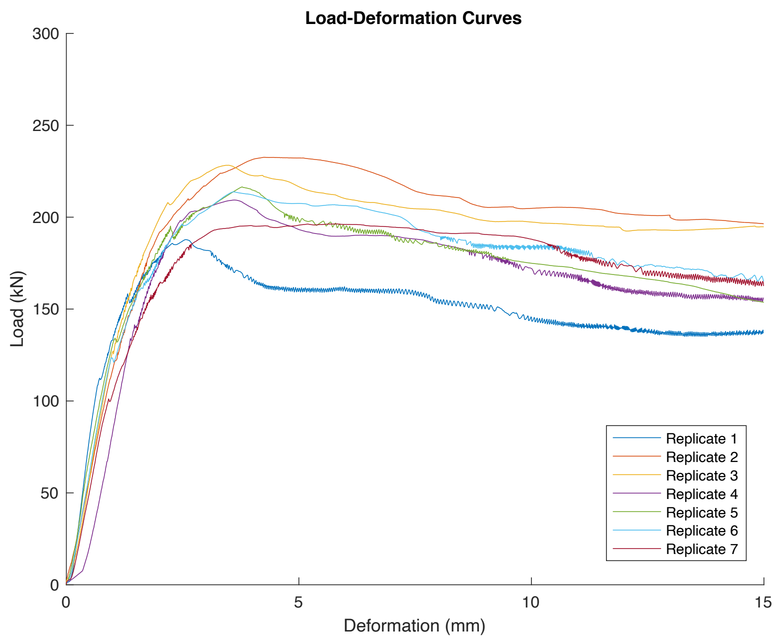

Figure C.35: d = 30M, 4.8 steel, E CLT, D = 3d

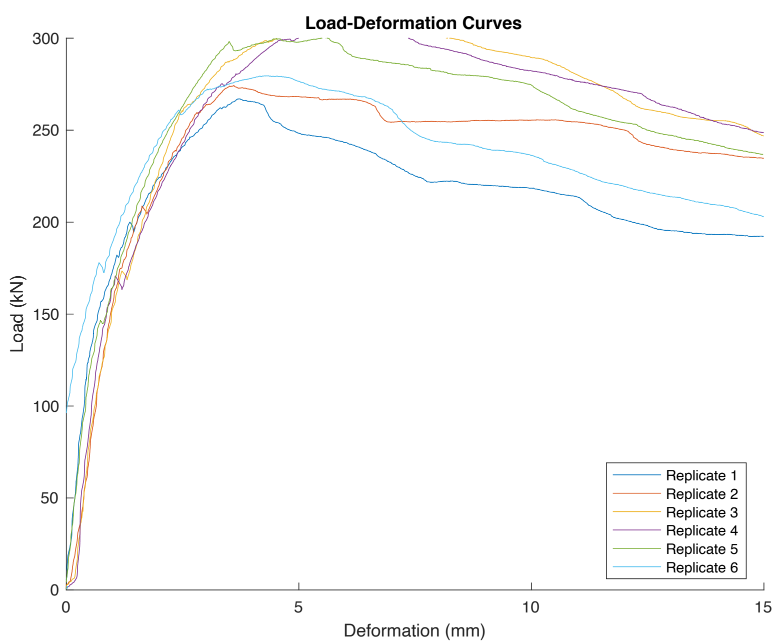

Figure C.36: d = 30M, 4.8 steel, E CLT, D = 4d

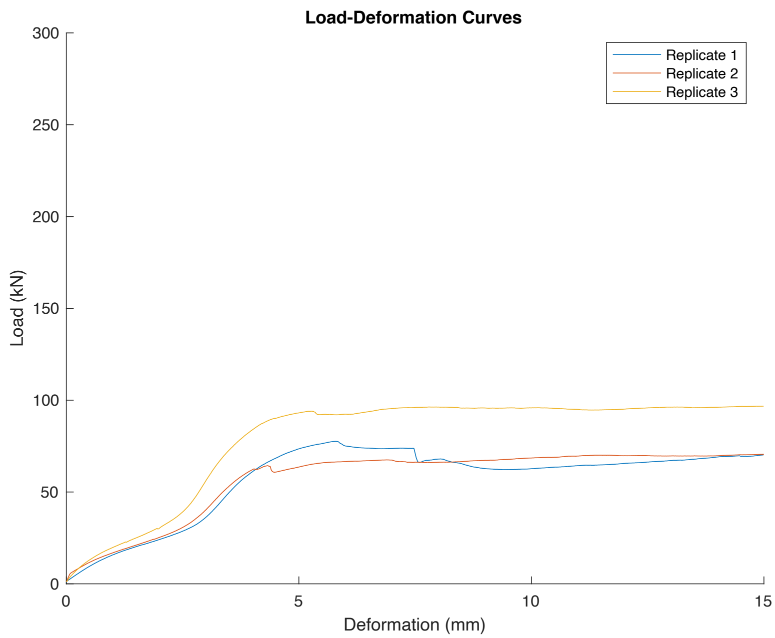

Figure C.37: d = 30M, 4.8 steel, V CLT, no grout

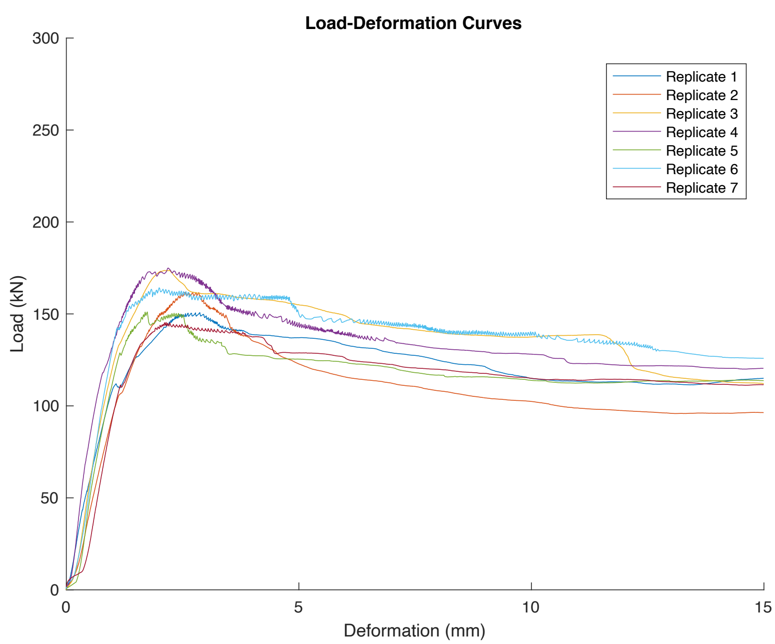

Figure C.38: d = 30M, 4.8 steel, V CLT, D = 2d

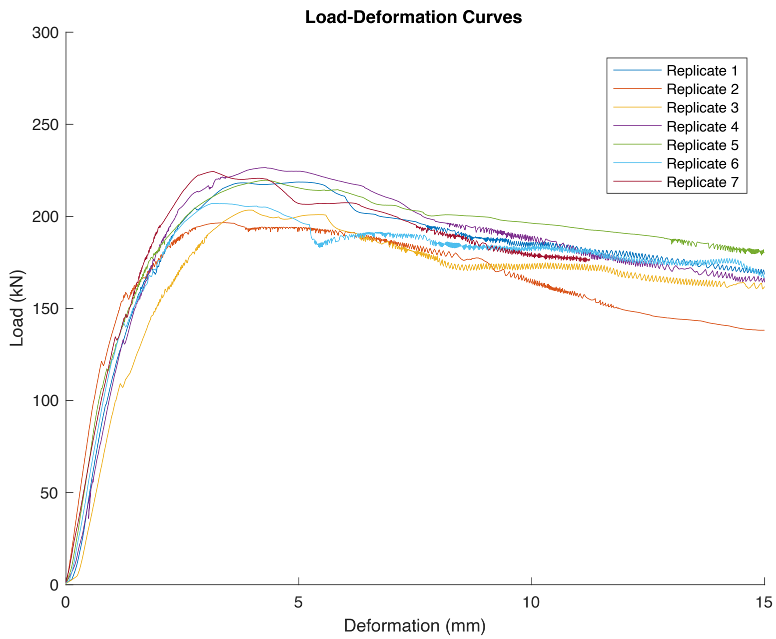

Figure C.39: d = 30M, 4.8 steel, V CLT, D = 3d

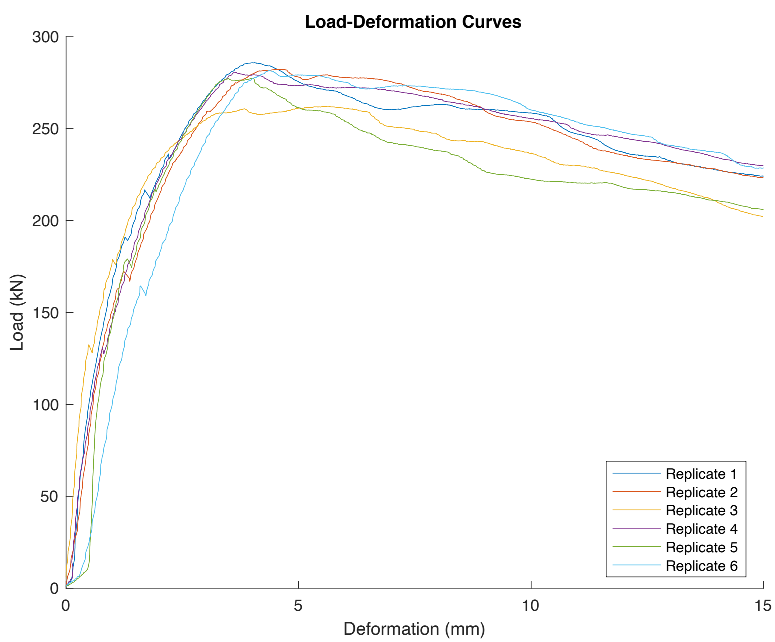

Figure C.40: d = 30M, 4.8 steel, V CLT, D = 4d

Appendix D

Tensile Test Reports

Full Tensile Report

Sample Identification:	Class-4.8 OAL-249.8mm
Sharp Of Test Specimens:	Round

Sample:	**1**	**2**	**3**
Sample Size:	12.47mm	12.41mm	12.44mm
Initial Gauge Length:	50.8mm	50.8mm	50.8mm
Yield Method (%Offset):	0.2%	0.2%	0.2%
Yield Load:	64.57kN	64.33kN	63.85kN
Yield Strength:	528.7Mpa	531.8Mpa	525.3Mpa
Ultimate Tensile Load:	68.4kN	68.2kN	68.4kN
Ultimate Tensile Strength:	560.4Mpa	563.8Mpa	563.1Mpa
Final Sample Size:	7.36mm	7.85mm	7.23mm
Final Gauge Length:	57.95mm	60.15mm	59.6mm
Type Of Failure:	Ductile	Ductile	Ductile

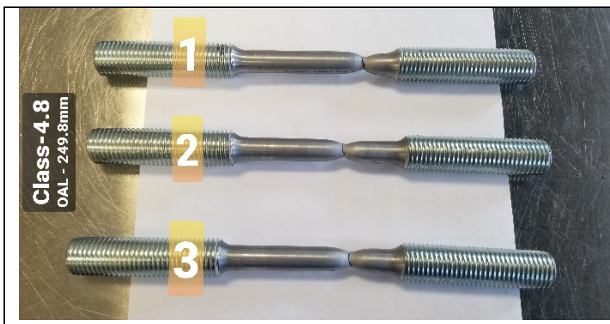

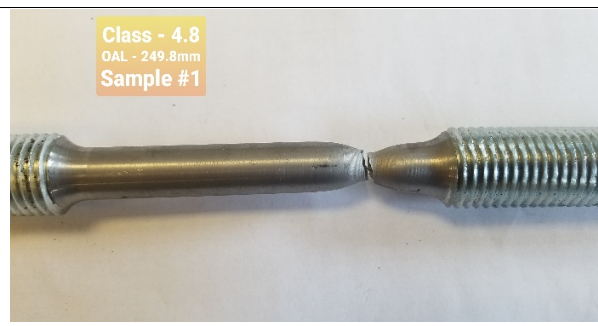

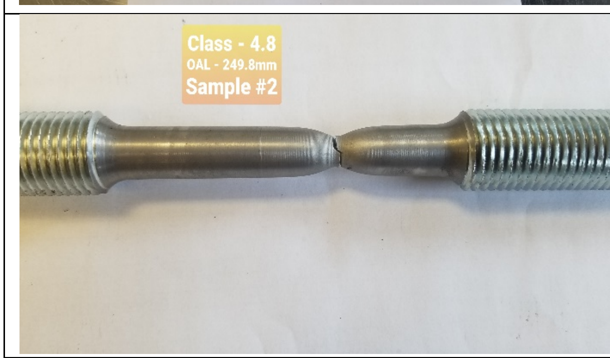

Full Tensile Report

Sample Identification:	Class – 8.8 OAL – 248.2mm
Sharp Of Test Specimens:	Round

Sample:	**4**	**5**	**6**
Sample Size:	12.31mm	12.35mm	12.28mm
Initial Gauge Length:	50.8mm	50.8mm	50.8mm
Yield Method (%Offset):	0.2%	0.2%	0.2%
Yield Load:	87.94kN	89.04kN	85.07kN
Yield Strength:	738.9Mpa	743.3Mpa	718.3Mpa
Ultimate Tensile Load:	104.9kN	105.8kN	103.0kN
Ultimate Tensile Strength:	881.3Mpa	883.6Mpa	869.9Mpa
Final Sample Size:	7.3mm	7.42mm	7.48mm
Final Gauge Length:	63.26mm	64.25mm	63.25mm
Type Of Failure:	Ductile	Ductile	Ductile

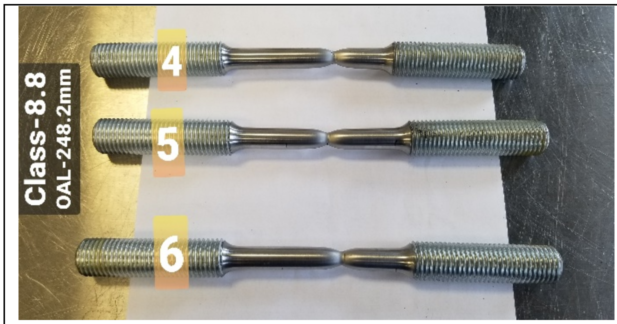

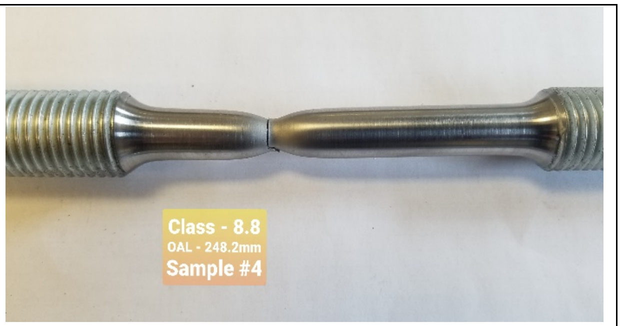

Appendix E

Material Data Sheets

Solid base to build on.

Epoxy Grout

Hilti Epoxy Grout is a Buy American-compliant, three component, 100% solids, VOC and BGE free, high performance epoxy grouting system. This specially formulated grout offers high strength providing excellent resistance to impact and vibration. Using the most advanced amine technology this grout meets today's needs of an effective and easy to use epoxy grout designed to help protect people and the environment. Hilti's Epoxy Grout comes with a non-corrosive hardener, avoiding the risk of burns like with other epoxy products and making it a DOT-non-hazardous product simplifying transportation and storage.

Order Information

Description	Package Contents	Qty	Item No.
Epoxy Grout	59 lb. bucket	1	00430898

Technical Data	Epoxy Grout			
	Standard	Aspect	Imperial	Metric
Compressive strength, psi (MPa) at 73°F (23°C)	ASTM C 579 B	8 h 16 h 1 day 3 days 7 days	6,000 12,000 12,500 14,000 15,000	(41) (83) (86) (97) (103)
Compressive modulus, psi (MPa)	ASTM D 695		568,000	(3,917)
Flexural strength, psi (MPa)	ASTM C 580	7 days	3,900	(27)
Tensile strength, psi (MPa)	ASTM C 307	7 days	2,100	(14)
Bond to concrete (complete concrete failure), psi (MPa)	ASTM C 882		≥ 550	(4)
Adhesion to steel (clean, sandblasted), psi (MPa)			2,500	(17)
Coefficient of thermal expansion, 10-5 / °C	ASTM D 696		1.74	
Heat distortion temperature, °F (°C)	ASTM D 648		170	(77)
Working time at 72 °F (22 °C), min			45	
Gel time at 72 °F (22 °C), min	ASTM D 2471		90	
Yield, 59 lb (26.8 kg)			0.40 ft^3	(0.011 m^3)
Packaging, three component kit in one plastic container		Part A: Resin Part B: Hardener Part C: Aggregate	0.58 gal 0.14 gal 48.0 lb.	(2.18 L) (0.51 L) (21.8 kg)
Shelf life		24 months from date of manufacture when stored properly in original unopened container		

The data shown above reflect typical results based on laboratory testing under controlled conditions. Reasonable variations from the data shown above may result.

Advantages

- Non-corrosive hardener — no risk of burns
- Non-hazardous per DOT shipping classification
- VOC and BGE free
- High early and ultimate strengths
- High vibration resistance
- Deep pour, low shrinkage
- Self-leveling
- Easy to use, all-in-one kit
- High resistance to a variety of chemicals
- Best in class epoxy grout for worker safety

Trades and Facilities

- Civil projects
- Concrete professionals
- Energy facilities
- General contractors / construction managers
- Industrial plants
- Ornamental steel artisans
- Steel erectors

Purposes and Uses

- Grouting of machinery and equipment with high load requirements
- Precision alignment under dynamic load conditions
- Structural grouting of baseplates, columns, beams, crane rails, bridge seats, dowels, etc.
- Chemical processing facilities

Application Instructions

Read product instructions and MSDS before use.

Preparation
The surfaces to be grouted must be solid, clean and free from oil, grease and other contaminants that may act as a bond breaker. Remove all loose material and laitance. Concrete surfaces must be dry, sound and roughened to obtain proper bond. The grout and the affected grouting area should be kept between 50 °F and 90 °F (10 °C and 32 °C) and shaded from direct sunlight. During cold weather it is important that the grouted areas be kept warm (above 50 °F or 10 °C) until the grout has cured completely. Store material at room temperature (70°F-80°F) for at least 24 hours before use. Set time and strength development are dependent on ambient temperature. Hot temperatures will accelerate the setting process of the grout while cold temperatures will have a retarding effect. Metal surfaces to come in contact with the epoxy grout should be sandblasted to a white metal finish and wiped clean with solvent before grout is applied. Apply grout immediately to prevent re-oxidizing or moisture condensation.

Formwork
Standard wood or metal forming may be used. The formwork must provide rapid, continuous grout placement and needs to retain grout without leakage. The forms should be protected with heavy coats of paste wax, grease or form release agent.

For baseplates, forms should be at least 1" (2.54 cm) higher than the bottom of the baseplate. The forms should have 45° angle chamfer strips at all vertical corners and horizontal grout grade elevation in order to eliminate sharp corners. The clearance for remaining sides (distance between the baseplate and the form) shall be 2-6" (50 to 152 mm).

Mixing
Pour the hardener into the resin container and mix with a slow speed mixer (400 - 600 rpm) for approximately 1-2 minutes until thoroughly blended (the mix will show a uniform color). Keep the mixing paddle submerged to avoid air entrapment. Pour mixed resin and hardener into a larger container. While mixing at low speed, slowly add the included aggregate and mix until thoroughly blended (aggregate must be completely wet). Always mix in complete units — do not mix smaller batches.

Application
Immediately after mixing, place grout from one side allowing it to flow to the opposite and adjacent sides thereby avoiding air entrapment. Provide vent holes where needed to prevent air entrapment. Where grout cannot be adequately worked to fill the cavity (because of large size or limited space), a head box will greatly assist flow.

Minimum application thickness per pour: 1" (25.4 mm)

Maximum application thickness per pour: 8" (203 mm)

Finishing
If a smooth finish is desired, the surface of the grout may be ground and painted with an appropriate paint or protective coating.

Clean-up
All tools and equipment may be cleaned with warm water and a strong detergent solution before material hardens.

Storage
Always keep in closed container in a dry warm place unexposed to sunlight.

Limitations
- Do not use if the container is damaged
- Aggregate (Part C) must be kept dry before use
- Do not add solvent, water or any other material to the grout

MET

THREADED RODS, NUTS AND WASHERS

- Metric threaded products for creating connections and joints
- Available in carbon steel and stainless steel for use in service classes 1, 2 and 3 (EN 1995 1-1)

MGS 1000

THREADED ROD

CODE	rod	L [mm]	pcs
MGS10008	M8	1000	10
MGS100010	M10	1000	10
MGS100012	M12	1000	10
MGS100014	M14	1000	10
MGS100016	M16	1000	10
MGS100018	M18	1000	10
MGS100020	M20	1000	10
MGS100022	M22	1000	10
MGS100024	M24	1000	10
MGS100027	M27	1000	10
MGS100030	M30	1000	10

Steel class 4.8 - zinc plated
DIN 975

MGS 1000

THREADED ROD

CODE	rod	L [mm]	pcs
MGS10888	M8	1000	1
MGS11088	M10	1000	1
MGS11288	M12	1000	1
MGS11488	M14	1000	1
MGS11688	M16	1000	1
MGS11888	M18	1000	1
MGS12088	M20	1000	1
MGS12488	M24	1000	1
MGS12788	M27	1000	1

Steel class 8.8 - zinc plated
DIN 975

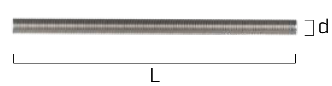

MGS 2200

THREADED ROD

CODE	rod	L [mm]	pcs
MGS220012	M12	2200	1
MGS220016	M16	2200	1
MGS220020	M20	2200	1

Steel class 4.8 - zinc plated
DIN 975

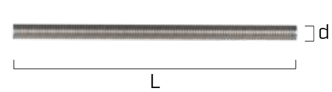

ULS 9021

WASHER

CODE	rod	d_{INT} [mm]	d_{EXT} [mm]	s [mm]	pcs
ULS8242	**M8**	8,4	24	2	200
ULS10302	**M10**	10,5	30	2,5	200
ULS13373	**M12**	13	37	3	100
ULS15443	**M14**	15	44	3	100
ULS17503	**M16**	17	50	3	100
ULS20564	**M18**	20	56	4	50
ULS22604	**M20**	22	60	4	50

* ISO 7093 differs from DIN 9021 in the surface hardness.

S235 steel - zinc plated
DIN 9021 (ISO 7093*)

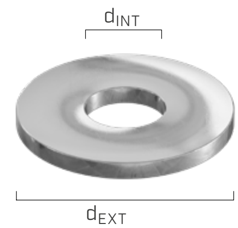

ULS 440

WASHER

CODE	rod	d_{INT} [mm]	d_{EXT} [mm]	s [mm]	pcs
ULS11343	**M10**	11	34	3	200
ULS13444	**M12**	13,5	44	4	200
ULS17565	**M16**	17,5	56	5	50
ULS22726	**M20**	22	72	6	50
ULS24806	**M22**	24	80	6	25

* ISO 7094 differs from DIN 440 R in the surface hardness.

S235 steel - zinc plated
DIN 440 R (ISO 7094*)

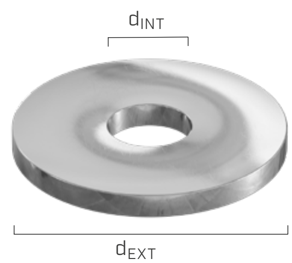

ULS 1052

WASHER

CODE	rod	d_{INT} [mm]	d_{EXT} [mm]	s [mm]	pcs
ULS14586	**M12**	14	58	6	50
ULS18686	**M16**	18	68	6	50
ULS22808	**M20**	22	80	8	25
ULS25928	**M22**	25	92	8	20
ULS271058	**M24**	27	105	8	20

S235 steel - zinc plated
DIN 1052

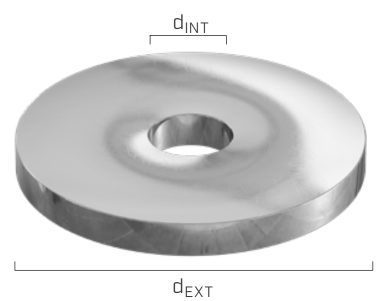

ULS 125

WASHER

CODE	rod	d_{INT} [mm]	d_{EXT} [mm]	s [mm]	pcs
ULS81616	**M8**	8,4	16	1,6	1000
ULS10202	**M10**	10,5	20	2	500
ULS13242	**M12**	13	24	2,5	500
ULS17303	**M16**	17	30	3	250
ULS21373	**M20**	21	37	3	250
ULS25444	**M24**	25	44	4	200
ULS28504	**M27**	28	50	4	100
ULS31564	**M30**	31	56	4	20

* ISO 7089 differs from DIN 125 A in the surface hardness.

S235 steel - zinc plated
DIN 125 A (ISO 7089*)

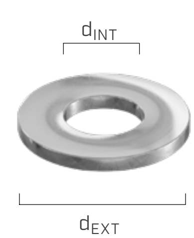

MUT 934

HEXAGONAL NUT

CODE	rod	h [mm]	SW [mm]	pcs
MUT9348	**M8**	6,5	13	400
MUT93410	**M10**	8	17	500
MUT93412	**M12**	10	19	500
MUT93414	**M14**	11	22	200
MUT93416	**M16**	13	24	200
MUT93418	**M18**	15	27	100
MUT93420	**M20**	16	30	100
MUT93422	**M22**	18	32	50
MUT93424	**M24**	19	36	50
MUT93427	**M27**	22	41	25
MUT93430	**M30**	24	46	25

* ISO 4032 differs from DIN 934 in diameters M10 and M12 for parameters h and SW and diameters M10, M12, M14 and M22.

Steel class 8 - zinc plated
DIN 934 (ISO 4032*)

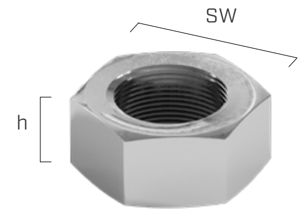

MUT 6334

CONNECTING NUT

CODE	rod	h [mm]	SW [mm]	pcs
MUT633410	**M10**	30	17	10
MUT633412	**M12**	36	19	10
MUT633416	**M16**	48	24	25
MUT633420	**M20**	60	30	10

Steel class 8 - zinc plated
DIN 6334

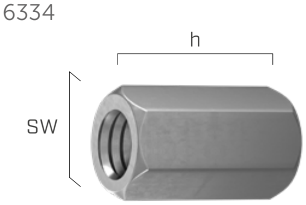

MUT 1587

BLIND NUT

CODE	rod	h [mm]	SW [mm]	pcs
MUT15878S	**M8**	15	13	200
MUT158710S	**M10**	18	17	50
MUT158712S	**M12**	22	19	50
MUT158714S	**M14**	25	22	50
MUT158716S	**M16**	28	24	50
MUT158718S	**M18**	32	27	50
MUT158720S	**M20**	34	30	25
MUT158722S	**M22**	39	32	25
MUT158724S	**M24**	42	36	25

Single-piece turned nut.

Steel class 8 - zinc plated
DIN 1587

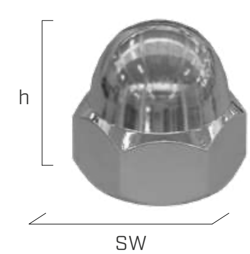

MGS AI 975

THREADED ROD

A2
AISI 304

CODE	rod	L [mm]	pcs
AI9758	**M8**	1000	1
AI97510	**M10**	1000	1
AI97512	**M12**	1000	1
AI97516	**M16**	1000	1
AI97520	**M20**	1000	1

A2 | AISI304 stainless steel
DIN 975

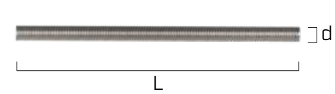

Appendix F

Matlab Code

The following pages are portions of the Matlab code written to calculate structural performance parameters and statistics. The original script is seven pages long. Please contact the author, Samuel Shulman, for the complete script.

```
%% Section 1: Description

% This matlab program imports load-deformation data from experimental data
files,
% plots them, and determines various structural performance parameters

% Written by Samuel Shulman in June/July 2021 for his Master's Thesis
% at the University of British Columbia.

%% Section 2: Clear command window and workspace

clear
clc

%% Section 3: Input data and create vectors

dia = 20;                       % Rod diameter = 20, 24, or 30
steel_class = 4;                % Steel class = 4 (4.8) or 8 (8.8)
clt = "E";                      % CLT grade = E or V
grout = "X";                    % Grout type = X (epoxy)
grout_dia = "2x";               % Grout diameter = 2x, 3x, or 4x (multiple of
rod diameter)
numtests = 7;                   % Number of tests (replicates)

data = cell(1, numtests);       % "data" is a vector of cells, each
containing a matrix of the load-deformation data of each replicate

[…]

%% Section 4: Initialize figure for load-deformation curves

figure;
%subplot(1,2,1);
hold on

%% Section 5: Import and organize data

for k = 1:numtests
  file = sprintf(dia + "M-" + steel_class + clt + grout + "-" + grout_dia +
"-%d.txt", k);
  data{k} = readtable(file);
  data{k}.avgDef = (data{k}.left + data{k}.right) / 2;          % adds column
for average deformation
  data{k}.def = (data{k}.avgDef - data{k}.avgDef(1)) * 25.4;    % adds column
of deformation zeroed with respect to the first reading and converts from
inches to mm
  data{k}.roundedDef = round(data{k}.def,1);                    % adds column
of deformation rounded to the nearest 0.1
  data{k} = removevars(data{k},[1 3:6]);                        % removes
unnecessary columns of data
  data{k} = movevars(data{k},"load","After","def");             % moves
deformation column before load column
  data{k}(any(isnan(data{k}.load),2),:) = [];                   % removes NaN
data (sometimes the last line of the data imports as NaN)
```

```
  for j = 1:size(data{k}.def,1)-1                               % removes all
data after 15 mm
      if data{k}.def(j) > 15
         data{k}(j:end,:) = [];
         break
      end
  end

  for j = 1:size(data{k}.load,1)-1                              % removes
rapidly descending data (i.e. readings after failure)
      if abs(data{k}.load(j) - data{k}.load(j+1)) > 100          % the
threshold value needs to be adjusted based on the data (25 for 24M-8VX-4x &
100 for 30M-4VX-3x)
         data{k}(j:end,:) = [];                                 % if curves
show sharp drop, reduce value
         break                                                  % if data is
cut off early, increase value
      end
  end

  %% Section 6: Calculations

  % Maximum force (kN) and maximum deformation (mm)

  [maxForce(k), idxMaxForce(k)] = max(data{k}.load);
  maxDef(k) = data{k}.def(idxMaxForce(k));

  % Ultimate force (kN) and ultimate deformation (mm)
    % If ultimate force is final force, ultimate deformation is final
deformation
    % If ultimate force is 80% max force, ultimate deformation is deformation
after max force correspoding to value closest to 80% max force

  ultForce(k) = max(0.8 * maxForce(k), data{k}.load(end));
  if ultForce(k) == data{k}.load(end)
      ultDef(k) = data{k}.def(end);
  else
      loadsAfterMax = data{k}.load(idxMaxForce(k):end);
      [minDiffUltForce(k), idxUltForce(k)] = min(abs(loadsAfterMax-
ultForce(k)));
      ultForce(k) = loadsAfterMax(idxUltForce(k));
      ultDef(k) = data{k}.def(find(data{k}.load == ultForce(k),1,'last'));
  end

[…]

  %% Section 7: Plot

  plot(data{k}.def,data{k}.load)            % plot load-deformation curves
%   plot(data{k}.def,data{k}.stiff)         % plot stiffness lines
   plot(propLimitDef(k),propLimit(k),"ro") % plot proportional limits
   plot(yieldDef(k),yieldLoad(k),"ko")     % plot yield points
%   plot(maxDef(k),maxForce(k),"bo")        % plot max forces
   plot(ultDef(k),ultForce(k),"mo")        % plot ultimate forces

end
```

```
[…]

% Create envelope curves
    % Loads are the average of the loads corresponding to the same rounded
    % deformation to the nearest 0.1 mm

stdLoads = zeros(151,numtests);
q = 1;

for k = 1:numtests
    for i = 0:0.1:15
        stdLoads(q,k) = mean(data{k}.load(abs(data{k}.roundedDef - i) <
0.01));
        q = q + 1;
    end
   q = 1;
end

[…]

%% Section 8: Statistics

k_s = (6.5 * numtests + 6) / (3.7 * numtests - 3);  % For calculating
characteristic values (EN 14358)

avgMaxForce = mean(maxForce);
avgMaxForceLog = mean(log(maxForce));
stdDevMaxForce = std(maxForce);
stdDevMaxForceLog = max(std(log(maxForce)),0.05);
covMaxForce = stdDevMaxForce / avgMaxForce * 100;
charMaxForce = exp(avgMaxForceLog - k_s * stdDevMaxForceLog);
hMaxForce = kstest((log(maxForce)-avgMaxForceLog)/stdDevMaxForceLog);   %
Kolmogrov-Smirnov statistic (h = 0 passes test)

[…]

%% Section 9: Results

[…]

% Master Table

[…]

Master = [repelem(dia,numtests)' repelem(steel_class,numtests)'
repelem(clt,numtests)' repelem(grout_dia,numtests)' maxForce ultForce
yieldLoad propLimit stiffness];
```